SPONTANEOUS EMISSION IN

MICROCAVITY LASERS

THESIS
Dustin Philip Ziegler
Captain, USAF

AFIT/GAP/ENP/97D-11

1998021O 042

DTIC QUALITY INSPECTED 3

DEPARTMENT OF THE AIR FORCE

AIR UNIVERSITY

AIR FORCE INSTITUTE OF TECHNOLOGY

Wright-Patterson Air Force Base, Ohio

The views expressed in this thesis are those of the author and do not reflect the official policy or position of the Department of Defense or the United States Government.

SPONTANEOUS EMISSION IN MICROCAVITY LASERS

THESIS

Presented to the Faculty of the School of Engineering

of the Air Force Institute of Technology

Air University

In Partial Fulfillment of the

Requirements for the Degree of

Master of Science

Dustin Philip Ziegler, B.S.
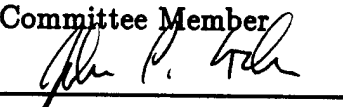
Captain, USAF

December, 1997

AFIT/GAP/ENP/97D-11

SPONTANEOUS EMISSION IN MICROCAVITY LASERS

Dustin Philip Ziegler, B.S.

Captain, USAF

Approved:

_____   _20 Nov 97_
Dr. David E. Weeks   Date
Thesis Advisor

_____   _24 Nov 97_
Dr. Won B. Roh   Date
Committee Member

_____   _21 Nov 97_
Dr. John P. Loehr   Date
Committee Member

Acknowledgements

My appreciation goes out to my two families, both in Vermont and in Boston, who listened to my woes and shared in my better moments. Thanks to all of you.

Saving perhaps the most important for last, my special gratitude and everlasting love for my wife Melissa, for the countless hours of support, the many cooked meals waiting for me in spite of her own graduate studies, and especially for being the something wonderful to come home to when things just didn't go quite right. Love always and forever.

<div align="right">Dustin Philip Ziegler</div>

Table of Contents

List of Figures

List of Tables

List of Symbols

List of Abbreviations

Abstract

An understanding of spontaneous emission processes within microcavities is crucial in addressing the need to make tomorrow's microlasers more efficient. One approach to improving the device efficiency is to reduce the threshold input current at which lasing begins to occur. It has been suggested that the threshold in a microcavity laser can be decreased by increasing the fraction of spontaneous emissions into the lasing mode. This can be accomplished by preferentially coupling the gain medium of the laser to the electromagnetic cavity mode of interest. It therefore becomes necessary to understand the mechanism by which this coupling takes place. This research develops a fully quantum mechanical description of the interaction between a gain medium modeled as a two level atom and a multimode electromagnetic field in a microcavity. Atomic transition probabilities are computed for systems in which the atom couples through a single photon process to electromagnetic cavity modes which range in number from two to 2000. Calculations performed for cavities with widely spaced modes demonstrate that atoms exhibit Jaynes-Cummings behavior when closely tuned to one mode. Detuning of the atom from the mode inhibits the exchange of energy, while increasing the strength of the coupling to the mode amplifies this exchange. Two level systems strongly coupled to many closely spaced modes exhibit spontaneous emission rates characteristic of an atom in free space.

SPONTANEOUS EMISSION IN MICROCAVITY LASERS

I. Introduction

1.1 Motivation

As stated in the New World Vistas, one of the goals of the Air Force laser programs heading into the twenty-first century is to develop very compact, highly efficient semiconductor laser devices [24]. The breadth of military applications for miniaturized laser devices continues to grow as portability and cost-efficiency of mass-manufacturing become increasingly important features across a variety of disciplines: optical control circuitry, information storage and retrieval, optical encryption and decryption technologies—just to name a few. In the past, the applications for semiconductor lasers were satisfied almost exclusively by traditional edge-emitting devices. These conventional "horizontal" lasers range in length from roughly 200 to 450 μm, though shorter devices have been fabricated [23]. The design is straightforward: an active region is formed by layering appropriate junction materials that also act as the optical waveguide in operation. The ends of the device are cleaved or etched to form mirror surfaces which are orthogonal to the junction (see Figure 1.1a). In this way, the cavity of the resonator is along the interface of the active region (horizontal). In these Fabry Perot resonators, relatively long cavity lengths are required to reduce the effects of loss at the mirrors. However, the resonant mode spacing, or Free Spectral Range, is inversely proportional to the cavity length, which in turn means long cavities support nearly a continuum of resonant modes which compete for the energy released by the active region at the junction. What is needed is a means of taking the non-lasing modes out of the competition.

a)

b)
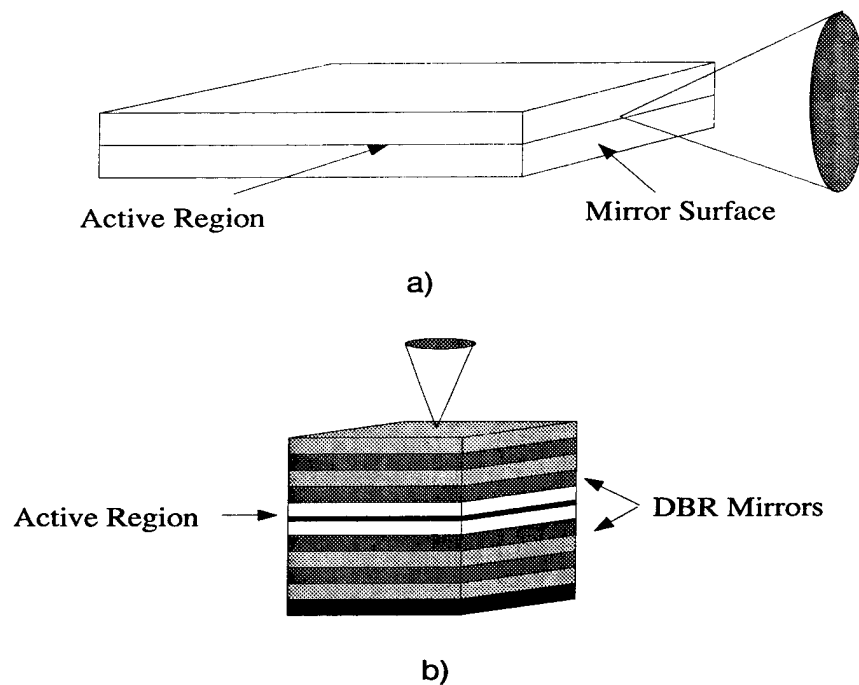
Figure 1.1   Diagrams for (a) conventional edge-emitting diode laser and (b) VCSEL
diode laser (After Ref. [23]).

1.2   Emergence of Vertical Cavity Surface Emitting Lasers

Within the past decade, research in the area of alternate semiconductor laser
designs has produced the Vertical Cavity Surface Emitting Laser (VCSEL). In con-
trast to the edge-emitting approach, the VCSEL design utilizes a layering technique
to form Distributed Bragg Reflectors (DBR) at either end of the cavity such that
the mirrors of this geometry are parallel to the active region in the middle (Figure
1.1 (b)). These mirrors are formed by layering pairs of alternately low and high
refractive index materials as shown in Figure 1.2.

VCSELs are fabricated using a bottom-up layering process using techniques
such as Molecular Beam Epitaxy or Metal-Organic Chemical Vapor Deposition to
grow the entire device on the substrate from the first DBR to the active region to the
second DBR. Although tolerances on the layering process are extremely tight, this
design eliminates the often complex cleaving or etching steps necessary to produce
the mirrors in the conventional laser diodes. In the final product, VCSEL cavities

measure in the micron to submicron range, roughly two orders of magnitude shorter than edge-emitting diodes. The advantages of this technology over the edge-emitting device are well documented and include single longitudinal mode operation (leading to higher output in the desired mode), smaller threshold currents, and the potential for application in large two-dimensional laser arrays [3, 23]. In what way can these devices be made more efficient? It has been suggested by Vurgaftman and Singh that the threshold current for microcavity lasers can be reduced even further through reductions in cavity dimensions [25]. It is instructive at this point to momentarily depart from the present discussion to address the basic principles of operation for laser diodes then return to the implications of cavity length reductions.

1.2.1 Overview of the VCSEL. At the risk of oversimplifying, the VCSEL can be described in terms of three basic components:

- an active gain medium;

- the pump energy, typically in the form of an applied electrical current or optical pumping that excites the active medium;

- an optical cavity formed by the DBR mirrors that encloses the active medium and allows for oscillation and subsequent amplification of emitted radiation;

It is the interactions between the active medium and the electromagnetic field in the cavity with which this thesis is chiefly concerned.

1.2.2 Emission Processes Within The Active Medium. In very elementary terms, the active medium consists of the region surrounding an interface between semiconductor materials and is characterized by an energy bandgap structure. A simple structure is shown in Figure 1.3. In this bandgap structure, charge carriers are excited from a lower energy bound-state *valence* band into a higher energy *conduction* band by the pump energy. Once excited, the carriers may transition back to the valence band, either directly or by way of intermediate transitions. The desirable
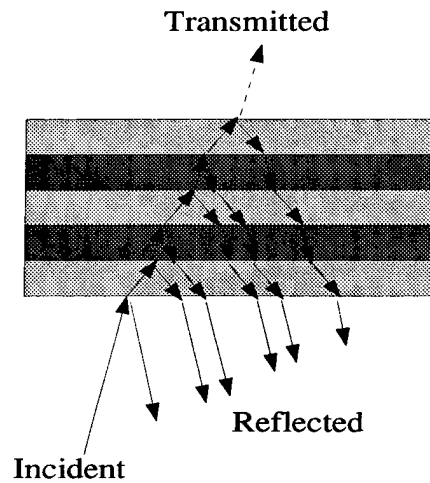
Figure 1.2   Multilayer reflections of the electric field within the DBR.

transitions are those for which the de-excitation is accompanied by the emission of photons of the intended lasing wavelength; other means of decay detract from the overall efficiency of the device and require higher pumping levels to overcome this effect. When a radiative decay is 'uninduced', or independent of the photon population in the cavity, the process is referred to as *spontaneous emission*. When a photon is emitted into the cavity, there is also a probability for it to interact with other carriers in the region in one of two ways: through *absorption*, where the photon is absorbed to excite the carrier, and *stimulated emission*, where the passage of a photon induces the excited carrier to de-excite and emit a photon of matching wavelength, polarization, phase, and direction. If a population inversion is achieved and maintained such that the number of conduction band carriers exceeds that in the valence band, then the subsequent avalanche of spontaneous emissions create a substantial flux of photons in the cavity. A fraction of these photons are emitted into a resonant mode of the cavity and remain in the cavity temporarily until absorbed or lost as output. While in the cavity the photons can initiate stimulated emission. When the gain in stimulated emission exceeds loss to output or absorption, then lasing threshold is achieved.
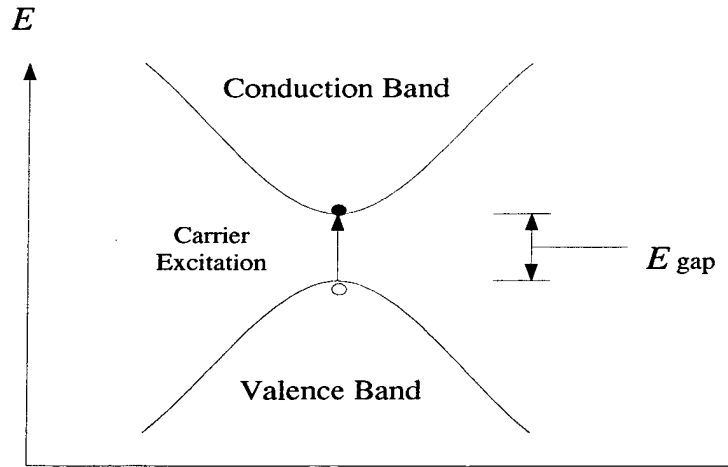
Figure 1.3   Simple energy bandgap structure.

1.3   Modified Spontaneous Emission

We now briefly return to the idea of modifying the probability of spontaneous emission into the lasing mode. In order to improve the efficiency of the laser, it is useful to reduce the power required to bring the laser to threshold. One method of accomplishing this is to preferentially couple the gain medium to the lasing mode and decrease the coupling to other modes. It has been suggested that the degree to which the medium couples to a mode can be enhanced by tuning the transition frequency in the medium to the mode frequency [28]. The Jaynes-Cummings Model, proposed in 1963, demonstrates that a two level system interacting with a single mode with which it is in resonance will exchange energy completely with that mode [13].

It is in this context that the research described in this thesis is presented. A theoretical model is presented which treats the electromagnetic field, gain medium, and their coupling within a microcavity laser quantum mechanically. This model is an extension of the Jaynes-Cummings theory of the interaction between an atomic spontaneous emission source and the vacuum field mentioned above.
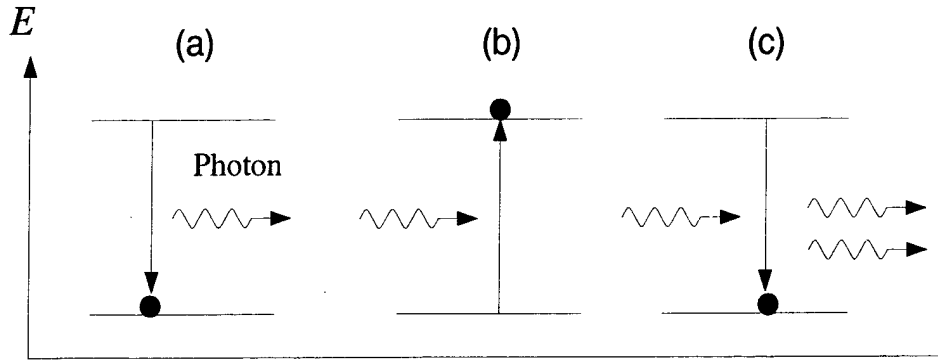
Figure 1.4 (a) Spontaneous Emission, (b) Absorption, and (c) Stimulated Emission.

1.4 Jaynes-Cummings Model

The Jaynes-Cummings Model (JCM) as presented by Meystre and Sargent [17] models the interaction between an atom represented by a two level system and a single electromagnetic mode in an enclosing optical cavity. The model assumes a single photon mechanism in which a single quantum of energy is either absorbed from the field by an atom in the ground state or emitted into the field mode by an excited atom [1]. The time evolution of the system is then given in terms of the evolution of the probability for the atom to spontaneously emit into the field and decay to the ground state. The JCM predicts a sinusoidal interchange of probability between the excited atom $(P(1))$ and excited field $(P(2))$ states [17]:

$$P(1) = \frac{\delta^2}{\delta^2 + 4 g^2} + \frac{4 g^2}{\delta^2 + 4 g^2} \cos^2(\frac{1}{2} \sqrt{\delta^2 + 4 g^2} \, t) \qquad (1.1)$$

$$P(2) = \frac{4 g^2}{\delta^2 + 4 g^2} \sin^2(\frac{1}{2} \sqrt{\delta^2 + 4 g^2} \, t) \qquad (1.2)$$

where g is a constant that describes how strongly the atom is coupled to the field mode and δ is the detuning of the atomic transition frequency from the field mode.

---

[1]The definition of the term 'photon' varies widely according to the context in which it is presented. In this thesis, 'photon' is used to indicate a single quantum of electromagnetic energy in a particular mode of the cavity. An interesting discussion of the definitions of the term is found in Ref. [17] in Section 12-1.

The resulting behavior of these probabilities is known as Rabi flopping after I.I. Rabi (1936), who explored the behavior of spin-$\frac{1}{2}$ magnetic dipoles in nuclear magnetic resonance [17]. The frequency $\mathcal{R} = \sqrt{\delta^2 + 4\,g^2}$ is the Rabi frequency for systems with no photons in the cavity when the atom is excited.[2] The probability exchange described by Equations 1.2 is illustrated in Figures 1.5a-d and 1.6a-d.

It is clear that as the coupling grows stronger, the frequency of the flopping increases, indicating a more rapid transition back and forth between the upper and lower atomic states. When the atom and field are perfectly tuned, complete exchange occurs. An increase in δ increases the frequency, but also reduces the amplitude of the exchange so that the energy in the system increasingly remains in the atom. However, for $g \gg \delta$, the exchange amplitude for a detuned atom approaches 1.0. The JCM demonstrates that the degree of exchange between the atom and field mode is suppressed through detuning and enhanced for increasing coupling strength.

As mentioned previously, the mode spacing, or Free Spectral Range (FSR), in the cavity is inversely proportional to the cavity length. For macroscopic cavities such as those used in typical gas discharge lasers, the mode spacing is very small. An atom near resonance with one mode is likely as well to be near resonance with adjacent modes. Conversely, as the cavity length is reduced, the mode spacing increases. In the limit of microcavity structures (roughly on the order of tens of microns or smaller), the mode spacing becomes very large (consider that the FSR for a 10 μm cavity is on the order of 10^{13} Hz compared to 10^8 Hz for a 1 m cavity). An atom near resonance with a given mode in a microcavity is much more detuned from the adjacent modes. Therefore, in the context of the microcavity, the single mode description contained in the JCM becomes applicable.

---

[2]The more general form of the Rabi frequency is $\mathcal{R} = \sqrt{\delta^2 + 4\,g^2\,(n+1)}$ where n is the number of photons in the cavity when the atom is excited.
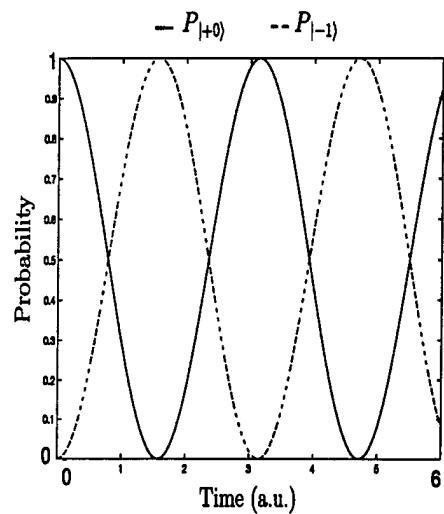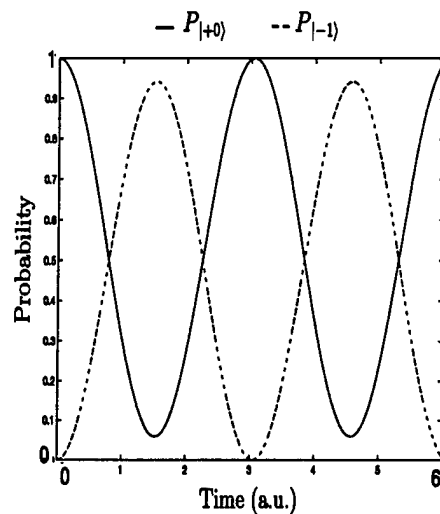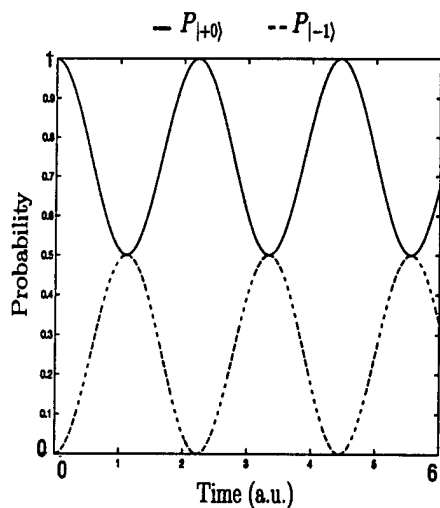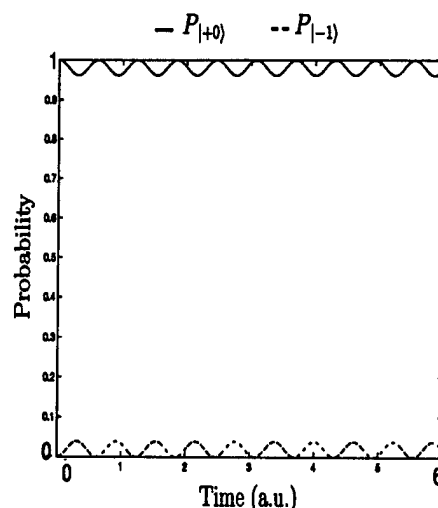
Figure 1.5   Detuning of the atom from the field mode increases the frequency of amplitude oscillation but reduces the probability for transition. (a) $\delta = 0$ (b) $\delta = g/2$ (c) $\delta = 2g$ (d) $\delta = 10g$.
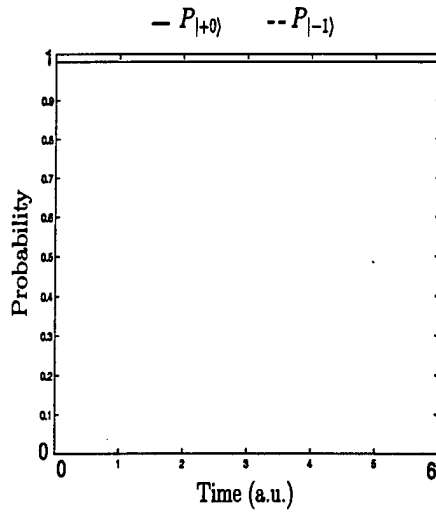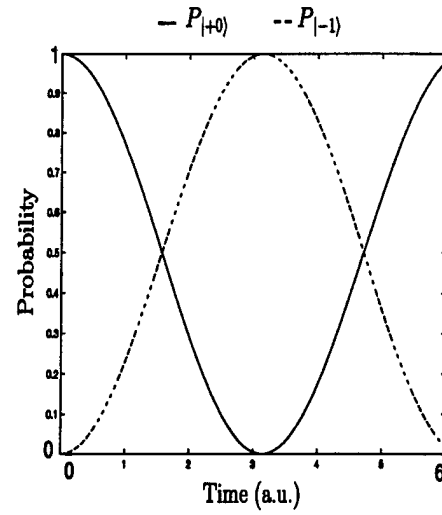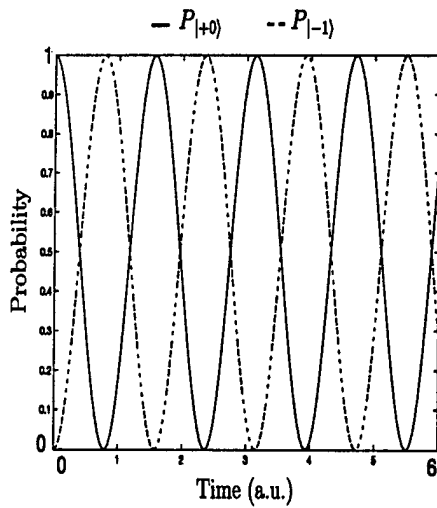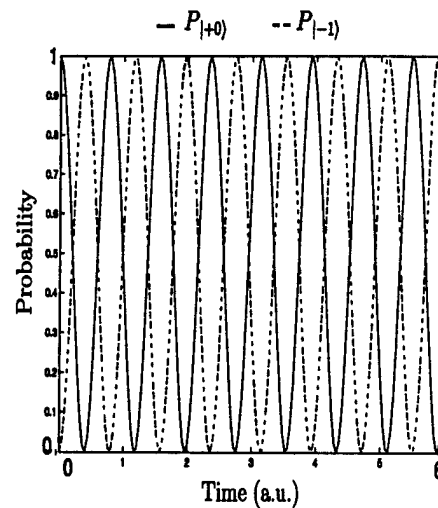
Figure 1.6   Increasing the coupling between the atom and the single field mode increases the flopping frequency but does not affect the amplitude in the JCM. $\delta = 0$ (a) Uncoupled (b) g_0 (c) $4 g_0$ (d) $8 g_0$

1.5 Scope

A truly quantum mechanical description of the microlaser system as a whole requires a quantized description of every facet of the problem. The individual atoms in the gain medium are in and of themselves complex systems. Because they're not isolated from one another, interactions occur which must be considered as well. Similarly, the atoms in the cavity walls must interact among themselves and with the gain medium, and the whole collection of material interacts with the field in the cavity. Broadening the field of view brings external influences into the picture. Each component of this system can take on a quantum mechanical description, and the resulting problem grows well beyond the number-crunching capabilities of even the best algorithms and high-performance computers. In order to make this problem tractable, a number of simplifications will be made:

- As in the JCM, the gain medium will be modeled by a single two-level atom. In effect, this corresponds to taking a vertical slice through the band structure shown in Figure 1.3. In principle, the medium is best modeled by a continuum of these slices, but the two level representation will have to suffice in this simplified model.

- A quantum mechanical description of the cavity wall material is not attempted and the walls are assumed to be perfectly electrically conducting (PEC). As a result, the only interactions are between the atom and the field, and there is no loss to the cavity walls.

- Because the wavelengths under consideration fall in the optical regime and are therefore roughly a thousand times larger than the dimensions of the atom in the cavity, the atom/field interaction will be approximated as the interaction of an electric point dipole in an electromagnetic field. Magnetic dipole, electric quadrupole, and higher multipole terms will be neglected.

- The two-level system is assumed to be stationary with regard to position or moving slowly enough within the cavity that variations in positions are small enough to be neglected on the timescale of the interactions. This carries the added benefit of allowing one to eliminate velocity dependent Doppler shifts from the picture.

- A one dimensional treatment of the electromagnetic field was adopted to simplify calculations. The results may be extrapolated to the three dimensional cubic cavity without significant extra work, where the spatial dependence of the electric and magnetic fields is slightly a slightly more complex product of sines and cosines in x, y, and z. In addition, the mode frequencies lose their harmonic spacing in the translation to the three dimensional cavity. [3]

- Cavity energies are low enough to warrant a strictly non-relativistic treatment.

These assumptions and constraints form the framework within which the following approach is pursued.

1.6 Methodology

As mentioned earlier, the model to be developed is an extension to the JCM outlined in Section 1.4. Where the JCM coupled the atom to a single mode of the electromagnetic field within the cavity, here the freedom to select multiple modes is added. In the model developed in this thesis, the atomic system is quantized in a fashion completely analogous to the spin-$\frac{1}{2}$ particle in a magnetic field. [4] Transitions between the two atomic levels are accomplished by means of operation on the state vector with the atomic raising and lowering operators (see Chapter 2). Quantization of the electromagnetic field is accomplished by first defining the mode structure by solving the classical cavity problem for a PEC cavity, then translating to a quantum

---

[3]The 1-D frequencies vary linearly with mode number m whereas in a 3-D cubic cavity the dependence is $(n_x^2 + n_y^2 + n_z^2)^{1/2}$.

[4]For an excellent discussion of spin-$\frac{1}{2}$ systems, see Cohen-Tannoudji et al, Ch. IV (Ref. [8])

mechanical picture by associating with each mode the characteristics of a quantized harmonic oscillator. A dipole interaction is assumed, and coupling coefficients are defined which determine the strength of interaction between the atom and each of the cavity modes. Together, the atomic, field, and coupling terms yield the full Hamiltonian of the system. The full Hamiltonian is diagonalized and the time evolution of the eigenstates is oscillatory with characteristic frequencies given by the energy eigenvalues. Finally, the transformation matrix that diagonalizes the Hamiltonian is used to transform back into the uncoupled basis to determine as a function of time the probability that the atom has undergone spontaneous emission.

The results obtained in Chapter 6 were obtained by computing the matrix elements of the full Hamiltonian for the system and diagonalizing the resulting matrix using FORTRAN 90 and a public domain Linear Algebra Package (LAPACK) diagonalizing routine. The resulting eigenvectors and eigenvalues were then used to propagate the system in time giving the evolution of the probabilities to be in each of the uncoupled states.

1.7 Notation

Where applicable I've adopted the Dirac Bra-Ket notation. State vectors are represented by $|\varphi\rangle \in \mathbb{V}$, where $\mathbb{V}$ is a vector space. Additionally, $|c\varphi\rangle = c|\varphi\rangle$ with c in general a complex constant. The scalar product is defined as $\langle\varphi_1|\varphi_2\rangle = c$ with the corresponding complex conjugate $\langle\varphi_2|\varphi_1\rangle = c^*$. Abstract operators are designated by a "hat" above the operator: $\hat{A}$, for example. The hat is dropped when a representation is taken, as with $\langle\alpha_i|A|\alpha_j\rangle$, where $\alpha_{i,j}$ are members of the basis in which A is represented. Note however, that $\hat{x}$, $\hat{y}$, and $\hat{z}$ are used as unit vectors in the classical field discussions to denote the direction of a vector quantity with respect to a set of x, y, and z coordinate axes, such as the classical electric field vector $\mathbf{E} = E_0\hat{x}$ directed along the x direction. Finally, the matrix elements of the

operator A are $A_{ij} = \langle u_i | A | u_j \rangle$ such that

$$
A \iff \begin{pmatrix}
A_{11} & A_{12} & \cdots & A_{1n} \\
A_{21} & A_{22} & \cdots & A_{2n} \\
\hdotsfor{4} \\
A_{n1} & A_{n2} & \cdots & A_{nn}
\end{pmatrix}
$$

1.8 Overview

The remainder of this thesis is devoted to presenting the theory, computational results, and implications of this quantum mechanical approach to the microcavity laser. To this end, a chapter has been devoted to each of these three aspects of the problem as outlined in the following paragraphs.

The focus of Chapter 2 is to present the theory underlying the quantum mechanical treatment of the atom. The analogy is made between the two level system and a spin-$\frac{1}{2}$ particle by means of the atomic raising and lowering (or spin-flip) operators. The resulting atomic Hamiltonian is then represented in the $| \pm \rangle$ eigenbases in matrix format.

In Chapter 3, expressions for the electric and magnetic fields are obtained for the classical PEC cavity. The amplitudes of these quantities are normalized by considering the total energy in the cavity, and the translation to a quantum mechanical operator form follows. As in Chapter 2, a matrix form is obtained by representing the Hamiltonian in the eigenbasis, in this case $|\{1_s\}\rangle$, where the $\{1_s\}$ notation indicates that the sth state has a single photon in the sth mode and none in any of the others. The uncoupled Hamiltonian is then obtained from the sum of the atomic and field Hamiltonians.

Chapter 4 develops the dipole interaction between the atom and field. The interaction Hamiltonian matrix is obtained by representing the Hamiltonian in the uncoupled atom/field basis $\{ | + \{0\}\rangle, | - \{1_s\}\rangle \}$.

The atom, field, and interaction Hamiltonians are brought together in Chapter 5. The chapter discusses how the eigenvectors of the diagonalized Hamiltonian are used to translate between the eigenbasis and the uncoupled basis mentioned above. The time evolution operator is introduced here, and the steps required to compute the time evolution of the bare state probabilities are outlined.

Chapter 6 contains the results of the calculations based on the theory presented in Chapters 2 through 5. A number of parameters, including cavity size, atomic transition frequency, and the coupling factor, are varied and the effects of these changes on the evolution of the system are extracted. Two regimes are of particular interest:

- atoms interacting with a field of widely spaced modes under weak coupling

- atoms strongly coupled to a large number of tightly spaced modes

In the limit of weak coupling and small cavities, the results obtained reproduce those of the JCM oscillations with predicted Rabi flopping frequencies. Likewise, for stronger coupling and large cavities where the atom easily accesses a large number of modes, the atom decays exponentially from the excited state with a rate comparable to an atom in free space. Chapter 6 concludes with a brief discussion of several unanticipated results.

The final chapter in this thesis, Chapter 7, presents a summary of the results and potential implications for microlaser performance. Recommendations on future studies in this area are provided at the closing.

Appendix A will describe the steps taken to verify the validity of the FORTRAN code written for this problem, while the code itself is presented as Appendix B. Appendix C contains several plots demonstrating an anomalous suppression of atomic de-excitation for moderate coupling strengths. Finally, Appendix D lists several useful conversion factors from the atomic unit system to the MKS and Gaussian unit systems.

II. The Atomic Hamiltonian, H_A

This chapter develops the Hamiltonian describing the atomic system. Recall from Section 1.5 that the simplification is made to represent the atom as a two-level system. While this significantly simplifies this aspect of the model, it is by no means intended as a realistic model of the material within a VCSEL or other microcavity laser.

2.1 Two Level System

Consider the two level system shown in Figure 2.1. The upper and lower states of the system are written $|+\rangle$ and $|-\rangle$ and are eigenstates of the atomic Hamiltonian, H_A:

$$H_A |\pm\rangle = \hbar\omega_\pm |\pm\rangle$$

with energy eigenvalues $\hbar\omega_\pm$. Note that the operator H_A can also be written

$$H_A = \mathbf{1} \, H_A \, \mathbf{1}$$

where $\mathbf{1}$ is the unit operator. The closure relation of quantum mechanics becomes useful at this point:

$$\sum_i |i\rangle\langle i| = \mathbf{1}$$

if the $|i\rangle$ form a complete orthonormal basis. The previous expression for H_A becomes

$$
\begin{aligned}
H_A &= \sum_i |i\rangle\langle i| \, H_A \, | \sum_j |j\rangle\langle j| \\
&= \sum_i |i\rangle \sum_j \langle i| H_A |j\rangle\langle j| \\
&= \sum_i |i\rangle \sum_j \hbar\omega_j \langle i|j\rangle\langle j| \, .
\end{aligned}
$$
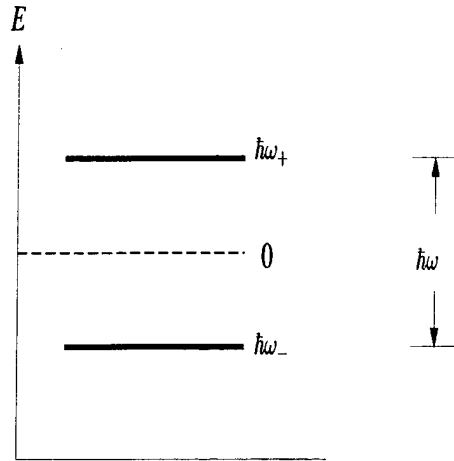
Figure 2.1   Renormalization of the atomic energy.

Recall that $\langle i|j \rangle = \delta_{ij}$ for orthonormal bases. Therefore,

$$
\begin{aligned}
H_A &= \sum_i |i\rangle \, \hbar\omega_i \, \langle i| \\
&= \sum_i \hbar\omega_i \, |i\rangle\langle i| \, .
\end{aligned}
\tag{2.1}
$$

For the convenience of subsequent discussion, suppose the zero-energy reference is renormalized to a value precisely halfway between the energies of the two states as in Figure 2.1. If the energy of transition between the two levels is

$$
\hbar\omega_+ - \hbar\omega_- = \hbar(\omega_+ - \omega_-) = \hbar\omega \, ,
$$

then renormalization of the energies presents a new set of measured values

$$
\langle +| \, H_A \, |+\rangle = \frac{\hbar\omega}{2}\langle +|+\rangle = \frac{\hbar\omega}{2}
$$

and

$$
\langle -| \, H_A \, |-\rangle = -\frac{\hbar\omega}{2}\langle -|-\rangle = -\frac{\hbar\omega}{2} \, .
$$

The operator H_A can finally be re-expressed (with the help of Equation 2.1) as

$$H_A = (\frac{\hbar\omega}{2})|+\rangle\langle+| + (-\frac{\hbar\omega}{2})|-\rangle\langle-|$$
$$= \frac{\hbar\omega}{2}(|+\rangle\langle+| - |-\rangle\langle-|). \tag{2.2}$$

2.2 Matrix Representation of H_A

At this point it is worthwhile to discuss the matrix representation of the atomic Hamiltonian. Consider the expansion of $|+\rangle\langle+|$ in the $|\pm\rangle$ basis:

$$|+\rangle\langle+| \Longleftrightarrow \begin{array}{c} \\ \langle+| \\ \langle-| \end{array} \begin{pmatrix} \langle+|+\rangle\langle+|+\rangle & \langle+|+\rangle\langle+|-\rangle \\ \langle-|+\rangle\langle+|+\rangle & \langle-|+\rangle\langle+|-\rangle \end{pmatrix}. \tag{2.3}$$

Those elements containing the scalar product $\langle\pm|\mp\rangle$ vanish by orthogonality, while the remaining element is 1, leaving

$$|+\rangle\langle+| \Longleftrightarrow \begin{pmatrix} 1 & 0 \\ 0 & 0 \end{pmatrix}.$$

This matrix can be written as the sum of two others:

$$|+\rangle\langle+| \Longleftrightarrow \begin{pmatrix} 1 & 0 \\ 0 & 0 \end{pmatrix} = \frac{1}{2}\left\{ \begin{pmatrix} 1 & 0 \\ 0 & 1 \end{pmatrix} + \begin{pmatrix} 1 & 0 \\ 0 & -1 \end{pmatrix} \right\}. \tag{2.4}$$

The first matrix in the brackets is the identity matrix, $\mathbf{1}$, while the second is the matrix representation of the Pauli $\hat{\sigma}_z$ spin operator. Performing similar operations for $|-\rangle\langle-|$ leads to the correspondences

$$|+\rangle\langle+| \Longleftrightarrow \frac{\mathbf{1} + \sigma_z}{2} \tag{2.5}$$

$$|-\rangle\langle-| \Longleftrightarrow \frac{\mathbf{1} - \sigma_z}{2}. \tag{2.6}$$

When the results of Equation 2.6 are substituted into Equation 2.2, an expression for H_A is obtained in terms of $\hat{\sigma}_z$:

$$\mathbb{H}_A = \frac{\hbar\omega}{2}\left(\frac{\mathbf{1}+\sigma_z}{2} - \frac{\mathbf{1}-\sigma_z}{2}\right)$$
$$= \frac{\hbar\omega}{2}\sigma_z \ .$$

And in operator form,

$$\hat{H}_A = \frac{\hbar\omega}{2}\hat{\sigma}_z \ . \tag{2.7}$$

III. The Multimode Electromagnetic Field Hamiltonian, H_F

Attention turns now to developing the Hamiltonian for the electromagnetic field in the cavity. Following the method of Chapter 2, the ultimate goal here is an expression for H_F, the field Hamiltonian, in the bare state representation. Initially, the classical modes of the cavity are derived in Gaussian units with a transition to atomic units for the quantum mechanical expressions. Throughout the classical cavity development, the quantities ϵ_0 and μ_0, which are both equal to 1 in these units, are retained as place holders to facilitate future studies that investigate dispersive cavities.

3.1 Classical Electromagnetic Cavity Modes.

The classical cavity discussion begins with Maxwell's equations for free space in Gaussian units,

$$\nabla \times \mathbf{E} + \frac{1}{c}\frac{\partial \mathbf{B}}{\partial t} = 0 \qquad \text{a)}$$

$$\nabla \times \mathbf{B} - \frac{\epsilon_0 \mu_0}{c}\frac{\partial \mathbf{E}}{\partial t} = 0 \qquad \text{b)}$$

$$\hspace{8cm} (3.1)$$

$$\nabla \cdot \mathbf{E} = 0 \qquad \text{c)}$$

$$\nabla \cdot \mathbf{B} = 0 \qquad \text{d)}$$

The curl of the first equation yields

$$\nabla \times \nabla \times \mathbf{E} + \frac{1}{c}\frac{\partial}{\partial t}(\nabla \times \mathbf{B}) = 0 . \qquad (3.2)$$
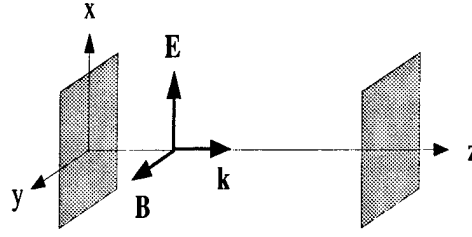
Figure 3.1   One dimensional PEC microcavity.

Substituting from Equation 3.1b and expanding the repeated curl above produces the wave equation in $\mathbf{E}$:

$$\nabla^2 \mathbf{E} - \frac{\epsilon_0 \mu_0}{c^2} \frac{\partial^2 \mathbf{E}}{\partial t^2} = 0 \; . \tag{3.3}$$

This equation can now be subjected to the boundary conditions for the PEC cavity. Choosing the z-axis as the direction along the cavity length and an $\mathbf{E}$ polarization in the $\hat{x}$ direction [1] (Figure 3.1), the first term becomes a second order derivative in z alone:

$$\nabla^2 \mathbf{E}(z,t) = \frac{\partial^2 E(z,t)}{\partial z^2} \hat{x} \; .$$

This leaves a differential equation in z and t which is solved by separation of variables,

$$\frac{\partial^2 E(z,t)}{\partial z^2} - \frac{\epsilon_0 \mu_0}{c^2} \frac{\partial^2 E(z,t)}{\partial t^2} = 0 \; .$$

Because the walls are perfect electrical conductors, the transverse ($\hat{x}$) component of the electric field vanishes at $z = 0$ and $z = L$ where L is the length of the cavity. Solutions are of the form

$$\mathbf{E}_m(z,t) = E_{0_m} \sin(kz) \exp^{-i\Omega_m t} \hat{x}; \tag{3.4}$$

$$k = \frac{m\pi}{L} \; , \quad m = 1,2,3,\cdots$$

---

[1]Note here that the hat denotes a vector direction and not an abstract operator as explained in Section 1.7.

with m^{th} mode amplitude E_{0_m}, propagation constant k, and angular mode frequency Ω_m. E_{0_m} will eventually need to be normalized when accounting for the total energy in the cavity, but for now it will remain as is. In order to find the cavity mode frequencies, Ω_m, this solution is now substituted back into the wave equation, Equation 3.3,

$$\nabla^2 \mathbf{E} - \frac{\epsilon_0 \mu_0}{c^2} \frac{\partial^2 \mathbf{E}}{\partial t^2} =$$

$$- k^2 E_0 \sin(kz) \exp^{-i\Omega_m t} \hat{x}$$

$$- \frac{\epsilon_0 \mu_0}{c^2} \left\{ -\Omega_m^2 E_0 \sin(kz) \exp^{-i\Omega_m t} \right\} \hat{x}$$

$$= \left\{ -k^2 + \frac{\epsilon_0 \mu_0 \Omega_m^2}{c^2} \right\} E_0 \sin(kz) \exp^{-i\Omega_m t} \hat{x} = 0$$

$$\implies k^2 = \frac{\epsilon_0 \mu_0 \Omega_m^2}{c^2} . \tag{3.5}$$

The frequencies are now defined according to

$$\Omega_m^2 = \frac{c^2}{\epsilon_0 \mu_0} \left\{ \frac{m^2 \pi^2}{L^2} \right\}$$

$$\Omega_m = \frac{m c \pi}{L \sqrt{\epsilon_0 \mu_0}} . \tag{3.6}$$

The solutions for $\mathbf{B}$ are found using $\mathbf{E}(z,t)$ in Equation 3.5 together with Equation 3.1b,

$$\nabla \times \mathbf{B}(z,t) = \frac{\epsilon_0 \mu_0}{c} \frac{\partial \mathbf{E}}{\partial t}$$

$$\frac{\partial B_y(z,t)}{\partial z} \hat{x} = - i \frac{\epsilon_0 \mu_0 \Omega_m}{c} E_{0_m} \sin(kz) \exp^{-i\Omega_m t} \hat{x}$$

$$\mathbf{B}_m(z,t) = - i \frac{\epsilon_0 \mu_0 \Omega_m}{c k} E_{0_m} \cos(kz) \exp^{-i\Omega_m t} \hat{y} .$$

Recall from Equation 3.5 that $\frac{\sqrt{\epsilon_0\,\mu_0}\,\Omega_m}{c} = k$ and the expression for the magnetic inductance in the cavity is obtained,

$$\mathbf{B}_m(z,t) = -\,i\,\sqrt{\epsilon_0\,\mu_0}\,E_{0_m}\,\cos(kz)\,\exp^{-i\Omega_m t}\,\hat{y}\ . \qquad (3.7)$$

3.2 Total Cavity Energy

From the last section, the expressions for the mode field quantities $\mathbf{E}_m(z,t)$ and $\mathbf{B}_m(z,t)$ are shown below,

$$
\begin{aligned}
\mathbf{E}_m(z,t) &= E_{0_m}\,\sin(k_m z)\,\exp^{-i\Omega_m t}\,\hat{x} \\
\mathbf{B}_m(z,t) &= -\,i\,\sqrt{\epsilon_0\,\mu_0}\,E_{0_m}\,\cos(k_m z)\,\exp^{-i\Omega_m t}\,\hat{y}\ .
\end{aligned} \qquad (3.8)
$$

In general, the total electric and magnetic fields in the cavity can be expanded in terms of these mode quantities,

$$\mathbf{E}(z,t) = \sum_m E_{0_m}\,\sin(k_m z)\,\exp^{-i\Omega_m t}\,\hat{x} \qquad (3.9)$$

$$\mathbf{B}(z,t) = \sum_m -\,i\,\sqrt{\epsilon_0\,\mu_0}\,E_{0_m}\,\cos(k_m z)\,\exp^{-i\Omega_m t}\,\hat{y}\ , \qquad (3.10)$$

where the amplitude E_{0_m} must now be normalized using the total energy in the cavity. The classical energy density $\mathcal{U}$ in the cavity is given by

$$\mathcal{U} = \epsilon_0\,\mathbf{E}\cdot\mathbf{E} + \frac{1}{\mu_0}\,\mathbf{B}\cdot\mathbf{B}\ .$$

Using the expansions in Equation 3.10, and averaging out the time dependence (the $\langle\ \rangle$ indicates the time averaging), the energy density becomes

$$\mathcal{U} = \sum_{m,m'}\left\{\epsilon_0\,\langle\mathbf{E}_m^*(z,t)\cdot\mathbf{E}_{m'}(z,t)\rangle + \frac{1}{\mu_0}\,\langle\mathbf{B}_m^*(z,t)\cdot\mathbf{B}_{m'}(z,t)\rangle\right\}$$

$$= \sum_{m,m'} \left\{ \frac{\epsilon_0}{2} E_{0_m} E_{0_{m'}} \sin^2(k_m z) + \frac{(\epsilon_0 \mu_0)}{2 \mu_0} E_{0_m} E_{0_{m'}} \cos^2(k_m z) \right\}$$

$$= \sum_{m,m'} \frac{1}{2} \left\{ \epsilon_0 E_{0_m} E_{0_{m'}} \sin^2(k_m z) + \frac{(\epsilon_0 \mu_0)}{\mu_0} E_{0_m} E_{0_{m'}} \cos^2(k_m z) \right\} .$$

Integration of this energy density over the volume of the cavity produces the total energy H in the cavity. Since the field quantities are expanded in orthogonal modes, integration over the volume eliminates those quantities $E_{0_m} E_{0_{m'}}$ for which $m \neq m'$,

$$H = \int_V dv \sum_m \frac{1}{2} \left\{ \epsilon_0 E_m^2 \sin^2(k_m z) + \frac{(\epsilon_0 \mu_0)}{\mu_0} E_m^2 \cos^2(k_m z) \right\}$$

$$= \sum_m \frac{1}{2} \int_V dv \left\{ \epsilon_0 E_m^2 \sin^2(k_m z) + \frac{(\epsilon_0 \mu_0)}{\mu_0} E_m^2 \cos^2(k_m z) \right\} . \qquad (3.11)$$

The volume of the 1-D cavity is L and the integral in Equation 3.11 is over z to yield the total energy,

$$H = \sum_m \frac{1}{2} \left\{ \epsilon_0 \frac{L}{2} E_{0_m}^2 + \frac{1}{\mu_0} \frac{L}{2} (\epsilon_0 \mu_0) E_{0_m}^2 \right\} . \qquad (3.12)$$

The expressions for **E** and **B** in Equation 3.8 may be reexpressed as

$$\mathbf{E}_m(z,t) = Q_m(t) \left[\frac{2\Omega_m^2}{\epsilon_0 L} \right]^{\frac{1}{2}} \sin \left(\frac{m \pi z}{L} \right) \hat{x}$$

$$\mathbf{B}_m(z,t) = \dot{Q}_m(t) \sqrt{\epsilon_0 \mu_0} \left[\frac{2}{\epsilon_0 L} \right]^{\frac{1}{2}} \cos \left(\frac{m \pi z}{L} \right) \hat{y}$$

where

$$E_{0_m} \exp^{-i\Omega_m t} = Q_m(t) \left[\frac{2\Omega_m^2}{\epsilon_0 L} \right]^{\frac{1}{2}}$$

and

$$-i E_{0_m} \exp^{-i\Omega_m t} = -i Q_m(t) \left[\frac{2\Omega_m^2}{\epsilon_0 L} \right]^{\frac{1}{2}} = \dot{Q}_m(t) \left[\frac{2}{\epsilon_0 L} \right]^{\frac{1}{2}} .$$

The $Q_m(t)$ and $\dot{Q}_m(t)$ are mode coordinate and mode velocity variables. These new expressions for **E** and **B** are substituted into Equation 3.12 to yield

$$
\begin{aligned}
\mathrm{H} &= \sum_m \frac{1}{2} \left\{ \epsilon_0 \frac{L}{2} \left[\frac{2\Omega_m^2}{\epsilon_0 L} \right] Q_m^2 + \frac{1}{\mu_0} \frac{L}{2} (\epsilon_0 \mu_0) \left[\frac{2}{\epsilon_0 L} \right] \dot{Q}_m^2 \right\} \\
&= \sum_m \frac{1}{2} \left\{ \Omega_m^2 Q_m^2 + \dot{Q}_m^2 \right\} .
\end{aligned} \tag{3.13}
$$

3.3   Translation to Quantized Field

The transition to a quantum mechanical expression for electric field as well as the total cavity energy involves a straightforward conversion of the Q_m^2 and $\dot{Q}_m^2$ variables to operators. Define $\hat{Q}_m$ and $\hat{P}_m$ as

$$
\hat{Q}_m = \left[\frac{\Omega_m}{\hbar} \right]^{\frac{1}{2}} Q \implies \Omega_m^2 Q_m^2 = \hbar \, \Omega_m \hat{Q}_m^2
$$

$$
\hat{P}_m = \left[\frac{1}{\hbar \, \Omega_m} \right]^{\frac{1}{2}} \dot{Q} \implies \dot{Q}_m^2 = \hbar \, \Omega_m \hat{P}_m^2
$$

such that the operator $\hat{H}_F$ corresponding to the total field energy is

$$
\hat{H}_F = \sum_m \frac{\hbar \, \Omega_m}{2} \left\{ \hat{Q}_m^2 + \hat{P}_m^2 \right\} \tag{3.14}
$$

while the electric field operator becomes

$$
\hat{E} = \sum_m \hat{Q}_m \left[\frac{2\Omega_m^2}{\epsilon_0 L} \right]^{\frac{1}{2}} \sin(k_m z) . \tag{3.15}
$$

The raising and lowering operators for a given field mode $(\hat{a}_m^\dagger, \, \hat{a}_m)$ corresponding to adding and removing, respectively, a photon from that mode can be constructed from the $\hat{Q}_m$ and $\hat{P}_m$ operators:

$$
\hat{a}_m = \frac{1}{\sqrt{2}} \left(\hat{Q}_m + i \hat{P}_m \right)
$$

$$\hat{a}_m^\dagger = \frac{1}{\sqrt{2}} \left(\hat{Q}_m - i\hat{P}_m \right) . \tag{3.16}$$

Solving these equations for $\hat{Q}_m$ and $\hat{P}_m$ in terms of $\hat{a}_m$ and $\hat{a}_m^\dagger$ gives

$$\hat{Q}_m = \frac{1}{\sqrt{2}} \left(\hat{a}_m^\dagger + \hat{a}_m \right) \tag{3.17}$$

$$\hat{P}_m = \frac{i}{\sqrt{2}} \left(\hat{a}_m^\dagger - \hat{a}_m \right) \tag{3.18}$$

which in turn can be inserted into Equation 3.14:

$$\begin{aligned}
\hat{H}_F &= \sum_m \frac{\hbar \Omega_m}{2} \left\{ \hat{Q}_m^2 + \hat{P}_m^2 \right\} \\
&= \sum_m \frac{\hbar \Omega_m}{2} \left\{ \hat{Q}_m^\dagger \hat{Q}_m + \hat{P}_m^\dagger \hat{P}_m \right\} \\
&= \sum_m \frac{\hbar \Omega_m}{2} \left\{ \frac{1}{2} \left(\hat{a}_m^\dagger + \hat{a}_m \right)^\dagger \left(\hat{a}_m^\dagger + \hat{a}_m \right) + \frac{1}{2} \left(\hat{a}_m^\dagger - \hat{a}_m \right)^\dagger \left(\hat{a}_m^\dagger - \hat{a}_m \right) \right\} \\
&= \sum_m \frac{\hbar \Omega_m}{2} \left\{ \frac{1}{2} \left(\hat{a}_m + \hat{a}_m^\dagger \right) \left(\hat{a}_m^\dagger + \hat{a}_m \right) + \frac{1}{2} \left(\hat{a}_m - \hat{a}_m^\dagger \right) \left(\hat{a}_m^\dagger - \hat{a}_m \right) \right\} \\
&= \sum_m \frac{\hbar \Omega_m}{2} \left\{ \hat{a}_m \hat{a}_m^\dagger + \hat{a}_m^\dagger \hat{a}_m \right\} .
\end{aligned}$$

The commutator $\left[\hat{a}_m, \hat{a}_m^\dagger \right]$ is developed in most quantum mechanics texts and evaluates to 1, allowing the substitution $\hat{a}_m \hat{a}_m^\dagger = \hat{a}_m^\dagger \hat{a}_m + 1$ and

$$\begin{aligned}
\hat{H}_F &= \sum_m \frac{\hbar \Omega_m}{2} \left\{ 2\hat{a}_m^\dagger \hat{a}_m + 1 \right\} \\
&= \sum_m \hbar \Omega_m \left\{ \hat{a}_m^\dagger \hat{a}_m + \frac{1}{2} \right\} . \tag{3.19}
\end{aligned}$$

The $\frac{\hbar \Omega_m}{2}$ contributed by all modes leads to the infinite zero-point energy alluded to in the first chapter. Once again, it is the changes in energy with respect to some reference that can be measured, so the problem can be rescaled to exclude the factor

of $\frac{1}{2}$ above. The resulting field Hamiltonian is

$$\hat{H}_F \;\; = \;\; \sum_m \hbar\,\Omega_m\,\hat{a}_m^\dagger \hat{a}_m \; . \tag{3.20}$$

When this operator acts upon a state vector describing all modes of the cavity, the total energy held in each mode is determined as the number of photons n_m in the mth mode times the energy $\hbar\Omega_m$ of a single photon in that mode:

$$H_F\,|\,n_1\,n_2\,\cdots\,n_m\rangle = \{n_1\,\hbar\,\Omega_1 + n_2\,\hbar\,\Omega_2 + \cdots + n_m\,\hbar\,\Omega_m\}\,|\,n_1\,n_2\,\cdots\,n_m\rangle \; . \tag{3.21}$$

The states labeled $|\,n_1\,n_2\,\cdots\,n_m\rangle = |\,\{n_s\}\rangle$ are in fact the eigenstates of the Hamiltonian H_F.

The electric field operator can now be expressed in terms of the raising and lowering operators:

$$\hat{E} = \sum_m \left(\hat{a}_m^\dagger + \hat{a}_m\right)\left[\frac{\hbar\,\Omega_m}{\epsilon_0 L}\right]^{\frac{1}{2}} \sin(k_m z) \; .$$

Meystre and Sargent refer to $\left[\frac{\hbar\,\Omega_m}{\epsilon_0 L}\right]^{1/2} = \mathcal{E}_m$ as the electric field per photon, giving

$$\hat{E} = \sum_m \left(\hat{a}_m^\dagger + \hat{a}_m\right)\,\mathcal{E}_m\,\sin(k_m z) \; . \tag{3.22}$$

3.4 Matrix Representation of H_F

The matrix elements of $\hat{H}_F$ are given by $\langle \{n_{s'}\} | H_F | \{n_s\} \rangle$, where

$$
\mathbb{H}_F = \hbar \begin{array}{c} \\ \langle n_1 | \\ \langle n_2 | \\ \vdots \\ \langle n_m | \end{array}
\begin{array}{cccc}
|n_1\rangle & |n_2\rangle & \cdots & |n_m\rangle \\
\end{array}
\left(
\begin{array}{cccc}
n_1 \Omega_1 & 0 & \cdots & 0 \\
0 & n_2 \Omega_2 & \cdots & 0 \\
\vdots & \vdots & \ddots & \vdots \\
0 & 0 & \cdots & n_m \Omega_m
\end{array}
\right) . \tag{3.23}
$$

By combining the atom and field Hamiltonians, H_A and H_F, an uncoupled Hamiltonian can be obtained,

$$
\hat{H}_{A+F} = \frac{\hbar \omega}{2} \hat{\sigma}_z + \sum_m \hbar \Omega_m \hat{a}_m^\dagger \hat{a}_m .
$$

Defining the bare state representation as $| \pm \{n_s\}\rangle = |\pm\rangle \otimes |\{n_s\}\rangle$ yields

$$
\mathbb{H}_{A+F} = \hbar \begin{array}{c} \\ \langle +00\cdots| \\ \langle -10\cdots| \\ \vdots \\ \langle -0\cdots1| \end{array}
\begin{array}{cccc}
|+00\cdots\rangle & |-10\cdots\rangle & \cdots & |-0\cdots1\rangle \\
\end{array}
\left(
\begin{array}{cccc}
\frac{\omega}{2} & 0 & \cdots & 0 \\
0 & \Omega_1 - \frac{\omega}{2} & \cdots & 0 \\
\vdots & \vdots & \ddots & \vdots \\
0 & 0 & \cdots & \Omega_{m_{max}} - \frac{\omega}{2}
\end{array}
\right) . \tag{3.24}
$$

This Hamiltonian describes the energy of the system when interactions between the atom and field are ignored. Note that since the matrix is already diagonal, the bare states are the eigenstates of H_{A+F} with eigenvalues given by the diagonal elements. For example, the time independent Schrödinger equation involving the $| - 010 \cdots \rangle$ state is

$$
(H_A + H_F) | - 010 \cdots \rangle = \left(\hbar \Omega_2 - \frac{\hbar \omega}{2} \right) | - 010 \cdots \rangle .
$$

IV. The Atom - Field Interaction, H_{int}

4.1 Dipole Operator $\hat{D}$

The classical energy of interaction between the atom and field is given by

$$H_{int} = -e\,\mathbf{r} \cdot \mathbf{E} = \mathbf{D} \cdot \mathbf{E} , \qquad (4.1)$$

where $\mathbf{D}$ is the dipole moment of the two level atom. The operator form of the equation above is obtained by recognizing the correspondence between the vector quantity $\mathbf{r}$ and the operator $\hat{\mathbf{r}}$:

$$\mathbf{D} = -e\mathbf{r} \iff \hat{\mathbf{D}} = -e\hat{\mathbf{r}} .$$

The matrix elements of $\hat{\mathbf{D}}$ define those transitions which are dipole allowed in the atomic system. By symmetry, the matrix elements $\langle i| - e\,\mathbf{r}|j\rangle$ vanish if i and j label the same state. Since $\mathbf{r}$ is antisymmetric,

$$\langle i| - e\,\mathbf{r}|j\rangle = \int d^3r\, \psi^*(\mathbf{r})\,\mathbf{r}\,\psi(\mathbf{r}) = 0, \quad i = j . \qquad (4.2)$$

While it is also possible for the matrix elements to vanish for certain $i \neq j$, this model will assume transitions between the two levels in the atomic system are dipole allowed. The eigenstates of H_A, $|\pm\rangle$ are used to represent the dipole matrix,

$$
\mathbb{D} = -e\,
\begin{array}{cc}
 & \begin{array}{cc} |+\rangle & \qquad |-\rangle \end{array} \\
\begin{array}{c} \langle+| \\ \langle-| \end{array} &
\begin{pmatrix}
\langle+|r|+\rangle & \langle+|r|-\rangle \\
\langle-|r|+\rangle & \langle-|r|-\rangle
\end{pmatrix}
\end{array}
$$

$$
= -e
\begin{pmatrix}
0 & \langle+|r|-\rangle \\
\langle-|r|+\rangle & 0
\end{pmatrix} .
$$

Let $\langle +| -er |-\rangle = -er_{+-} = D_{+-}$ and $\langle -| -er |+\rangle = D_{-+} = D_{+-}^*$:

$$\mathbb{D} \quad = \quad \begin{pmatrix} 0 & D_{+-} \\ D_{+-}^* & 0 \end{pmatrix}$$

$$= \quad D_{+-} \begin{pmatrix} 0 & 1 \\ 0 & 0 \end{pmatrix} + D_{+-}^* \begin{pmatrix} 0 & 0 \\ 1 & 0 \end{pmatrix}$$

$$= \quad D_{+-} \sigma_+ + D_{+-}^* \sigma_- \quad . \tag{4.3}$$

The matrices σ_+ and σ_- correspond to the atomic raising and lowering operators, $\hat{\sigma}_+$ and $\hat{\sigma}_-$. This can be seen by their action on the states $|+\rangle$ and $|-\rangle$ with their vector representations, $(1\ 0)$ and $(0\ 1)$:

$$\hat{\sigma}_+ |-\rangle \ \leftrightarrow \ \begin{pmatrix} 0 & 1 \\ 0 & 0 \end{pmatrix} \begin{pmatrix} 0 \\ 1 \end{pmatrix} = \begin{pmatrix} 1 \\ 0 \end{pmatrix}$$

$$\hat{\sigma}_- |+\rangle \ \leftrightarrow \ \begin{pmatrix} 0 & 0 \\ 1 & 0 \end{pmatrix} \begin{pmatrix} 1 \\ 0 \end{pmatrix} = \begin{pmatrix} 0 \\ 1 \end{pmatrix} \quad .$$

Because this system is limited to two levels, raising of the upper and lowering of the lower states is not allowed. The dipole operator is given by

$$\hat{D} = D_{+-}\hat{\sigma}_+ + D_{+-}^*\hat{\sigma}_- \quad . \tag{4.4}$$

4.2   Interaction Hamiltonian

Equations 3.22 and 4.4 together form the quantized interaction Hamiltonian, H_{int}. Combining the two equations,

$$\hat{H}_{int} \quad = \quad \hat{D} \cdot \hat{E}$$

$$= \left(D_{+-} \hat{\sigma}_+ + D_{+-}^* \hat{\sigma}_- \right) \sum_m \left(\hat{a}_m^\dagger + \hat{a}_m \right) \mathcal{E}_m \, \sin(kz)$$

$$= \sum_m \left\{ \left(D_{+-} \hat{\sigma}_+ + D_{+-}^* \hat{\sigma}_- \right) \left(\hat{a}_m^\dagger + \hat{a}_m \right) \mathcal{E}_m \, \sin(kz) \right\}$$

$$= \sum_m \hbar \left\{ g_m \hat{a}_m^\dagger \hat{\sigma}_+ + g_m \hat{a}_m \hat{\sigma}_+ + g_m^* \hat{a}_m^\dagger \hat{\sigma}_- + g_m^* \hat{a}_m \hat{\sigma}_- \right\} \qquad (4.5)$$

where $g_m = \frac{1}{2\hbar} D_{+-} \cdot \mathcal{E}_m \, \sin(kz)$ and $g_m^* = \frac{1}{2\hbar} D_{+-}^* \cdot \mathcal{E}_m \, \sin(kz)$ are the coupling constant and its complex conjugate that describe the strength with which a given atomic transition and field mode interact. With the definitions $D_{+-} = -e\,r_{+-}$ and $\mathcal{E}_m = \left[\frac{\hbar \Omega_m}{\epsilon_0 L} \right]^{1/2}$, the explicit form of g_m is

$$g_m = -\frac{e\,r_{+-}\,\cos\theta}{2\,\hbar} \left[\frac{\hbar \Omega_m}{\epsilon_0 L} \right]^{1/2} \sin(kz)$$

where $\cos\theta$ represents the projection of the electric field polarization vector along the dipole moment of the atom. When the electric field lies along the dipole axis, coupling is maximized; conversely, a dipole aligned perpendicular to the field will not couple to that field. In the development of the quantized field in Chapter 3, the polarization of the electric field was taken to be in the $\hat{x}$ direction and as a simplification the orientation of the dipole moment is taken to lie in the $\hat{x}$ direction as well. The $\cos\theta$ factor can then be replaced by 1. The coupling terms are then given by

$$g_m = -\frac{e\,r_{+-}}{2\,\hbar} \left[\frac{\hbar \Omega_m}{\epsilon_0 L} \right]^{1/2} \sin(kz) \,. \qquad (4.6)$$

Note from Equation 4.5 that there are four terms of interaction: $g_m \hat{a}_m^\dagger \hat{\sigma}_+$, $g_m \hat{a}_m \hat{\sigma}_+$, $g_m^* \hat{a}_m^\dagger \hat{\sigma}_-$, and $g_m^* \hat{a}_m \hat{\sigma}_-$. The first term describes a process in which the states of the atom and m^{th} field mode are simultaneously raised. Similarly, the fourth term describes the lowering of both the atomic and field mode states. The second and third terms involve 'cross processes' in which an exchange of energy occurs wherein the excitation of the atom is accompanied by a lowering of the field and vice-versa. It is shown in Meystre and Sargent that the contribution of the cross terms to the

4-3

Hamiltonian is on the order of $\frac{1}{\Omega_m - \omega}$ while in comparison the contribution of the remaining terms is $\frac{1}{\Omega_m + \omega}$ [17]. In general, the key interactions dealt with in this analysis involve atomic and field frequencies which are roughly of the same order of magnitude, so the $g_m \hat{a}_m^\dagger \hat{\sigma}_+$ and $g_m^* \hat{a}_m \hat{\sigma}_-$ terms are neglected. This approximation is analogous to the Rotating Wave Approximation in semi-classical treatments of the atom-field interaction. The final form of the interaction Hamiltonian is

$$\hat{H}_{int} = \sum_m \hbar \left\{ g_m \hat{a}_m \hat{\sigma}_+ + g_m^* \hat{a}_m^\dagger \hat{\sigma}_- \right\} . \tag{4.7}$$

4.3 Matrix Representation of H_{int}

Using the properties of the field and atom raising and lowering operators, the bare state representation of H_{int} is given by

$$\mathbb{H}_{int} \quad = \quad \hbar \quad \begin{array}{c} \\ \langle +00\cdots| \\ \langle -10\cdots| \\ \vdots \\ \langle -\cdots 1_m| \end{array} \overset{\displaystyle |+00\cdots\rangle \quad |-10\cdots\rangle \quad \cdots \quad |-\cdots 1_m\rangle}{\begin{pmatrix} 0 & g_1 & \cdots & g_m \\ g_1^* & 0 & \cdots & 0 \\ \vdots & \vdots & \ddots & \vdots \\ g_m^* & 0 & \cdots & 0 \end{pmatrix}} . \tag{4.8}$$

The full Hamiltonian H_{tot} is given by

$$
\begin{aligned}
\hat{H}_{tot} \quad &= \quad \hat{H}_A + \hat{H}_F + \hat{H}_{int} \\
&= \quad \frac{\hbar \omega}{2} \hat{\sigma}_z + \sum_m \hbar \Omega_m \hat{a}_m^\dagger \hat{a}_m + \sum_m \hbar \left\{ g_m \hat{a}_m \hat{\sigma}_+ + g_m^* \hat{a}_m^\dagger \hat{\sigma}_- \right\} ,
\end{aligned} \tag{4.9}
$$

and the matrix elements of H_{tot} are then $\langle \pm \{1_s\} \mid H_{tot} \mid \pm \{1_{s'}\}\rangle$ where,

$$
\mathbb{H}_{tot} \quad = \quad \hbar \quad
\begin{array}{c}
\\
\langle +00\cdots\mid \\
\langle -10\cdots\mid \\
\vdots \\
\langle -0\cdots 1_m \mid
\end{array}
\begin{array}{cccc}
\mid +00\cdots\rangle & \mid -10\cdots\rangle & \cdots & \mid -0\cdots 1_m\rangle \\
\left(\begin{array}{cccc}
\frac{\omega}{2} & g_1 & \cdots & g_m \\
g_1^* & \Omega_1 - \frac{\omega}{2} & \cdots & 0 \\
\vdots & \vdots & \ddots & \vdots \\
g_m^* & 0 & \cdots & \Omega_m - \frac{\omega}{2}
\end{array}\right)
\end{array}
\quad . \quad (4.10)
$$

V. Time Evolution of the System

5.1 Time Evolution in the Bare State Basis

Discussion of the time evolution of the system begins with the time-dependent Schrödinger Equation,

$$i\hbar \frac{d}{dt}|\psi(t)\rangle = \hat{H}_{tot}|\psi(t)\rangle \ . \tag{5.1}$$

Solution of this equation for a time-independent Hamiltonian yields

$$|\psi(t)\rangle = \exp\left[\frac{-i\hat{H}_{tot}t}{\hbar}\right]|\psi(0)\rangle \ . \tag{5.2}$$

In the bare state representation,

$$\langle B\,|\,\psi(t)\rangle = \langle B\,|\ \exp\left[\frac{-i\hat{H}_{tot}t}{\hbar}\right]|\psi(0)\rangle \tag{5.3}$$

where the shorthand notation $|B\rangle = |\pm\{1_s\}\rangle$ has been adopted and $\hat{U}(t) = \exp\left[\frac{-i\hat{H}_{tot}t}{\hbar}\right]$ is the time evolution operator. Using the completeness of the bare state basis, Equation 5.3 can be rewritten

$$\langle B\,|\,\psi(t)\rangle = \sum_{B'}\langle B\,|\ \exp\left[\frac{-i\hat{H}_{tot}t}{\hbar}\right]|B'\rangle\langle B'\,|\,\psi(0)\rangle \ . \tag{5.4}$$

The matrix form of $\hat{H}_{tot}$ is non-diagonal in the bare state basis, making the exponential of the Hamiltonian difficult to evaluate. If the time evolution operator is represented in the eigenbasis of $\hat{H}_{tot}$, also known as the dressed state basis, the expression is greatly simplified. The completeness of the dressed states $|D\rangle$ allows Equation 5.4 to be re-expressed as

$$\langle B \,|\, \psi(t)\rangle =$$

$$\sum_{B'}\sum_{D}\sum_{D'}\langle B \,|\, D\rangle\langle D \,|\, \exp\left[\frac{-i\,\hat{H}_{tot}\,t}{\hbar}\right] \,|\, D'\rangle\langle D' \,|\, B'\rangle\langle B' \,|\, \psi(0)\rangle \, . \quad (5.5)$$

The exponential is expanded in a Taylor series,

$$\exp\left[\frac{-i\,\hat{H}_{tot}\,t}{\hbar}\right] = 1 - \frac{i\,\hat{H}_{tot}\,t}{\hbar} - \frac{\hat{H}_{tot}^2\,t^2}{2\,\hbar^2} + \cdots \, ,$$

and the quantity $\langle D \,|\, \exp\left[\frac{-i\,\hat{H}_{tot}\,t}{\hbar}\right] \,|\, D'\rangle$ is evaluated term by term in the expansion. The dressed states are by definition orthogonal, and the expansion terms evaluate as

$$\langle D \,|\, 1 \,|\, D'\rangle \;=\; 1\,\langle D \,|\, D'\rangle = \delta_{D,D'}$$

$$\hspace{10cm}(5.6)$$

$$\langle D \,|\, -\frac{i\,\hat{H}_{tot}\,t}{\hbar} \,|\, D'\rangle \;=\; -\frac{i\,E_{D'}\,t}{\hbar}\,\langle D \,|\, D'\rangle = -i\,\omega_{D'}\,t\,\delta_{D,D'}$$

$$\vdots$$

where $E_{D'}$ is the eigenvalue corresponding to the eigenstate D' and $\omega_{D'}$ is the associated eigenfrequency. Equation 5.6 can be re-summed to give the resulting expression for $\langle B \,|\, \psi(t)\rangle$,

$$\langle B \,|\, \psi(t)\rangle = \sum_{B'}\sum_{D}\langle B \,|\, D\rangle\,\exp\left[-i\,\omega_D\,t\right]\,\langle D \,|\, B'\rangle\langle B' \,|\, \psi(0)\rangle \, . \qquad (5.7)$$

There are an infinite number of modes in the cavity and therefore an infinite number of bare states. The matrix form for the time evolution in the bare state basis is

$$
\begin{bmatrix} \langle B_1 \,|\, \psi(t) \rangle \\ \vdots \end{bmatrix} =
$$

$$
\begin{bmatrix} \langle B_1 \,|\, D_1 \rangle & \cdots \\ \vdots & \ddots \end{bmatrix}
\begin{bmatrix} e^{-i\omega_1 t} & 0 \\ 0 & \ddots \end{bmatrix}
\begin{bmatrix} \langle D_1 \,|\, B_1 \rangle & \cdots \\ \vdots & \ddots \end{bmatrix}
\begin{bmatrix} \langle B_1 \,|\, \psi(0) \rangle \\ \vdots \end{bmatrix}
$$

or

$$
\mathbb{C}_B(t) \;=\; \mathbb{T}\,\mathbb{U}\,\mathbb{T}^T\,\mathbb{C}_B(0) \tag{5.8}
$$

where $\mathbb{C}_B(t)$ are the expansion coefficients of $\psi(t)$ in the bare state representation,

$$
\mathbb{C}_B \;=\; \begin{pmatrix} c_{+00\cdots}(t) \\ c_{-10\cdots}(t) \\ \vdots \\ c_{-0\cdots 1_m}(t) \end{pmatrix}, \tag{5.9}
$$

$\mathbb{T}$ is the matrix obtained by diagonalizing H_{tot} that transforms from the dressed states representation to the bare state representation,

$$
\mathbb{T} \;=\;
\begin{array}{c}
\\
\langle +00\cdots| \\
\langle -10\cdots| \\
\vdots \\
\langle -0\cdots 1_m|
\end{array}
\begin{array}{cccc}
|es_1\rangle & |es_2\rangle & \cdots & |es_m\rangle \\
\end{array}
\begin{pmatrix}
c_{11} & c_{12} & \cdots & c_{1m} \\
c_{21} & c_{22} & \cdots & c_{2m} \\
\vdots & \vdots & \ddots & \vdots \\
c_{m1} & c_{m2} & \cdots & c_{mm}
\end{pmatrix}, \tag{5.10}
$$

and $\mathbb{U}$ is the time evolution operator in the dressed state representation,

$$
\mathbb{U} \;=\;
\begin{pmatrix}
\exp^{-iE_1 t/\hbar} & 0 & \cdots & 0 \\
0 & \exp^{-iE_2 t/\hbar} & \cdots & 0 \\
\vdots & \vdots & \ddots & \vdots \\
0 & 0 & \cdots & \exp^{-iE_m t/\hbar}
\end{pmatrix}. \tag{5.11}
$$

The last two terms in Equation 5.8 are the transpose of $\mathbb{T}$ and the initial state of the system in the bare state representation.

The probability for finding the system in a given bare state is found by squaring the absolute value of the appropriate expansion coefficient. For example, the probability of finding the system in a state with an excited atom and no photons in the field at time t is

$$P(+00\cdots) = c^*_{+00\cdots}(t)\, c_{+00\cdots}(t) = |\, c_{+00\cdots}(t)|^2 \quad . \tag{5.12}$$

The recipe now exists to compute the probabilities for the atom/field system to be in any given state at a particular time. This provides insight into how the atom couples to the various field modes as a function of time.

5.2 Truncation of $\mathbb{H}_{tot}$

As mentioned in the previous section, the infinite number of field modes requires an infinite number of basis vectors to represent the system. As a result, the Hamiltonian is infinitely large. In practice, we must decide how to truncate the matrix. In other words, we need to anticipate how many modes the atom can be expected to couple to. There are two (related) ways to answer this. The first is to compare the relative sizes of the coupling terms on the off diagonals to the corresponding term on the diagonal. For a given value of r_{+-} and L, the coupling terms g_m in the first row and column can be written as a constant times the square root of the mode frequency times the spatial mode amplitude modulation $\sin(kz) = \sin(\frac{m\pi z}{L})$, giving

$$g_m = \kappa\, \Omega_m^{1/2} \sin\left(\frac{m\,\pi\,z}{L}\right) \;,$$

where $\kappa = -\frac{e\, r_{+-}}{2\,\sqrt{\hbar\,\epsilon_0 L}}$. The diagonal matrix elements are

$$\Omega_m - \frac{\omega}{2} \;,$$

5-4
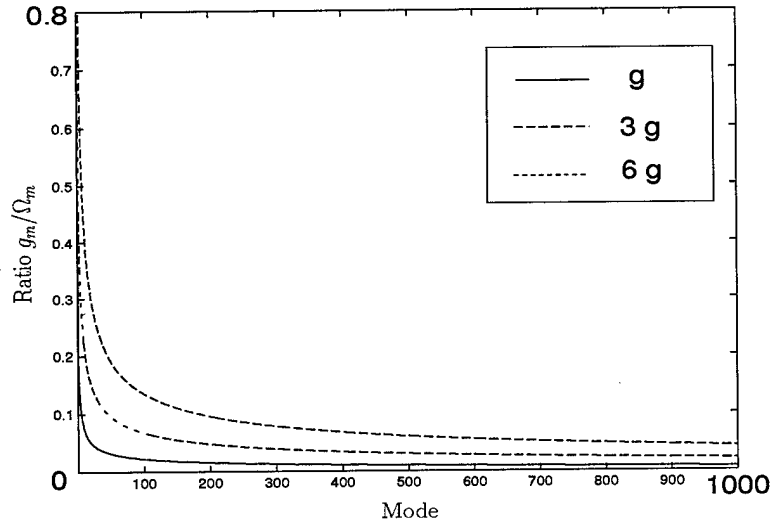
Figure 5.1   Ratio of the off-diagonal Hamiltonian terms to the diagonals as mode
number increases for several. In this case $\omega \sim \Omega_1$.

and the ratio of the off-diagonals to the diagonals becomes

$$\frac{\kappa \, \Omega_m^{1/2} \, \sin\left(\frac{m\pi z}{L}\right)}{\Omega_m - \frac{\omega}{2}}.$$

If ω is comparable to the fundamental mode frequency, and we temporarily ignore
the sinusoidal modulation in favor of examining the envelop of the ratio values, then
the ratio varies approximately as

$$\frac{\kappa}{\Omega_m^{1/2}}$$

for large m. A plot of this ratio is shown in Figure 5.1 for several values of κ.
If enough modes are added, the off-diagonals eventually become negligible com-
pared to the diagonals. As these coupling terms become negligible, the remainder
of the Hamiltonian matrix takes on the appearance of the uncoupled Hamiltonian
of Equation 3.24. The Hamiltonian can then be said to be block-diagonal, with a
coupled symmetric block and a diagonal uncoupled block (with mode frequencies

5-5

much greater than the atomic frequency). This block diagonal form of $\mathbb{H}_{tot}$ is

$$
\left(
\begin{array}{cc}
\left[
\begin{array}{cccc}
\frac{\omega}{2} & g_1 & \cdots & g_m \\
g_1^* & \Omega_1 - \frac{\omega}{2} & \cdots & 0 \\
\vdots & \vdots & \ddots & \vdots \\
g_m^* & 0 & \cdots & \Omega_m - \frac{\omega}{2}
\end{array}
\right] & 0 \\
0 & \left[
\begin{array}{cccc}
\Omega_{m+1} & 0 & \cdots & 0 \\
0 & \Omega_{m+2} & \cdots & 0 \\
\vdots & \vdots & \ddots & \vdots \\
0 & 0 & \cdots & \Omega_{m_{max}}
\end{array}
\right]
\end{array}
\right) . \qquad (5.13)
$$

Hence, the atom is more or less uncoupled from these higher modes. [1] Note that if a threshold is chosen below which the coupling terms are effectively zero, then Figure 5.1 illustrates that larger coupling strengths necessitate more modes and thus larger matrices. This serves as the basis for truncating the matrix. Using the definitions in Equations 5.9 and 5.10, the initial probability amplitudes of the eigenstates (i.e. the expansion coefficients) are given by

$$
\mathbb{C}_D(0) = \mathbb{T}^{\mathrm{T}} \mathbb{C}_B(0) \qquad (5.14)
$$

$$
\Rightarrow
\begin{pmatrix}
c_{es_1}(0) \\
c_{es_2}(0) \\
\vdots \\
c_{es_m}(0)
\end{pmatrix}
=
\begin{pmatrix}
c_{11} & c_{21} & \cdots & c_{m1} \\
c_{12} & c_{22} & \cdots & c_{m2} \\
\vdots & \vdots & \ddots & \vdots \\
c_{1m} & c_{2m} & \cdots & c_{mm}
\end{pmatrix}
\begin{pmatrix}
1 \\
0 \\
\vdots \\
0
\end{pmatrix}
=
\begin{pmatrix}
c_{11} \\
c_{12} \\
\vdots \\
c_{1m}
\end{pmatrix} .
$$

The probability that the atom is initially in the ith eigenstate is found by squaring c_{1i}. Recall from above that by adding field modes, the Hamiltonian can be made large enough that it approaches block-diagonal form. The transformation matrix $\mathbb{T}$ that diagonalizes the Hamiltonian will therefore also be block diagonal. The

---

[1] It is important to note that regardless of the magnitude of ω, the matrix can always be made large enough to block diagonalize it by adding modes.

block for which the Hamiltonian is non-diagonal will transform in some complex way giving rise to mixtures of eigenstates comprising the bare states of that block. Conversely, the diagonal block is, of course, diagonalized by the identity matrix. The transformation matrix becomes

$$
\mathbb{T} = \left(
\begin{bmatrix}
c_{11} & c_{12} & \cdots & c_{1m} \\
c_{21} & c_{22} & \cdots & c_{2m} \\
\vdots & \vdots & \ddots & \vdots \\
c_{m1} & c_{m2} & \cdots & c_{mm}
\end{bmatrix}
\qquad 0 \qquad
\begin{bmatrix}
1 & 0 & \cdots & 0 \\
0 & 1 & \cdots & 0 \\
\vdots & \vdots & \ddots & \vdots \\
0 & 0 & \cdots & 1
\end{bmatrix}
\right) . \qquad (5.15)
$$

It was shown above that the distribution of eigenstate probability amplitudes for the excited atom bare state at $t = 0$ was given by

$$
\begin{pmatrix}
c_{es_1}(0) \\
c_{es_2}(0) \\
\vdots \\
c_{es_m}(0)
\end{pmatrix}
=
\begin{pmatrix}
c_{11} \\
c_{12} \\
\vdots \\
c_{1m}
\end{pmatrix} .
$$

A sample plot of the initial eigenstate probabilities for a coupled Hamiltonian in which none of the coupling terms were neglected is shown in Figure 5.2. It confirms that the eigenstate amplitudes do indeed eventually vanish, so that such plots as these can be used to select an appropriate number of modes for a particular coupling strength. In this way, the amount of computation can be reduced while obtaining the same results (see Figure 5.3).
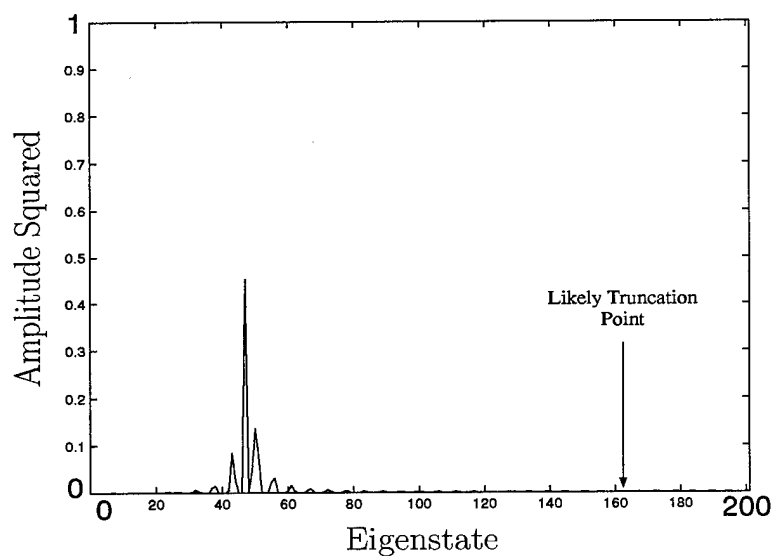
Figure 5.2   Probabilities of the eigenstates comprising the initial excited atom state of the system. This system can be truncated at roughly 160 modes while still producing the same result, as shown below.
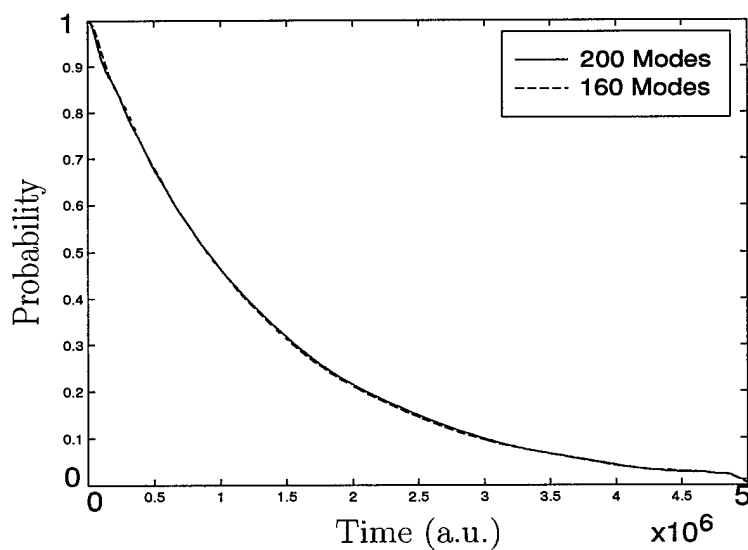
Figure 5.3   Comparison of $P_{+00...}$ for the arbitrarily large (200 mode) and truncated (160 mode) matrices.

5.3   A Closer Look at $\mathbb{H}_{tot}$

Now that the groundwork has been laid to perform the calculations, a closer look at the nature of the Hamiltonian, $\mathbb{H}_{tot}$, should provide some insights towards how the system might behave under several limiting circumstances. The previous section demonstrated how the Hamiltonian becomes block diagonalized when the ratio of the couplings terms to the bare state frequencies $(\Omega_m - \omega/2)$ on the diagonal vanishes.

Consider Figure 5.1 once again. As mentioned earlier, the ratio vanishes much more quickly for weak coupling. It seems reasonable to assume that $\kappa = -\frac{e\, r_{+-}}{2\sqrt{\epsilon_0}\, L}$ can be chosen such that the atom couples to a very small number of modes, perhaps even one mode. In that event, eigenstate plots similar to Figure 5.2 should reveal that only two eigenstates (corresponding to the two dominant configurations of the system) participate. For one mode coupling, the system will exhibit Jaynes-Cummings behavior. We shall see in the next chapter that this is in fact the case.

On the other hand, when κ is significantly larger, the atom should couple to many more modes. This in turn implies that there will be many more eigenstates with non-trivial amplitudes arising from the diagonalization of $\mathbb{H}_{tot}$. It is intuitive to believe that an atom coupled strongly to a large number of modes should decay to a ground state with a small likelihood of returning to the excited state. The atom in free space can be considered the limiting case where the atom couples to an infinite number of infinitesimally spaced modes of an infinitely long cavity. The second half of Chapter 6 explores this regime of strong coupling and narrow mode spacing.

The next chapter details the results of these calculations for various values of coupling strength, cavity size, and atom-field detuning. For fields composed of many modes, numerical solutions are required. The diagonalization of the Hamiltonian is carried out by a public domain linear algebra routine that returns eigenvalues and eigenvectors which are then used to propagate the system and translate the result to the bare state basis.

VI. Spontaneous Emission Results

In this chapter the results of the calculations based on the previously developed theory are presented. In the first section, the one-mode Jaynes-Cummings problem is extended to the two-mode case to demonstrate the JCM behavior of a simple multimode system in which the atom is near resonance under weak coupling with one of the modes. In this regime of coupling strengths, the influence of the other modes can be neglected. For strong coupling, the single-mode simplification breaks down and the atom is shown to couple also to the off-resonant mode. The field is then expanded to 100 modes under a variety of coupling strengths and detunings to explore the influence of the additional modes. Section 6.2 demonstrates that an atom accessing a large number of closely spaced modes spontaneously decays from an excited state with a rate comparable to an atom in free space. All calculations and results are presented in atomic units, and conversions to MKS and Gaussian systems are provided in Appendix D.

There are essentially four parameters available to adjust in this model: the atomic transition frequency ω, the position of the two-level system z, the cavity length L, and the value assigned to r_{+-}. In selecting values for r_{+-}, it should be noted that it is possible to choose a coupling strength that is high enough to couple the atom strongly to the highest frequency modes in the field. One could then argue that there would be influences from even higher modes not accounted for in the Hamiltonian. Such behavior is characterized by noticeable amplitudes in the probabilities of the outlying bare states as shown in Figure 6.1. In order to remedy this, either the coupling constant must be reduced or the number of modes must be increased until the outlying states no longer participate. In all calculations presented here, the coupling was kept low enough that a significant number of the highest states exhibited negligible amplitude in the probability plots and the amplitudes of
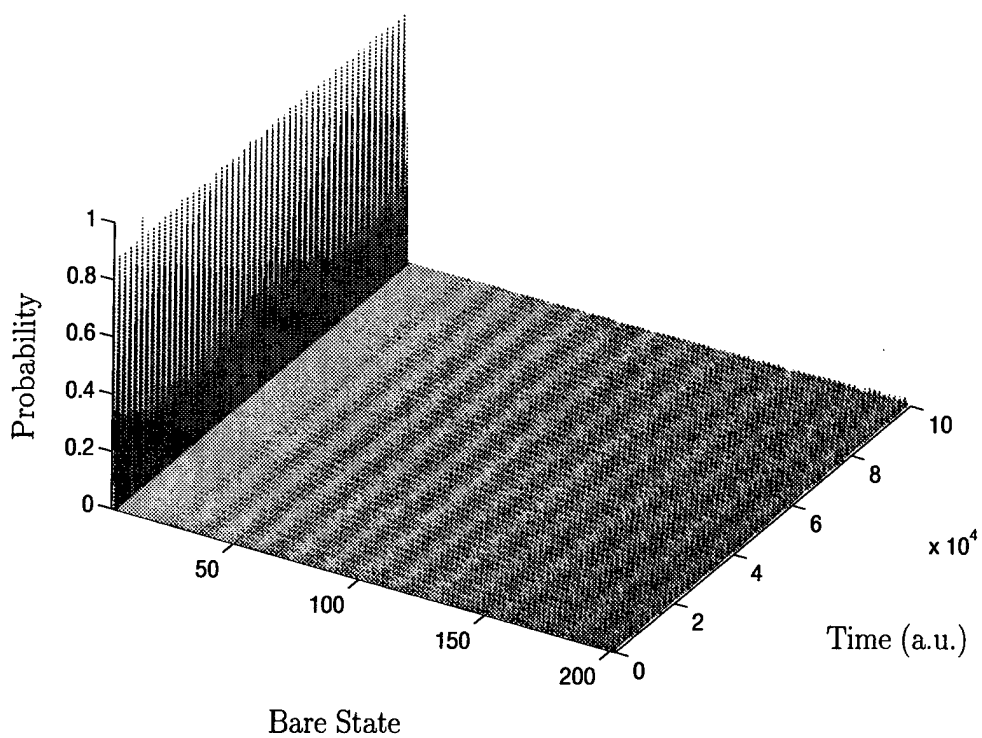
Figure 6.1   Plot of all bare state probabilities for a case in which the coupling strength is too high for the size of the Hamiltonian. The probability of the state corresponding to the excited atom is plotted at the left on the bare state axis. Note the growing amplitude of the probabilities for the higher-numbered bare states.

the highest eigenstates were negligible (recall the discussion on matrix truncation in Chapter 5).

One may also adjust the coupling strength to each mode by varying z. Doing so affects each mode differently through the $\sin(kz)$ term in g. It follows, then, that a particular choice of position may cause one or more of the coupling terms to vanish if the atom is located at a node. For example, Figure 6.2 shows how the choice of position can affect coupling. In the top diagram, the atom is located at a position where the electric field amplitude of the fundamental mode is maximum. Consequently, the coupling of the atom to this mode is stronger than to the second cavity mode in (b). Since the amplitude of the second mode vanishes at $\frac{L}{2}$, the coupling constant $g = D_{+-} \cdot \mathcal{E}_m \sin(kz)$ also vanishes. Unless otherwise noted, the calculations presented below were performed for a two level system located away from the center of the cavity at $\frac{L}{2}$. While this has the disadvantage of modulating the coupling values in a predictable yet uneven fashion, it avoids the undesirable effect of decoupling half of all of the modes (the center position decouples the even-m modes) in the cavity.

6.1   Jaynes-Cummings Behavior

As mentioned in Section 1.4, the JCM predicts an oscillatory interchange of probability between an excited atom state and a single excited field state for which the frequency of the excited mode is closely tuned to the atomic transition (also referred to as the resonant atom or resonant field case). Figure 1.5, reproduced here as Figure 6.3 shows this complete interchange. Now suppose that a single mode is added to the existing field at the next cavity mode frequency (twice the fundamental frequency). When the coupling strength is 'weak', an atom tuned near either frequency will couple only to that mode as predicted by the JCM. Figure 6.4 shows the change in how the atom is coupled to the field modes as the atomic transition frequency is 'dialed' from resonance with the fundamental mode to resonance with
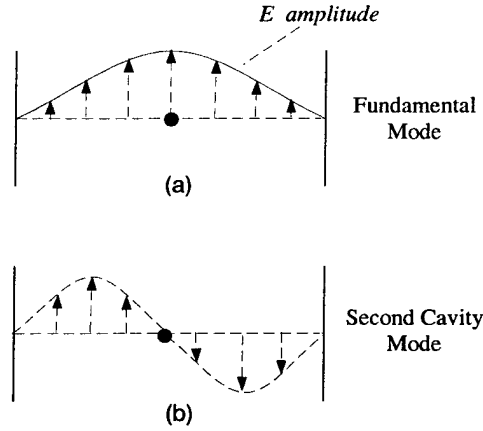
Figure 6.2   Strength of coupling for a given mode is modulated by the atom's position in the cavity. Coupling is maximized at the antinodes (a) and zero at the nodes (b).

the second cavity mode. The atom is located $\frac{1}{3}$ of the way along the cavity so that the $\sin(kz)$ factor in the coupling constant contributes equally to both modes.

The Rabi frequency can be calculated for the two mode system for comparison with the analytical one-mode result, where the frequency of probability exchange went as $\frac{\mathcal{R}}{2} = \frac{1}{2}\sqrt{\delta^2 + 4\,g^2}$. The probability exchange represented by Figure 6.4a has a half-period of $T_{1/2} = 1.865 \times 10^6$ in atomic units (recall that the flopping frequency exhibits a $\cos^2$ temporal dependence in Equation 1.2, such that a period spans *three* peaks instead of two for cos). This corresponds to an angular frequency of

$$\frac{\mathcal{R}_{data}}{2} = \frac{2\,\pi}{2\,T_{1/2}} = 3.369 \times 10^{-6} \text{ in atomic units of frequency.}$$

For $\delta = 0$, $\Omega_1 = 2.278 \times 10^{-3}$, $\langle r_{+-} \rangle = 0.01$, $L = 10\,\mu m = 1.890 \times 10^5$, $\epsilon_0 = .0795$, $e = 1$ and $\hbar = 1$, all in atomic units, the JCM result for $\frac{\mathcal{R}}{2}$ is

$$\begin{aligned}
\frac{\mathcal{R}_{JCM}}{2} &= \frac{1}{2}\sqrt{\delta^2 + 4\,g^2} = g \\[2mm]
&= \frac{e\,r_{+-}\,\mathcal{E}_m}{2\,\hbar}\,\sin(kz) \\[2mm]
&= \frac{e\,r_{+-}\,\left[\frac{\hbar\,\Omega_m}{\epsilon_0\,L}\right]^{\frac{1}{2}}}{2\,\hbar}\,\sin(kz)
\end{aligned}$$

6-4
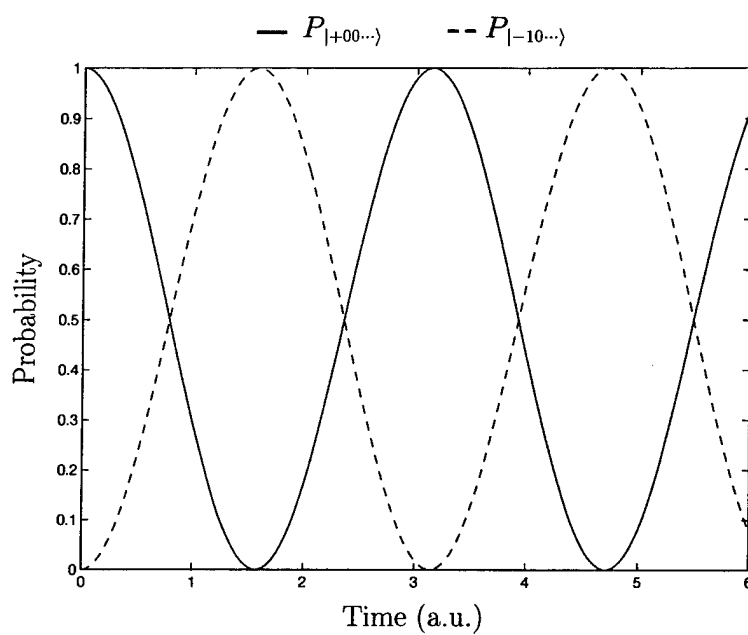
Figure 6.3 Characteristic complete probability exchange predicted by the analytical one mode JCM solution for a resonant atom (from Chapter 1).
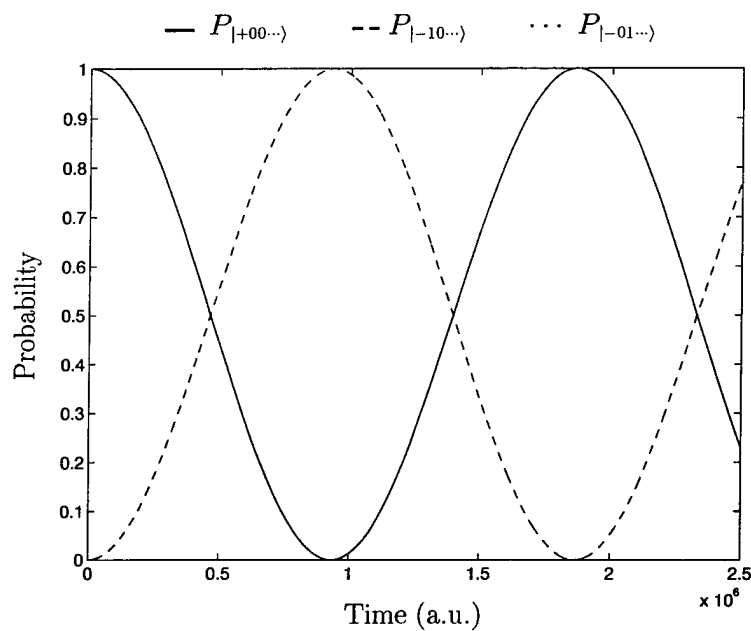
(a) Atom interacts only with first mode showing complete flopping. $P_{|-01\cdots\rangle}$ is zero.
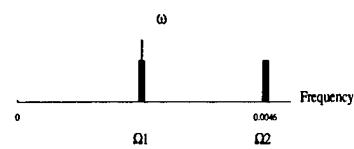
(b) Atom is resonant with the first mode.
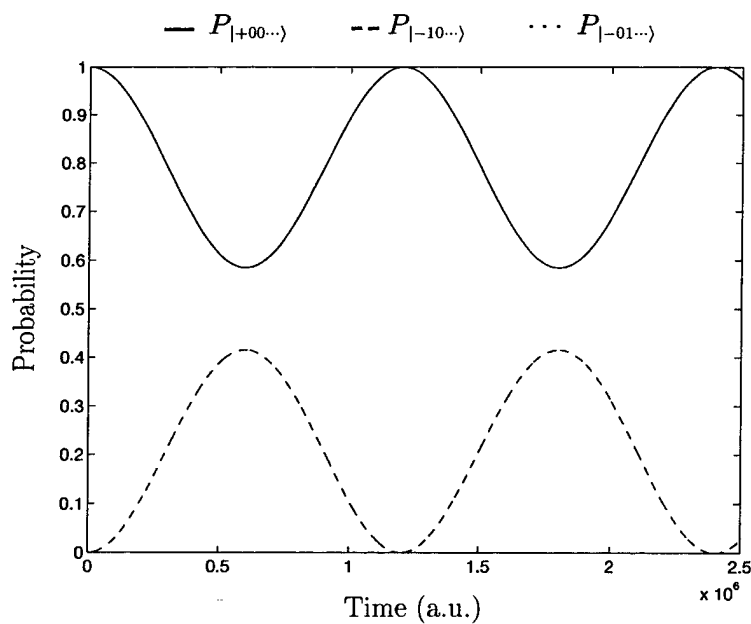
(c) Atom continues to interact with first mode, but with reduced amplitude exchange.
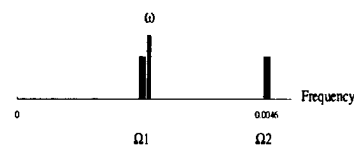
(d) Atom is slightly detuned from the first mode.

6-6
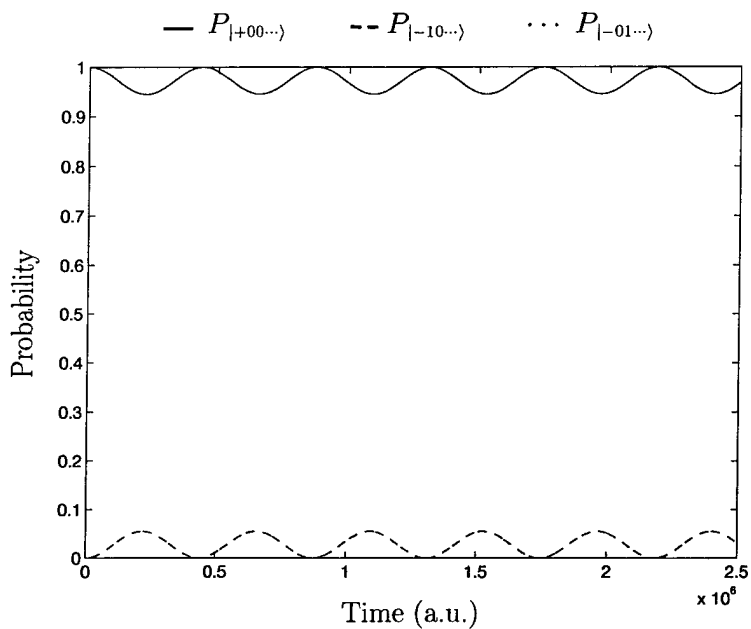
(e) Very little interaction with first mode, none with the second.
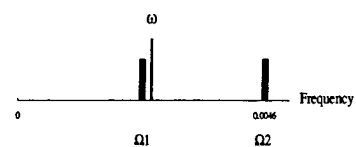
(f) Moderate detuning of atom from the first mode.
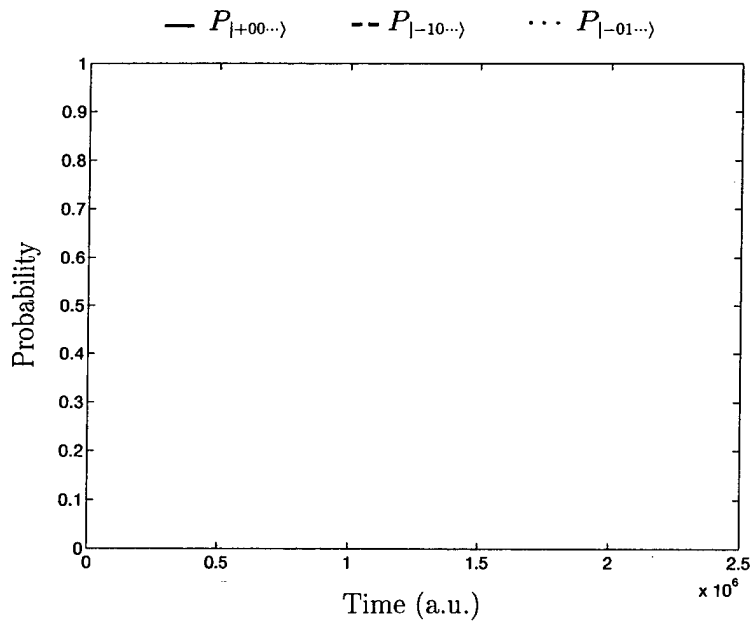
(g) Atom is completely uncoupled from the two modes.
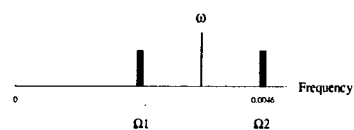
(h) Equal detuning from both modes.
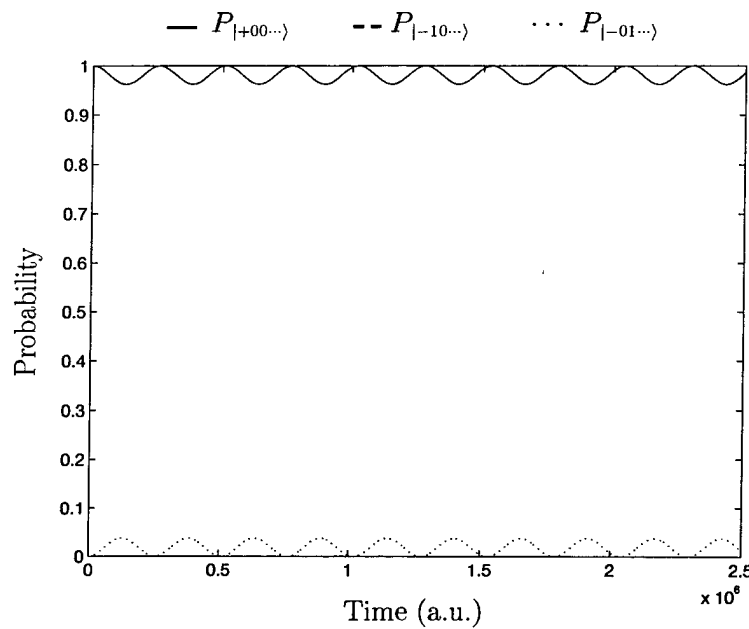
(i) Atom begins to couple to second mode. $P_{|-10\cdots\rangle}$ is now zero.
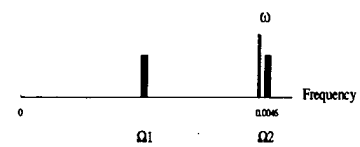
(j) Moderately detuned from second mode.
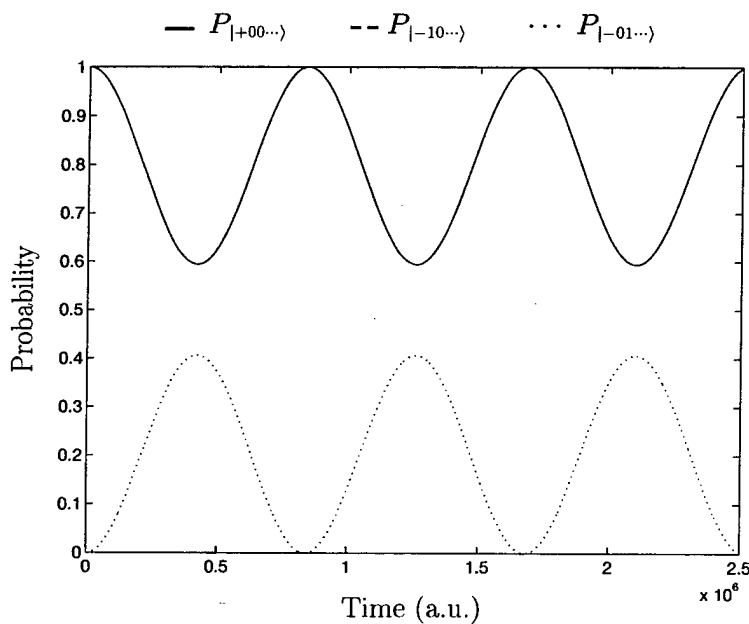
(k) Atom couples more strongly to second mode as detuning is reduced.
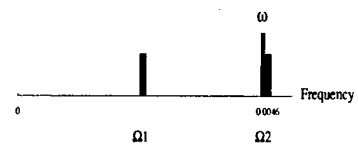
(l) Atom only slightly detuned from the second mode.
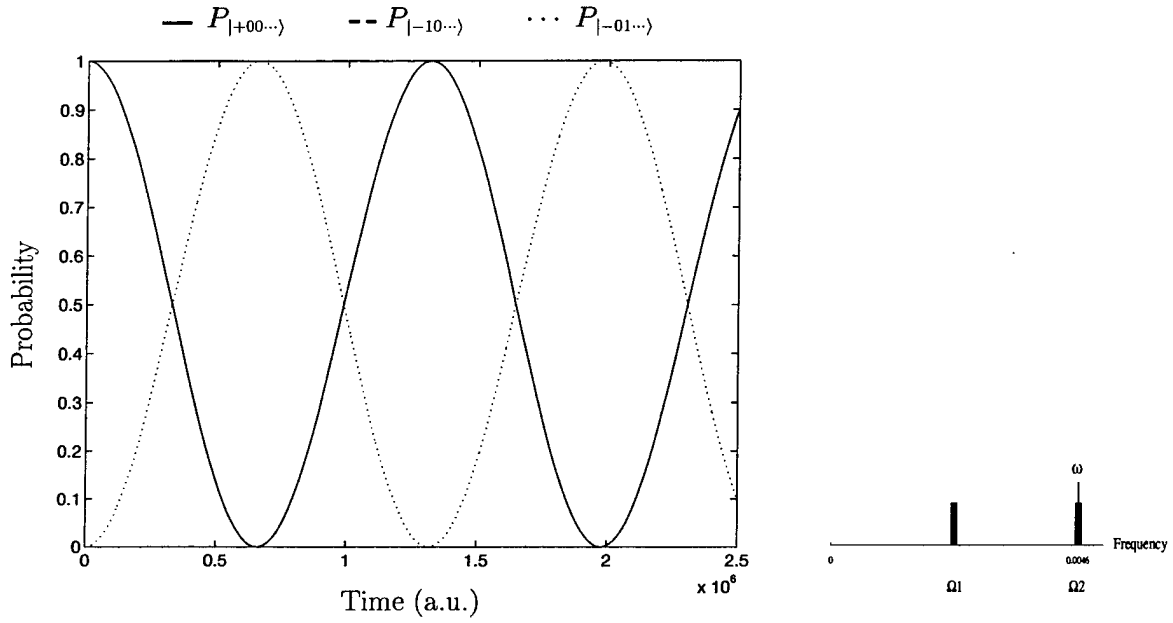
(m) Atom now completely flops through interactions with second cavity mode.

(n) Resonant with second mode

Figure 6.4   (a - n) JCM behavior of a two-mode system with atomic transition frequency tuned from resonant with fundamental mode (a,b) to resonant with second cavity modes (m,n). $L = 10\,\mu m$, $\langle r_{+-} \rangle = 0.01$.
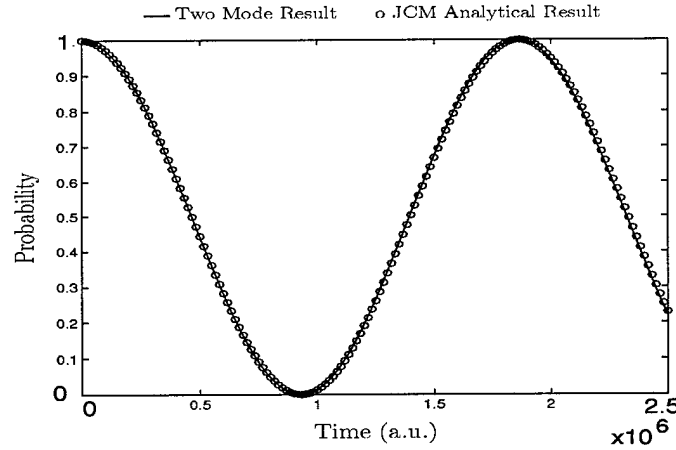
Figure 6.5   Overlay of the two mode calculation of excited state probability with the one mode JCM prediction.

$$= \frac{(0.01)}{2} \sqrt{\frac{2.278 \times 10^{-3}}{(.0795)(1.890 \times 10^5)}} \, (.866)$$

$$= 3.371 \times 10^{-6} \text{ in atomic units.}$$

$$\boxed{\frac{\mathcal{R}_{data}}{2} = 3.369 \times 10^{-6} \text{ au} \qquad \frac{\mathcal{R}_{JCM}}{2} = 3.371 \times 10^{-6} \text{ au}} \qquad (6.1)$$

As expected, the flopping frequency predicted by the JCM is very close to the frequency exhibited by the two mode system. An overlay of the excited-atom state probabilities from the JCM and two mode calculations confirms the result (see Figure 6.5). To place the value of the coupling strength in somewhat of a historical context, the value of $e \, r_{+-}$ used in the investigation of the ammonia maser by Jaynes and Cummings [13] was 1.47×10^{-18} esu $= .5787$ au which corresponds to a coupling strength in this scenario of $g_{maser} = 1.95 \times 10^{-4}$.

However, if the coupling constant is significantly increased, an atom tuned to a given mode can be forced to couple to other modes as well. This is demonstrated most simply for the two mode field by increasing the coupling by a factor of 200 over the Jaynes-Cummings-like case in Figure 6.4a [1]. Figure 6.6a indicates a significant

---

[1]recall the value of the coupling in Figure 6.4a was $r_{+-} = .01$. Calculations indicate that r_{+-} values over 50 are possible for certain high quantum-number states in simple hydrogenic atoms.
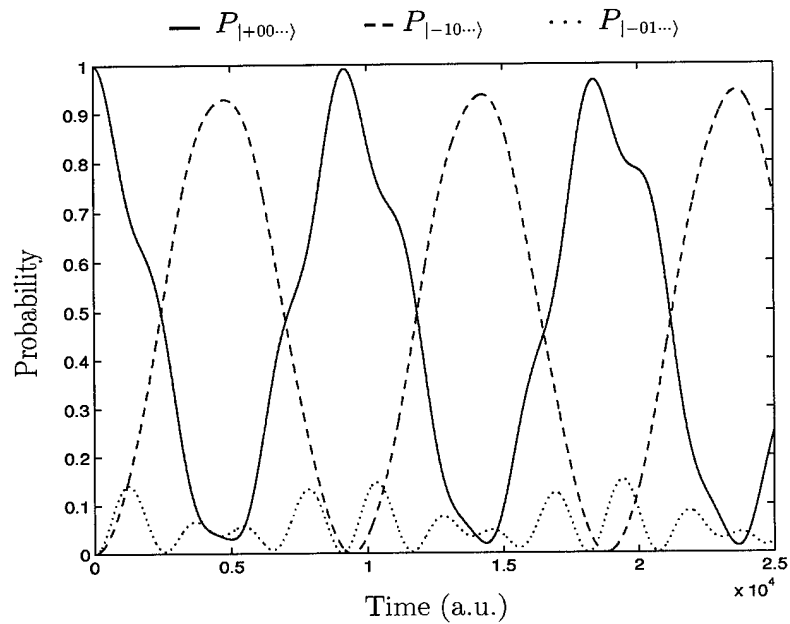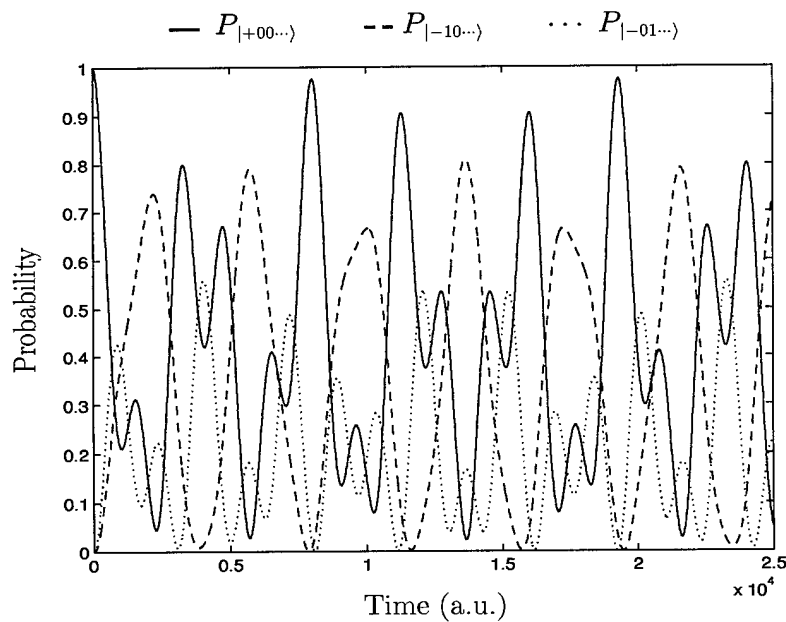
Figure 6.6   Departure from JCM behavior in the strong coupling regime with atomic transition frequency tuned to the fundamental mode: (a) $r_{+-} = 2.0$; (b) $r_{+-} = 5.0$.

departure from the JCM, and complete breakdown of the one mode approximation is achieved in 6.6b for a factor of 500 increase in coupling. It is clear that a single mode field is insufficient to adequately describe the spontaneous emission properties of the atom beyond the weakly coupled limit. In order to demonstrate that the presence of many more modes has a minimal impact on the Jaynes-Cummings behavior of the system, we now consider a field expanded to 100 modes in which the atom may be slightly detuned from a mode near the center of the frequency range, such as the 49th mode. In light of the earlier discussion of the effect of atomic position on the coupling terms in the full Hamiltonian, the atom is placed at a position selected to decouple a minimum of modes. In this case, the atom is placed $\frac{19}{53} \times L$ away from one wall. Since the nth mode has $n+1$ nodes spaced $\frac{1}{n} \times L$ apart, we are assured that the atom is positioned at precisely one node, the 19th node of the 53rd mode. As before, the cavity is small by macroscopic standards, $L = 10 \text{ m}\mu = 1.8897 \times 10^5$ a.u., and the mode spacing is equivalent to the fundamental mode frequency, 2.2278×10^{-3} in atomic frequency units (roughly in the infrared). Once again, recall that the effect of detuning the atom from the field mode in the JCM is to reduce the amplitude of probability exchange and increase the flopping frequency. Figure 6.7a shows the interaction when the atom is perfectly tuned to the mode— clearly the complete flopping observed in the tuned JCM. The analytical results can be overlaid on the solid line to show how closely the JCM flopping is duplicated (see Figure 6.7b). Now the atom is detuned from the mode by 5% of the mode spacing. The detuning causes a reduction in the exchange amplitude as shown in Figure 6.8a, and the overlay of the JCM prediction for this detuning in Figure 6.8b reveals excellent agreement with the numerical results. Now the frequency dial is adjusted to bring the atom to 10% detuning. The amplitudes of exchange are further reduced as expected, and the familiar overlay of the JCM data again indicates the agreement between analytical one mode and numerical 100 mode results (Figure 6.9a,b). As a final check, the atom is detuned to 20% and the probabilities are plotted in Figures 6.10a and 6.10b.

If we now hold the atomic frequency fixed at 10% detuning as in Figure 6.9, we can see how small increases in coupling strength (via r_{+-}) can cause the detuned atom to exchange more completely with the field mode. In Figure 6.11, the amplitude of the exchanges does indeed increase as r_{+-} is raised from .05 to .10, but the overlay plot shows a de-phasing between the JCM prediction and the numerical results. Notice also in Figure 6.12, where $r_{+-} = .15$, that $P_{+00...}$ doesn't quite return to one after the initial decay, and the differences between the analytical and numerical periods of exchange oscillation are increasing. The irregularities that begin to appear in $P_{+00...}$ are amplified for $r_{+-} = .20$ (Figure 6.13). This is a sign that the coupling is strong enough for the surrounding modes to begin to interact with the atom. Finally, a plot of all of the bare state probabilities in Figure 6.14 confirms that this is the case. Thus, in contrast to the JCM, where the coupling strength can be increased *ad infinitum* until the effect of detuning is negligible (in Equations 1.2) and exchange is complete, an upper limit is placed on the degree to which total probability exchange can be recovered in the multiple field mode cavity.

The next section investigates the other extreme of coupling strength and mode spacing, in which a two level system interacts with many closely spaced field modes under the influence of substantially higher coupling strengths.
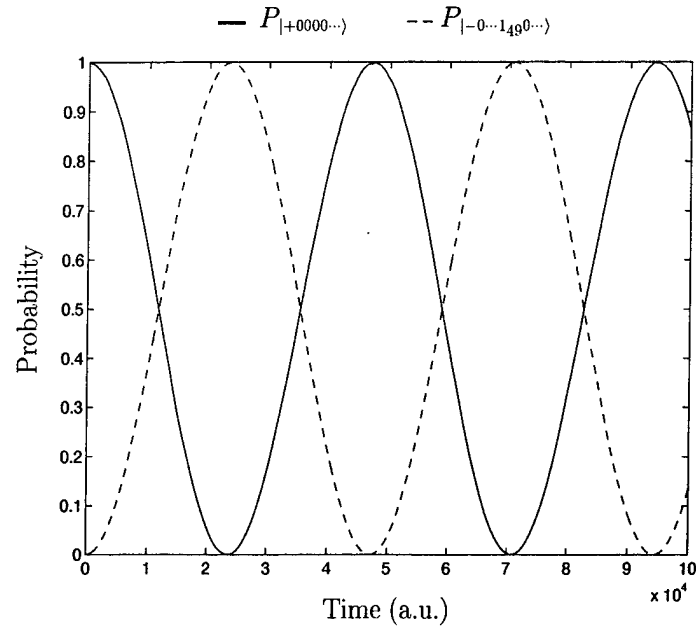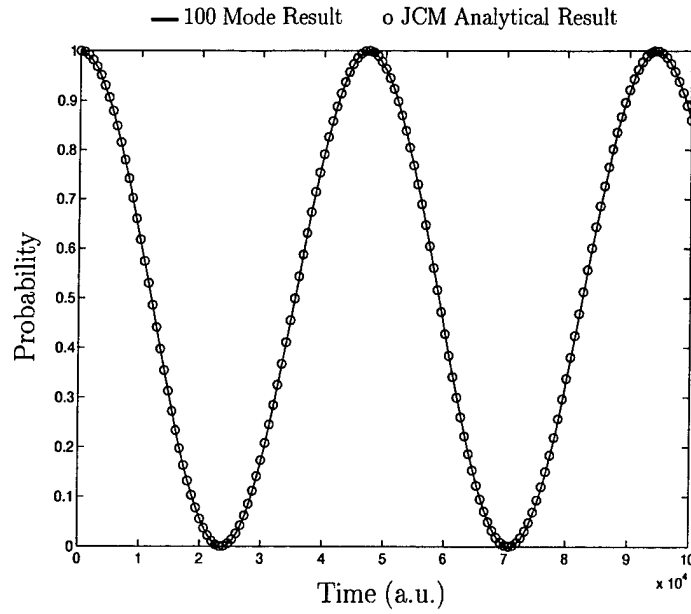
Figure 6.7   (a,b) The atom is resonant with a cavity mode at a frequency of .11163
a.u. in a cavity with mode spacing .00228 a.u. In (b), the analytical
results from the JCM are superimposed on the numerical data.
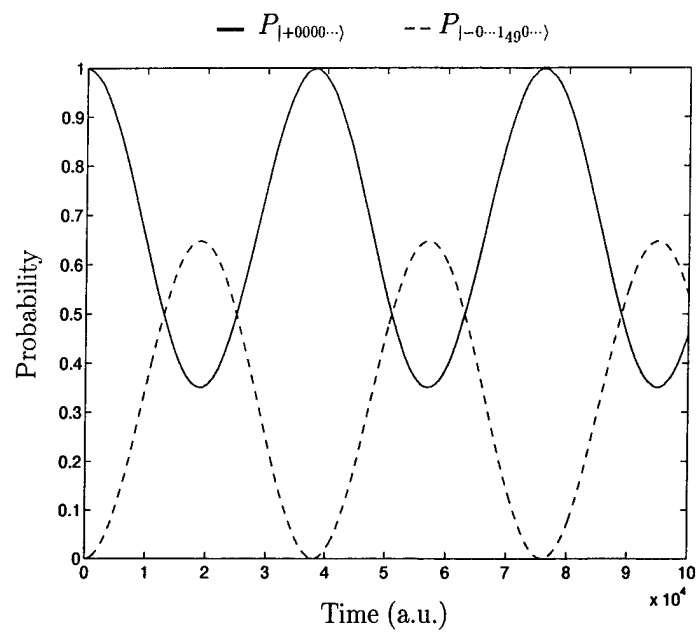
(a)
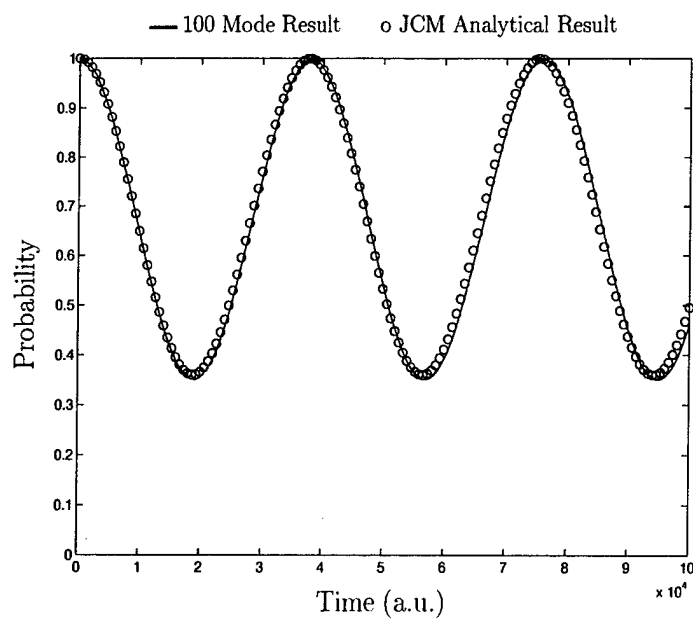
(b)

Figure 6.8   (a,b) Reduction in the amplitudes of probability exchange result from detuning the atom from the field mode. Here the detuning is 5%.
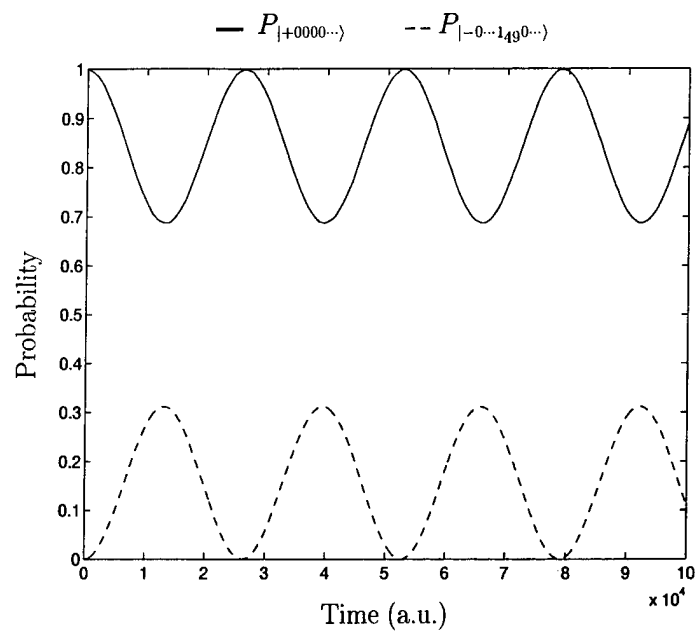
(a)
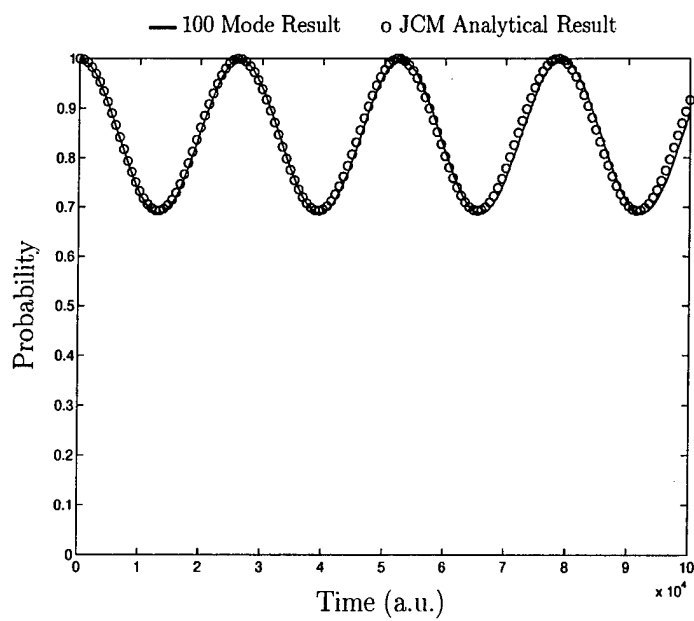
(b)

Figure 6.9   (a) The atom is detuned 10% from the field mode. In (b), the analytical results from the JCM are superimposed on the numerical data.

6-16

$$-P_{|+0000\cdots\rangle} \qquad --P_{|-0\cdots1_{49}0\cdots\rangle}$$

(a)

$$\text{— 100 Mode Result} \qquad \text{o JCM Analytical Result}$$
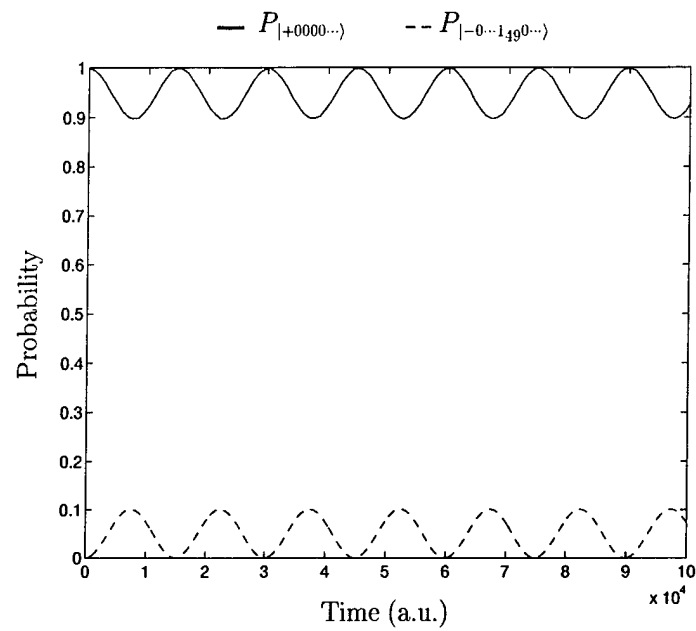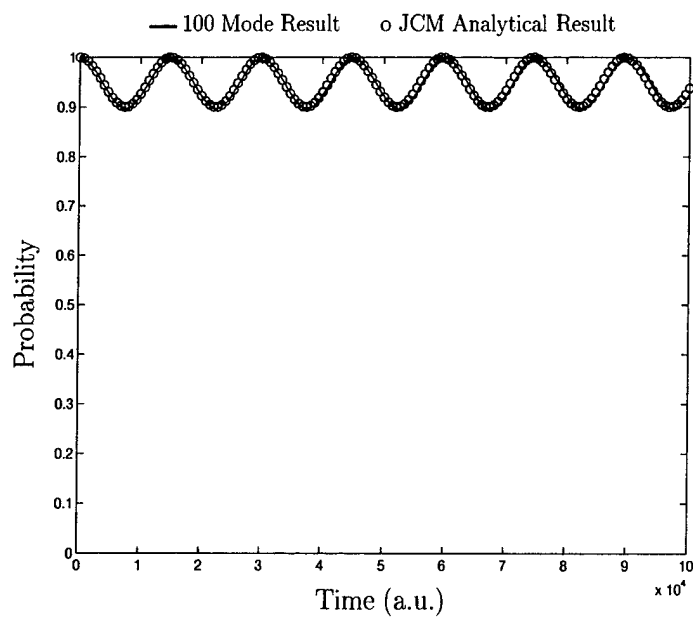
(b)

Figure 6.10   (a) Detuning of 20% of the mode spacing. Again, in (b), the analytical results from the JCM are superimposed on the numerical data.

$— P_{|+0000\cdots\rangle}$ $-- P_{|-0\cdots 1_{49}0\cdots\rangle}$

(a)

— 100 Mode Result   o JCM Analytical Result
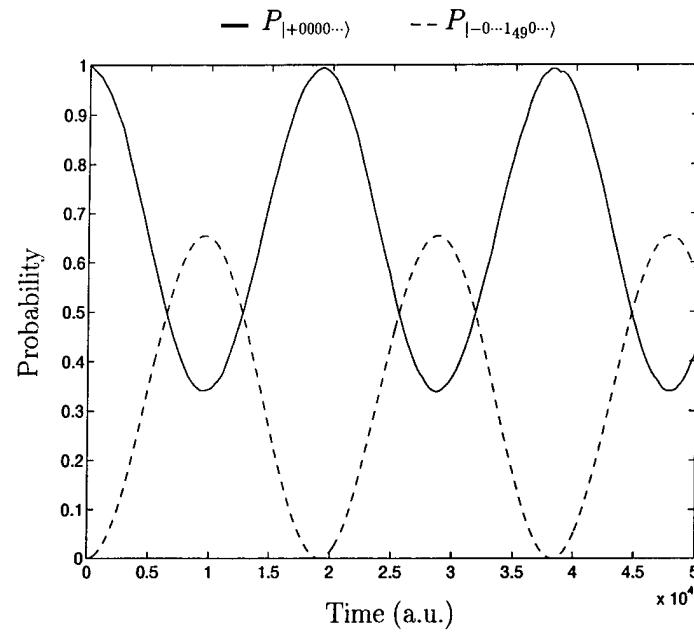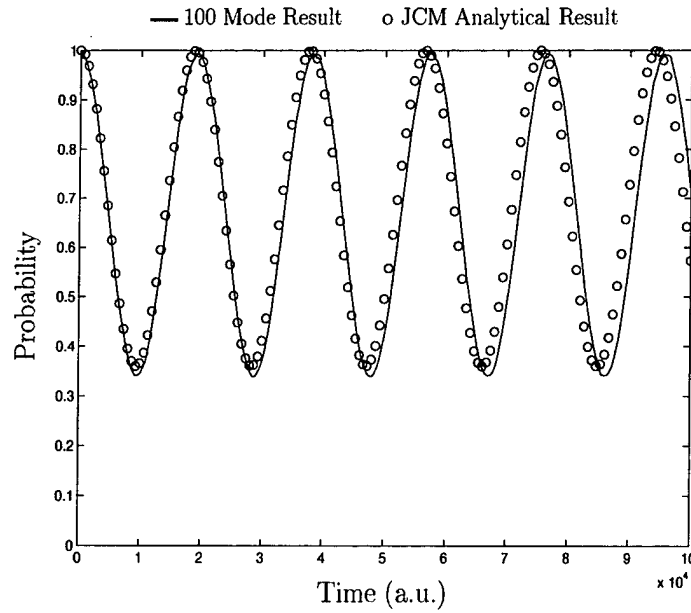
(b)

Figure 6.11   (a,b) The atom is detuned 10% from a field mode in the cavity, and the coupling strength has been doubled through an increase in r_{+-} from .05 to .10. A comparison of the JCM prediction to the numerical results in (b) reveals a subtle difference in the frequencies of the probability oscillations.
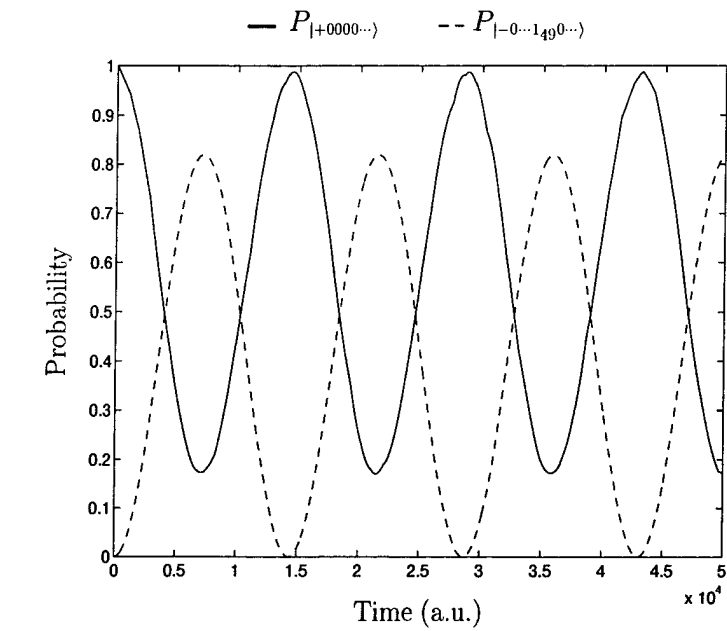
(a)
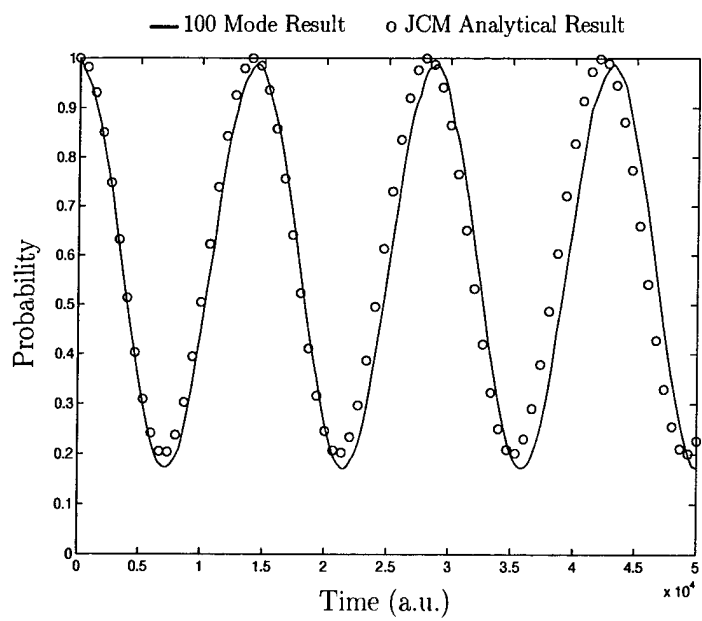
(b)

Figure 6.12   (a,b) Further increase in r_{+-} increases the degree to which energy is exchanged between the atom and field.
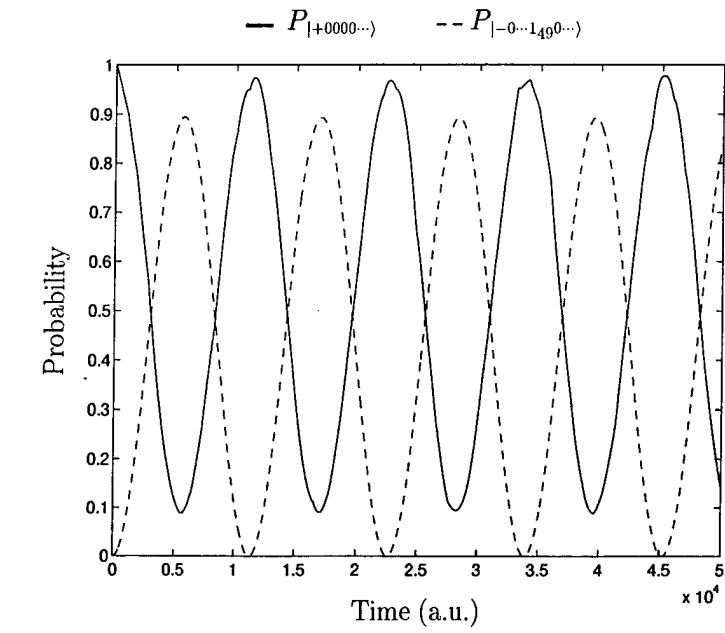
(a)
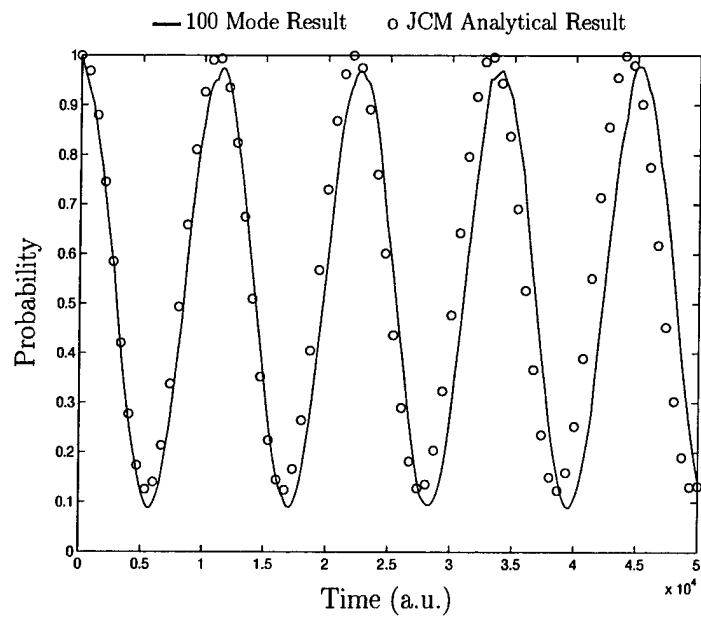
(b)

Figure 6.13   (a) The exchange is further increased, but the irregularities appearing in $P_{+00...}$ indicate coupling to additional modes. (b) A non-trivial difference in the oscillation periods is quite apparent.
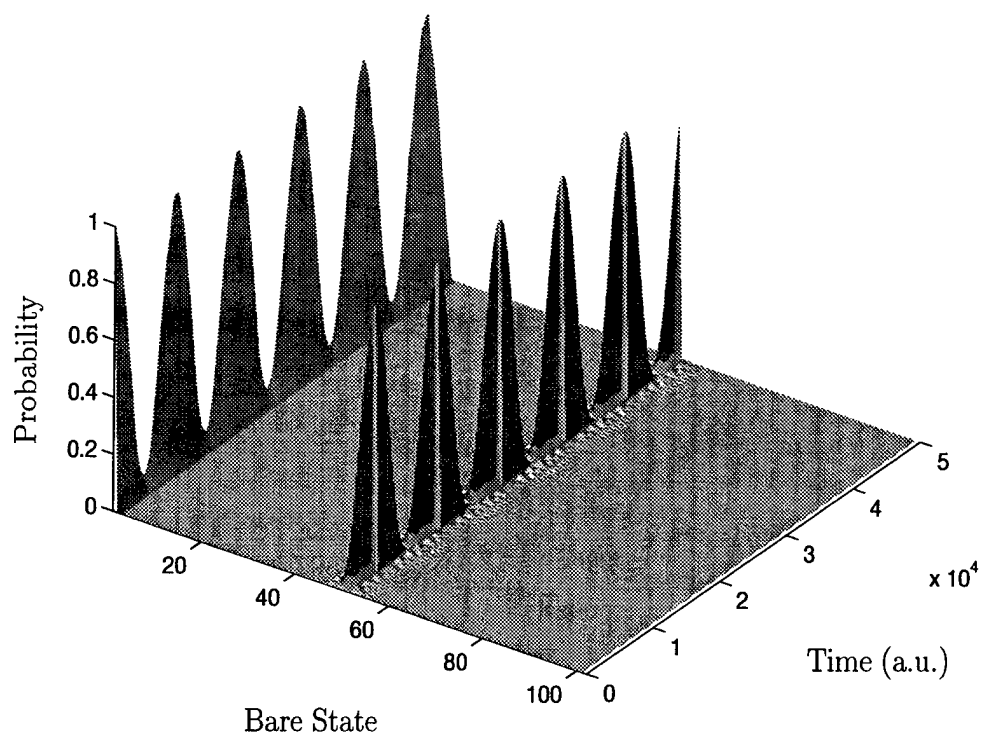
Figure 6.14   The structure along the first bare state describes the evolution of the excited atom state. Here the atom is coupling strongly to the 49th mode in the field, although the ripples near the base of the excited mode probability indicate that coupling to a number of off-resonant modes is non-negligible.

Parameter	Value
# Modes	200
L	1.8897×10^9 au $= 10$ cm
Ω_1	2.2782×10^{-7} au $= 1.5$ GHz
ω	1.1391×10^{-5} au $= 75$ GHz
z	$.6774 \times 10^9$ au $= 3.58$ cm

Table 6.1   Fixed parameter values for the progression from weak coupling to strong coupling. r_{+-} is varied to demonstrate the transition.

6.2 Free Space-Like Spontaneous Emission

The results from Section 6.1 showed that an atom tuned to a single mode in a multimode field exhibited Jaynes-Cummings-like behavior for systems with weak coupling and widely spaced modes. Here, the narrow mode spacing and strong coupling regime is explored. Figure 6.6 hinted at the fact that the inclusion of additional modes for stronger coupling can produce markedly different behavior than is predicted by the JCM. In fact, under the influence of strong coupling with a large number of modes, the atom exhibits spontaneous emission rates similar to those of an excited atom in free space. The excited atom state probability is shown to follow a decay which is approximately exponential in the high coupling regime, and the rate of this decay is compared to the rate of decay predicted for an atom in a one dimensional cavity by the Wigner-Weisskopf theory [17].

To demonstrate this, we begin with an uncoupled system in which the atom is resonant with a mode of the cavity—in this case, the 50th cavity mode—but $g = 0$. Imagine now that there is a dial controlling the value of r_{+-} with which the atom-field interaction may be adjusted. This dial has four settings: the initial zero coupling $r_{+-} = 0.0$ and three higher settings of $r_{+-} = 0.225$, $r_{+-} = 0.450$, and $r_{+-} = 4.500$. By progressing through these settings, we can see how the behavior of the system evolves towards a nearly free space decay of excited atom state probability. The fixed parameters (number of modes, L, Ω_1, ω, and z) for this series of scenarios are summarized in Table 6.1. In Figure 6.15a, the atom is completely uncoupled from

the field. As a result, the atom remains in the excited state. The accompanying plot of the eigenstate amplitudes shows that the system is described entirely by one eigenstate, consistent with the uncoupled scenario. In the next two figures, the coupling has been turned up so that the atom interacts not only with the resonant mode, but also with several off-resonant modes as well. The off-resonant coupling is indicated by the increasingly rapid and erratic probability evolutions. Finally, the last figure in the series, Figure 6.18, demonstrates what appears to be an exponential decay in the $| +000\cdots\rangle$ probability. When all bare state probabilities are plotted as in Figure 6.19, the extent of participation by the large number of modes becomes evident.

The decay from this multimode analysis is compared in Figure 6.20 to the exponential decay predicted by the Wigner-Weisskopf Theory. The presentation of this theory in Meystre and Sargent is based on a three dimensional vacuum of sufficient size that the modes form a continuum. When the theory is appropriately reduced to the one dimensional case through the application of the 1-D mode density and the limitations on the orientations of the dipole moment and field polarization, the predicted decay rate Γ is

$$\Gamma = \frac{|\, e\, r_{+-}\,|^2\, \omega}{c\,\epsilon_0\,\hbar}$$

such that the excited atom state probability falls as $\exp^{-\Gamma t}$.

Using the values of ω and r_{+-} that produced Figure 6.18a, the one dimensional Wigner-Weisskopf theory predicts an exponential free space decay rate of $\Gamma = 2.115 \text{x} 10^{-5}$ in inverse atomic units of time ($8.744 \times 10^{11}\ s^{-1}$), while an exponential fit to the results in Figure 6.18 gave a decay rate of 3.70×10^{-6} in inverse atomic units of time ($1.53 \times 10^{11} s^{-1}$). Figure 6.18a is reproduced in Figure 6.20 with an overlay of the Wigner-Weisskopf prediction for comparison. However, it must be stressed that the behavior of the two level system in the closely spaced mode cavity is not irreversible as in the free space spontaneous decay. The theory of Wigner and Weisskopf predicts a strictly exponential decay and does not allow the possibility of

revivals in the excited atom state probability after a finite period of time. In contrast, these revivals do occur for the quantized system presented here. Figure 6.21 illustrates this probability revival that occurs when the temporal axis of Figure 6.18a is extended by a factor of 100. The revivals are a result of the phasing properties of the eigenstates. Since each eigenstate evolves at its own eigenfrequency, then it is reasonable to expect that there exists times at which groups of the eigenstates are in phase (recall that at $t = 0$ all eigenstates are in phase), causing resurgences in the amplitude of the initial bare state of the system.
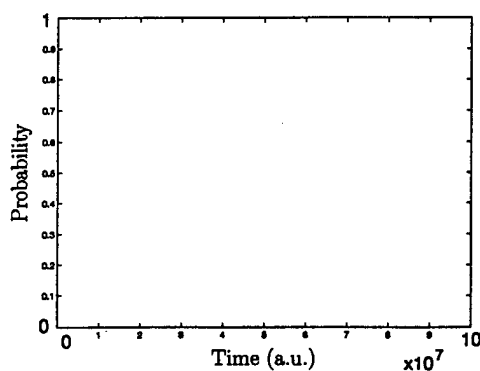
(a) Excited Atom State Probability
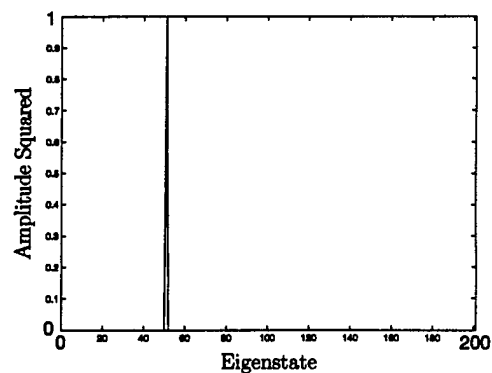
(b) Eigenstate Amplitudes

Figure 6.15 $| + 000 \cdots \rangle$ probability and eigenstate amplitudes for $r_{+-} = 0.0$. The atom is completely uncoupled from the field and remains in the excited state.
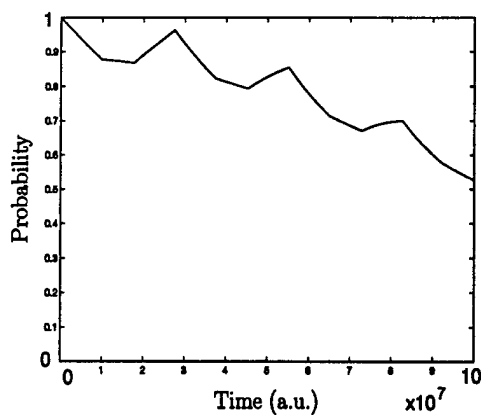
(a) Excited Atom State Probability
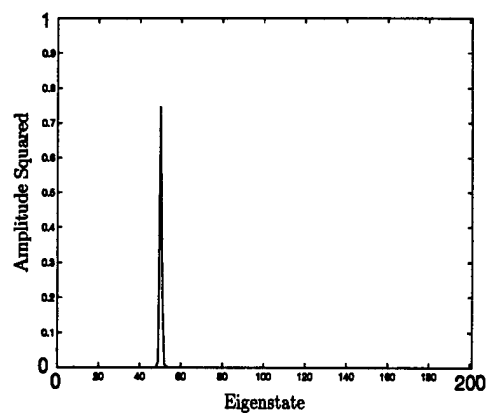
(b) Eigenstate Amplitudes

Figure 6.16 $| + 000 \cdots \rangle$ probability and eigenstate amplitudes for $r_{+-} = 0.225$. Coupling to several off-resonant modes introduces irregularities in the time evolution.
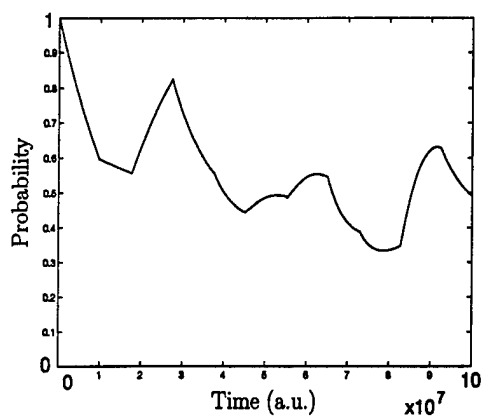
(a) Excited Atom State Probability
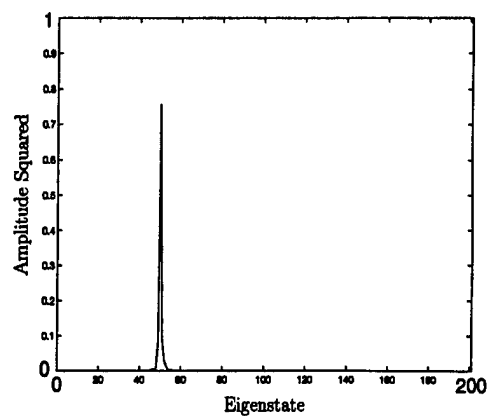
(b) Eigenstate Amplitudes

Figure 6.17 $|+000\cdots\rangle$ probability and eigenstate amplitudes for $r_{+-} = 0.45$.
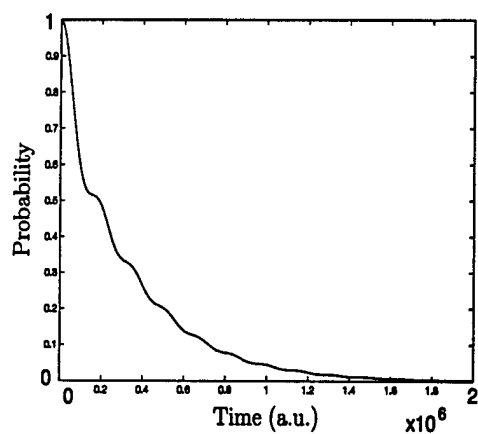
(a) Excited Atom State Probability
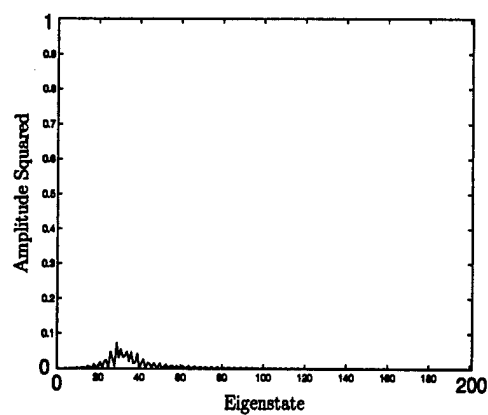
(b) Eigenstate Amplitudes

Figure 6.18 $|+000\cdots\rangle$ probability and eigenstate amplitudes for $r_{+-} = 4.50$.
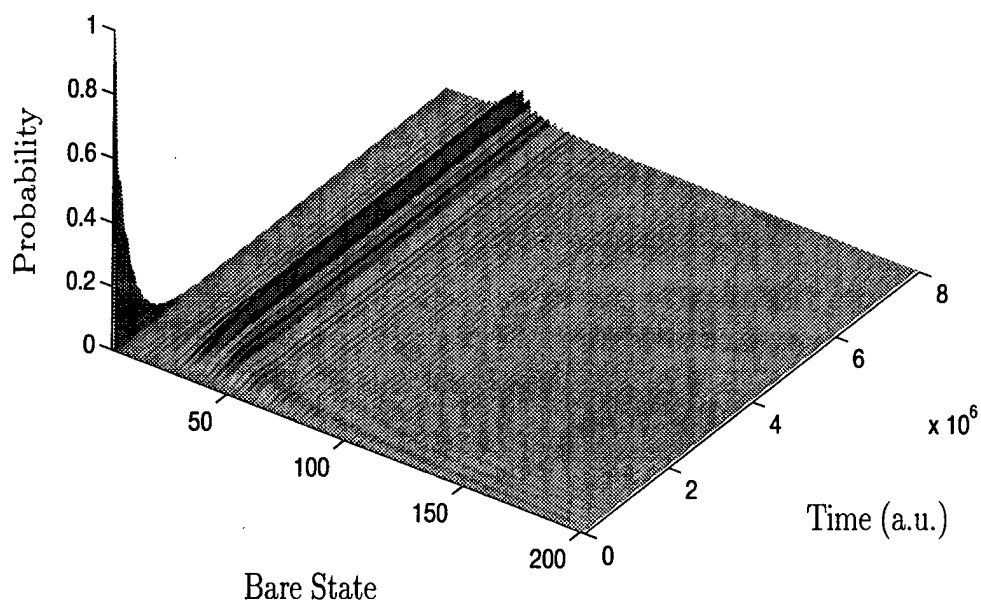
Figure 6.19   Evolution of the bare state probabilities for $r_{+-} = 4.5$. The exponential decay of the excited atom state results from the strong coupling with many modes.
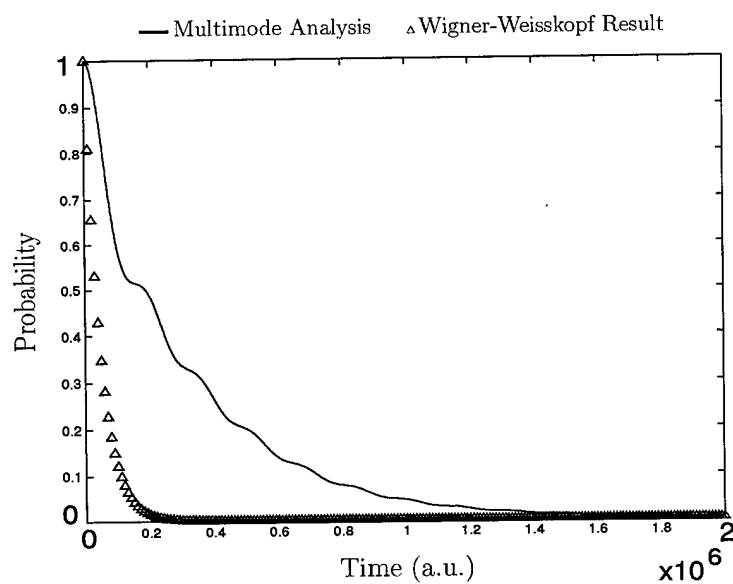
Figure 6.20   Comparison of Wigner-Weisskopf spontaneous emission decay and re-
sults from Figure 6.18a.
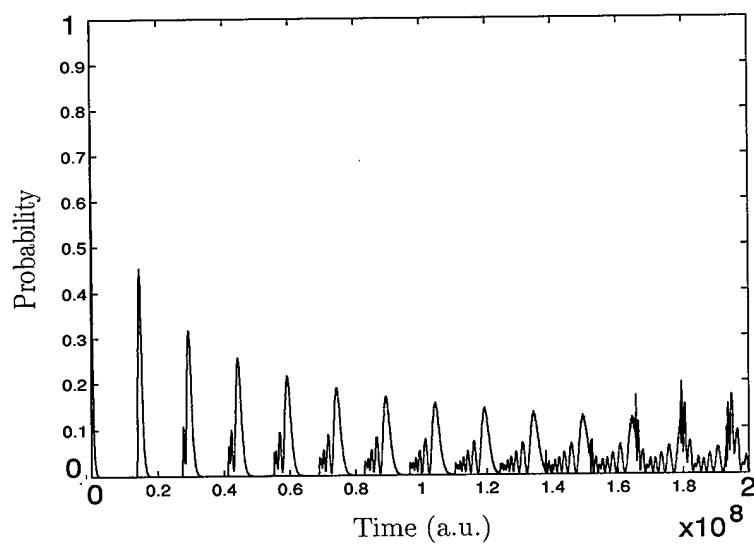
Figure 6.21   Revivals in the excited atom state probability appear when the system
is allowed to evolve for much longer timescales (note the change in the
Time axis from Figure 6.18).
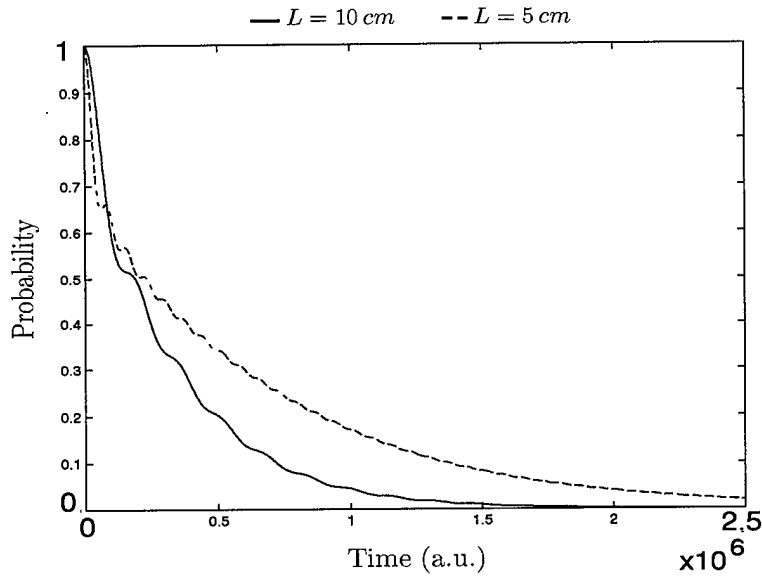
Figure 6.22   The atom decays from its excited state more slowly in the smaller cavity in which the mode spacing is larger.

Now consider the effect of reducing the cavity size on the decay rate. As the cavity size is reduced, the mode spacing becomes larger. An atom tuned near one mode of the cavity becomes more detuned from the rest of the modes. Therefore, if ω and r_{+-} are held fixed while L is reduced, then the atom will couple less to the off-resonant modes and the decay rate should decrease. Figure 6.22 compares the decays of a cavity of length $L = 10cm = 1.8897 \times 10^9$ a.u. (solid line) and the cavity reduced by half to $L = 5cm = 9.4486 \times 10^8$ a.u. (dashed line). The two level system was still positioned at $\frac{19}{53} L$. Even for such a relatively small change in cavity length, the decay is noticeably more gradual for the smaller cavity.

6.3   Unanticipated Effects

The results of the previous two sections illustrated that appropriate choices of the various parameters lead to the recovery of results for two limiting cases in agreement with two independent well-established theories of spontaneous emission. However, the appropriate choices did not reveal themselves easily. In exploring the various combinations of coupling strengths, atomic transition frequencies, cavity

lengths, and matrix truncation points, several regimes were discovered in which the behavior of the coupled atom-field system could be characterized as anomalous. In the first case, a two-level system exhibiting complete Rabi flopping with a mode could be caused to decouple from the mode by drastically increasing the number of modes in the field. As the mode number increased, the amplitude of the probability exchanges decreased as if the atom were being detuned from the field. The same effect also manifested itself in the investigation of free space-like behavior discussed in Section 6.2: the exponential spontaneous decay illustrated in Figure 6.18 became more gradual and eventually evolved to a probability curve which dropped quickly from 1 to a steady state value near .7 when the number of modes was expanded to 1000. It seems likely that this may be a result of an ill-conditioned Hamiltonian matrix, in spite of the fact that the diagonalization routine indicated convergence of the solutions and the conservation of probability and energy were verified (see Appendix A). The first step in addressing this problem will be to investigate the stability of the Hamiltonian under a variety of coupling strengths and matrix sizes, and analyze in depth the method by which the diagonalization is carried out by the LAPACK routine. If numerical instability in the matrix is ruled out as a cause for this behavior, then the conclusion which remains is that this is simply the way the system behaves under those conditions, and the 'problem' so to speak lies in the interpretation of these results.

A similar phenomenon occurred for the Jaynes-Cummings-like system in which the atom was perfectly tuned near a single cavity mode. When the perfectly tuned 100 mode system in Section 6.1 was subjected to gradually increasing coupling strengths through increases in r_{+-}, the spontaneous emission was again suppressed. An increase of a factor of ten in r_{+-} resulted in a 5% reduction in the exchange amplitude. However, recall from Section 6.1 (Figures 6.11-6.13) that the detuned atom behaved in the opposite fashion—the exchanges in the probability plots became more complete as r_{+-} was increased. Several plots illustrating the decoupling effect

on the perfectly tuned atom are included in Appendix C, but no further explanation is provided here for this behavior.

VII. Conclusion

The scale of today's microlaser devices are quickly approaching sub-micron dimensions as military and commercial requirements push the envelop of fabrication technologies. Microcavity structures such as the VCSEL offer the promise of large arrays of highly efficient lasers to meet a variety of needs. The forward progress in making these microcavity lasers more efficient inevitably relies on a thorough understanding of the spontaneous emission processes within. This thesis develops a fully quantum mechanical model of the spontaneous interaction between a two-level atom comprising the gain medium and a multimode electromagnetic field within an optical resonator cavity. The research described in the previous chapters provides a foundation for future exploration into the behavior of

7.1 Quantization of the Atom, Field, and Their Interaction

One of the first steps in addressing a problem quantum mechanically is to develop a Hamiltonian for the system under observation. In this case the system consists of a two-level atom interacting with a multimode electromagnetic field within a one dimensional perfectly conducting cavity. As a simplification, only processes in which a single photon was either emitted from or absorbed by the atom were considered. Chapter 2 describes the steps taken to construct the atomic Hamiltonian. The result is given in Equation 2.7 as

$$\hat{H}_A = \frac{\hbar \omega}{2} \, \hat{\sigma}_z$$

where $\hat{\sigma}_z$ is the Pauli z spin operator. A representation in the orthogonal two level atomic basis $\{\,|+\rangle\,,\,|-\rangle\,\}$ can be taken in which the matrix elements of H_A are

$$\langle\,+\,|\,H_A\,|\,+\,\rangle \;\; = \;\; +\frac{\hbar \omega}{2}$$

$$\langle -\,|\,H_A\,|-\rangle \;=\; -\frac{\hbar\omega}{2}$$

In Chapter 3, the classical wave equation is solved subject to the boundary conditions for a PEC cavity. The expression for the electric and magnetic fields are normalized to the total electromagnetic energy in the cavity and the field is quantized by associating each mode with a quantum mechanically treated harmonic oscillator. The Hamiltonian H_F for the field is

$$\hat{H}_F \;=\; \sum_m \hbar\,\Omega_m\,\hat{a}_m^\dagger \hat{a}_m$$

with photon raising and lowering operators $\hat{a}_m^\dagger$ and $\hat{a}_m$ (Equation 3.20). The basis with which to represent H_F consists of states in which there are no photons in any of the modes or one photon in one of the modes: $\{\,|\,0000\cdots\rangle,\ |\,0\cdots 1_m\,0\cdots\rangle\,\}$. The matrix elements of H_F are

$$\langle\,0000\cdots\,|\,H_F\,|\,0000\cdots\,\rangle \;=\; 0$$
$$\langle\,1_1\,00\cdots\,|\,H_F\,|\,1_1\,00\cdots\,\rangle \;=\; \hbar\,\Omega_1$$
$$\vdots \quad=\quad \vdots$$
$$\langle\,00\cdots 1_m\,|\,H_F\,|\,00\cdots 1_m\,\rangle \;=\; \hbar\,\Omega_m$$

Since H_A and H_F commute, the uncoupled operator H_{A+F} can be constructed:

$$\hat{H}_{A+F} = \frac{\hbar\omega}{2}\,\hat{\sigma}_z + \sum_m \hbar\,\Omega_m\,\hat{a}_m^\dagger \hat{a}_m$$

with an eigenbasis formed from the direct product of the atomic and field bases $\{\,|+\{0\}\rangle,\ |-\{1_s\}\rangle\,\}$. These eigenstates of the uncoupled Hamiltonian H_{A+F} are the bare states of the system and are useful in describing the state of the system before and after transitions have taken place. Chapter 4 treats the interaction between

the atom and the field. The interaction is given by

$$\hat{H}_{int} = \sum_m \hbar \left\{ g_m \hat{a}_m \hat{\sigma}_+ + g_m^* \hat{a}_m^\dagger \hat{\sigma}_- \right\}$$

where $\hat{\sigma}_+$ and $\hat{\sigma}_-$ are the atomic raising and lowering operators and g_m and its conjugate characterize the strength of coupling between the atom and m^{th} mode of the field. In the bare state representation, H_{int} couples the excited atom state, $| + \{0\}\rangle$, to each of the states $| - \{1_s\}\rangle$. The full Hamiltonian is therefore given in Equation 4.9 as

$$
\begin{aligned}
\hat{H}_{tot} &= \hat{H}_A + \hat{H}_F + \hat{H}_{int} \\
&= \frac{\hbar\omega}{2} \hat{\sigma}_z + \sum_m \hbar\,\Omega_m\, \hat{a}_m^\dagger \hat{a}_m + \sum_m \hbar \left\{ g_m \hat{a}_m \hat{\sigma}_+ + g_m^* \hat{a}_m^\dagger \hat{\sigma}_- \right\}
\end{aligned}
$$

The matrix representation of H_{tot} in the bare state basis is non-diagonal when the coupling terms are non-zero, so it is useful to find a basis in which the Hamiltonian is diagonal. The transformation matrix $\mathbb{T}$ that diagonalizes the matrix $\mathbb{H}_{tot}$ consists of elements which are the projections of the eigenbases, or dressed states, onto the bare states. The time evolution of the bare state expansion coefficients of the system wavefunction is then computed using Equation 5.8:

$$\mathbb{C}_B(t) = \mathbb{T}\,\mathbb{U}\,\mathbb{T}^t\,\mathbb{C}_B(0)$$

The probability to find the system in a particular bare state at time t is obtained by squaring the absolute value of its expansion coefficient in $\mathbb{C}_B$. The behavior of the system is analyzed by inspecting the way in which these probabilities evolve in time. The results of these analyses obtained in Chapter 6 for the limiting cases of an atom weakly coupled to a single field mode and an atom strongly coupled to many modes are summarized below. Following Section 7.2, recommendations are provided for future studies beyond the scope of this project.

7.2 Overview of the Results

7.2.1 Jaynes-Cummings Limit.

In the limit of weak coupling, an atom in a two mode field was shown to behave in a manner consistent with the Jaynes-Cummings Model, an analytical model which describes the interaction of a two level atomic system with a single field mode. The presence of additional modes was shown to have minimal impact for an atom near resonance with and weakly coupled to one mode, but increases in the coupling strengths through r_{+-} caused the atom to begin coupling to off-resonant modes.

7.2.2 Free Space-Like Behavior.

When the two level atom was placed in a field of many tightly spaced modes and the dipole matrix element proportional to r_{+-} was increased by a factor of $\sim$100 over those used in the Jaynes-Cummings limit, the atom coupled to a large number of modes and decayed exponentially to the lower state. The decay rate exhibited by the atom was comparable to the rate calculated using the Wigner-Weisskopf Theory of spontaneous emission for an atom in free space: 3.70×10^{-6} in inverse atomic units of time ($1.53 \times 10^{11} s^{-1}$) from a fit of the data compared to the Wigner-Weisskopf result of 2.115×10^{-5} in inverse atomic units of time ($8.744 \times 10^{11} s^{-1}$). Investigation of the effect of changing the cavity size indicated that reduction in L caused a decrease in decay rate, a result attributable to the increase in mode spacing and therefore decrease in the effective coupling of the atom the modes in the cavity.

7.2.3 Anomalous Results.

In the pursuit of these investigations, several regimes of parameter values produced results which were counterintuitive and without explanation. In one regime, it was discovered that the addition of a significant number (500 - 800) of modes to a system which clearly exhibited either Jaynes-Cummings or free space-like behavior caused that behavior to change drastically. In both cases, the atom in the presence of the expanded field tended to remain almost to the point of exclusion in the excited state. It can be seen by looking at the

form of the Hamiltonian matrix that it is possible to make the matrix large enough through the addition of modes, and hence, states, that the ratio of the largest to smallest elements can become quite large ($\sim 10^4 - 10^5$). This indicates a rather ill-conditioned matrix which may have caused numerical instabilities in the diagonalization of the Hamiltonian. Without an in-depth analysis of the diagonalization methods used by the LAPACK routine employed, it is difficult to draw any concrete conclusions regarding possible connections between the anomalous results and the condition number of the system. In another regime, a moderate increase in coupling strengths could cause a suppression of decays out of the excited atomic state for an atom perfectly tuned to a cavity mode and previously exhibiting complete probability exchanges. As shown in Section 6.1, however, the detuned atom did not experience this suppression. This phenomenon is not easily attributed to the conditioning of the matrix, and no explanation can be offered here.

7.3 Recommendations for Future Study

As alluded to in the abstract, the research detailed in this thesis carries an exploratory element to it. Along the way I've encountered more than a few dead ends, numerous dead ends that turned out not-so-dead, and a great many questions as yet without answers. It is in that context that I provide my recommendations for possible future studies for which this research may in part serve as a foundation.

1. The anomalies referred to in the previous section need to be investigated in depth. While it is quite possible that numerical instabilities are in part to blame for the behavior of the large matrices, the inhibition of spontaneous decay due to coupling increases for a perfectly tuned atom manifests itself in what appear to be stable systems.

2. In this analysis, the simplification was made to treat the cavity as a perfect conductor. However, the cavities within VCSELs and other microcavity lasers are by no means perfect conductors. A natural complement to this research is

an exploration of the imperfectly conducting, or lossy, cavity. In more realistic treatments of microcavities, there is a certain penetration of the radiation into the walls of the resonator, and for all practical purposes it is necessary to artificially introduce loss at one end to obtain an output for the photons oscillating within. One key implication of a lossy cavity is the introduction of a finite linewidth to the emitted radiation. The details of integrating this linewidth into the Hamiltonian are to be worked out, but it may be plausible to assume that each cavity mode with its inherent lineshape can be discretized into a collection of tightly packed modes of infinitesimal linewidths whose amplitudes follow a Lorentzian shape. The behavior of an atom coupled to a single longitudinal mode could be ascertained by examining the interaction of the atom with the modes under the Lorentzian profile.

3. A related offshoot addresses the problem of the dispersive cavity. Instead of the atom in a vacuum cavity, the gain medium should be modeled to more accurately reflect the characteristic of the semiconductor materials used in laser diodes. This has several implications. First, the behavior of the medium itself must be addressed. Secondly, the dispersive nature of the semiconductor materials which fill the cavity has an impact on the mode structure of the electromagnetic field. The two level system modeled here more accurately describes the quantum dot structures which are yet another area of current interest in microcavity edge emitting and surface emitting lasers.

4. In its infancy, this research was intended to explore the three dimensional cubic cavity. In order to simplify some of the issues related to the coupling terms, the problem evolved into the one dimensional cavity addressed here.

All of these recommendations are based on a need to actively pursue an understanding of the spontaneous processes in microcavity devices. This thesis constitutes a first step towards addressing the interactions between the gain medium and the multimode field that influence laser efficiencies at an atomic level. Ultimately, this

research complements the existing body of knowledge employed by Air Force scientists and Research Planners in improving current microcavity technologies and assessing the direction of tomorrow's laser programs.

Appendix A. Verification of the FORTRAN 90 Code

One of the most important steps in carrying out a numerical analysis of a complex problem such as this is to verify that the computer code used produces valid results. This is, of course, a misleading statement—the analyses are usually employed to address problems for which 'valid' results are the unknowns. However, it is typically the case that exploratory research is built upon prior results in which there is sufficiently high confidence. This appendix describes the steps that were taken to validate the FORTRAN 90 code in Appendix B to as high a degree as possible. The process of validation involved certain checks described briefly as follows:

Does the code compute the cavity mode frequencies correctly?

The mode frequencies were computed manually on a PC using a simple 16-bit precision function created in *Mathematica* for a variety of cavity lengths. These were used as a baseline for comparison with the results from the code. The purpose was to catch gross errors in the algorithms versus compare the numerical accuracy of the machines used. Quite obviously, the capabilities of the SGI Origin 2000 for producing high accuracy, high precision results heavily outweigh the Pentium 66. However, a comparison showed that the results agreed to seven or eight significant digits.

Does the code construct the full Hamiltonian correctly?

Once again, the objective was to catch errors in the way the matrix elements were computed. Sample matrices were generated by another *Mathematica* routine and compared to the results from the code, then both of these were checked against a matrix generated by hand. In matrices as large as 100×100, the diagonals and coupling terms sampled at random compared as favorably with the code as the frequencies above.

Are the results from the diagonalization routine reliable?

To verify the performance of the LAPACK diagonalization routine and its interface with my code, the eigenvalues and eigenvectors of 1, 2, 5, 20, and 100 mode systems were compared with those generated by the built-in Eigensystem function in *Mathematica.* An additional self-consistency check is provided in the code: for each run, a routine computes the product of the eigenvector matrix with its transpose. Since these matrices perform unitary transformations of the Hamiltonian, the product $\mathbb{T}^T\mathbb{T}$ should result in the identity matrix. One of the outputs of the code is a sum of the elements of this product which in all cases should produce the total number of columns or rows (an $n \times n$ identity matrix logically has n entries of 1 for its diagonals). This sum was confirmed following each run.

Does the code evolve the system in time properly?

Part of this verification is provided as the body of Section 6.1. The code results for 1, 2, 5, and 20 mode systems were overlaid on the analytical (for the 1 mode system) and *Mathematica* results with no discernible differences in the plots.

Is probability conserved for the system as it evolves in time?

It is a basic necessity that at all points in time the total probability for observing the system in one of its states is 1. In order to confirm this, the probability amplitudes for all states must be squared and summed for all times t. One of the routines in the code calculates these sums for every time sampled and writes them to a file. In all cases, the sum of the probabilities was 1 to within 5 significant digits.

Is energy conserved for the system as it evolves in time?

Since there is no loss mechanism built into the system, it is expected that a cavity which contains a specified total energy at time $t = 0$ should have that same total energy at each time step thereafter. A routine was built into the code to compute the total energy in the system for each iteration over the time variable. The results of this were then written to yet another file. Because the analyses all started with

the system in the excited atom state, the initial energy in the cavity was the energy of the excited atomic state: $\frac{\hbar\omega}{2}$. The results written to the energy conservation file consistently demonstrated at every time step that the total energy in the cavity remained $\frac{\hbar\omega}{2}$.

Can the original full Hamiltonian be reconstructed using the eigenvectors and eigenvalues from the diagonalizing routine?

The most compelling test of the diagonalizing routine is the reconstruction of the original full Hamiltonian from the diagonal Hamiltonian and the transformation matrix both obtained from the LAPACK routine. A comparison of the reconstructed and original Hamiltonians provides a figure of merit Υ in assessing the accuracy of the LAPACK solutions. The reconstructed Hamiltonian is found from

$$\tilde{\mathbb{H}}_{tot} = \mathbb{T}\,\mathbb{H}'\,\mathbb{T}^{\mathbf{T}}$$

where $\mathbb{H}'$ is the diagonalized dressed state (diagonal) representation of the Hamiltonian. $\tilde{\mathbb{H}}_{tot}$ can then be subtracted element-wise from $\mathbb{H}_{tot}$, the differences squared, then the square root of the sum of the resulting squares computed, and finally normalized to the matrix size by dividing by n^2. For the a sampling of the matrices evaluated in this thesis, the values of Υ fell around 10^{-13}. In other words, the original and reconstructed Hamiltonians agreed element by element out to around the tenth or eleventh digit.

Appendix B. Source Code

```
!-----------------------------------------------------------------------------------------
!       Main Program:
!
!       This program computes the time evolution of the bare states for a
!       quantized coupled atom-field system in a one-dimensional perfect electrically
!       conducting cavity.  The atomic system is quantized as a 2-level system and the
!       field is comprised of from 1 to n normal modes, where n can be as large as
!       computational resources will allow.  A coupled Hamiltonian is created based
!       on user input parameters, then is diagonalized using a public domain
!       LAPACK routine.  The eigenvalues and eigenvectors are then used with
!       the user-specified initial state of the system to determine the time
!       evolution in terms of the bare states.  The components are:
!
!               decs_module - Module containing the global declarations
!               funct_module - Module containing several common functions
!               readin1_1d - Subroutine to read the user specified parameter values
!               fullham_1d - Subroutine to construct the full Hamiltonian and
!                               diagonalize using the LAPACK routine dsyevd.for
!               timedev_1d - Subroutine to compute the time evolution of the
!                               system in the bare state basis
!
!-----------------------------------------------------------------------------------------
        PROGRAM main1D
        USE     decs_module
        USE funct_module
        IMPLICIT NONE

        CALL readin_1d
        CALL fullham_1d
        CALL timedev_1d

        END
```

```
!-------------------------------------------------------------------------
!       Modules:
!
!       The following two modules are structures which contain information
!       or functions which are global entities.  The module decs_module
!       contains the global declarations, while funct_module contains
!       two functions used by several subroutines.
!-------------------------------------------------------------------------
        MODULE decs_module
        IMPLICIT NONE
!       Constants:
                DOUBLE PRECISION c
                DOUBLE PRECISION pi
                DOUBLE PRECISION eps0
                DOUBLE PRECISION mu0
                DOUBLE PRECISION me
                DOUBLE PRECISION hbar
                DOUBLE PRECISION e
  ! Values from Bransden&Joachain
                PARAMETER (c    = 137.036D0             )      !  1/alpha
                PARAMETER (pi   = 3.14159265359D0       )
                PARAMETER (hbar = 1.0D0                 )
                PARAMETER (eps0 = 0.07957747155D0       )      !  1/4Pi
                PARAMETER (mu0  = 6.69176247674D-4      )      !  4Pi/c^2
                PARAMETER (e    = 1.0D0                 )
                PARAMETER (me   = 1.0D0                 )
!       Array-related declarations:
                DOUBLE PRECISION, ALLOCATABLE :: a_f_array(:,:)
                DOUBLE PRECISION, ALLOCATABLE :: intarray(:,:)
                DOUBLE PRECISION, ALLOCATABLE :: fullarray(:,:)
                DOUBLE PRECISION, ALLOCATABLE :: tempfull(:,:)
                DOUBLE PRECISION, ALLOCATABLE :: afreqarray(:)
                DOUBLE PRECISION, ALLOCATABLE :: ffreqarray(:)
                DOUBLE PRECISION, ALLOCATABLE :: phot_numarray(:)
                DOUBLE PRECISION, ALLOCATABLE :: gvector(:)
                DOUBLE PRECISION, ALLOCATABLE :: eigenvalues(:)
                DOUBLE PRECISION, ALLOCATABLE :: bareinitial(:)

                INTEGER              imax
                INTEGER              iterate
                INTEGER              countmax
                CHARACTER(2)         amethod
                CHARACTER(2)         fmethod
                CHARACTER(2)         gmethod
                DOUBLE PRECISION     gstart
                DOUBLE PRECISION     testval
                INTEGER              lworkfactor
!       Atomic system declarations:
                DOUBLE PRECISION rba
                DOUBLE PRECISION a_freqhalf
                DOUBLE PRECISION z
!       Field declarations:
                INTEGER m            !  mode_number
                INTEGER mmax         !  total number of modes
                INTEGER phot_num     !  number of photons
                DOUBLE PRECISION l   !  cavity dimensions
!       Initial conditions:
                INTEGER istate       !  specifies the initial state of atom
!       Time-development declarations:
                DOUBLE PRECISION tmax
                DOUBLE PRECISION tmin
                DOUBLE PRECISION tstep
        END MODULE decs_module

!       Module containing common functions for field frequencies
!       and mode spatial distributions
        MODULE funct_module
        USE decs_module
        IMPLICIT NONE

        CONTAINS
!       Function to calculate the radiation frequencies
                DOUBLE PRECISION FUNCTION r_freq (mode,dim)
                        INTEGER mode                 !  mode numbers
```

```fortran
            DOUBLE PRECISION dim                !  cavity dimensions
            r_freq = c*pi*mode/dim
            RETURN
        END FUNCTION
!   Function to calculate the value of the field spatial
!   distribution at a given location for a given mode
    DOUBLE PRECISION FUNCTION g_spatial(mode,dim,pos)
            INTEGER mode                  !  mode numbers
            DOUBLE PRECISION dim          !  cavity dimensions
            DOUBLE PRECISION pos          !  atom position in cavity

            g_spatial = SIN(mode * pi * pos / dim)

            RETURN

            END FUNCTION
    END MODULE funct_module
```

```
!-----------------------------------------------------------------------
!        Subroutine readin_1d:
!
!        Opens a stream to the file 'microcav.dat' and reads
!        the user input, assigning values to the appropriate variables.
!        The conversions from MKS to atomic units occur in this
!        subroutine where necessary.
!
!-----------------------------------------------------------------------
         SUBROUTINE readin_1d
         USE decs_module          !  declarations
         USE funct_module         !  common functions
         IMPLICIT NONE
         INTEGER i, j             !  iterators
         CHARACTER(1) fgheader    !  header letter at top of f_or_g.inp file
         CHARACTER(13) dummy      !  dummy for reading in (skipping over) strings
         CHARACTER(8) day         !  used for date stamp in message file
         CHARACTER(10) clock      !  used for time stamp in message file
         DOUBLE PRECISION lmicrons  !  accepts input cavity length
         in microns
         DOUBLE PRECISION zmicrons  !  input position in microns
         DOUBLE PRECISION atomic    !  input transition wavelength/frequency depending on amethod
         DOUBLE PRECISION fund_freq !  sets fundamental mode frequency if fmethod is manual
         DOUBLE PRECISION step      !  used for creating the gvector array of coupling constants
         DOUBLE PRECISION tempwave  !  temporary holder for read-in field wavelengths/frequencies
         DOUBLE PRECISION tempg     !  temporary holder for read-in g values
!        Open a message file for run-time error statements and other
!        miscellaneous junk (time/date stamped)
         OPEN (unit=7, file='messages.dat',status='replace')
         CALL DATE_AND_TIME(DATE=day,TIME=clock)
         WRITE (7, 1) day,clock
         WRITE (7, '("Messages:")')
!        Open the input file
         OPEN (unit=8, file='micro_1d.inp',status='old')
!        Read in the values
         READ(8,15) amethod
         READ(8,15) fmethod
         READ(8,15) gmethod
         READ(8,30) gstart
         READ(8,10) dummy
         READ(8,30) atomic
         READ(8,30) rba
         READ(8,10) dummy
         READ(8,30) lmicrons
         READ(8,30) zmicrons
         READ(8,20) mmax
         READ(8,20) phot_num
         READ(8,10) dummy
         READ(8,20) iterate
         READ(8,10) dummy
         READ(8,20) istate
         READ(8,35) tmin
         READ(8,35) tmax
         READ(8,35) tstep
         READ(8,35) testval
         READ(8,20) lworkfactor
!        Initialization of input-dependent quantities
         imax = mmax+1            !  array dimensions
!        Convert from input microns to the a.u. used internally
         l=lmicrons*18897.26877774
         z=zmicrons*18897.26877774
!        Flag to make sure 2-level system is in the cavity!
         IF(z.GT.1 .AND. gmethod.EQ.'a') THEN
                    WRITE(7,'("micro_1d.in Error -- Verify z<1")')
                    STOP
         END IF
!        Array initialization block
         ALLOCATE(intarray(imax,imax))
         ALLOCATE(a_f_array(imax,imax))
         ALLOCATE(fullarray(imax,imax))
         ALLOCATE(tempfull(imax,imax))
         ALLOCATE(afreqarray(iterate))
```

```fortran
        ALLOCATE(ffreqarray(mmax))
        ALLOCATE(eigenvalues(imax))
        ALLOCATE(bareinitial(imax))
        ALLOCATE(phot_numarray(imax))
        ALLOCATE(gvector(imax))
        intarray = 0.0
        a_f_array = 0.0          ! matrices
        fullarray = 0.0
        eigenvalues = 0.0        ! vectors
        bareinitial = 0.0
!       This block calculates atomic frequencies based on input file values
        SELECT CASE(amethod)
                CASE('AW','aw')   ! Single frequency is calculated based on atomic wavelength
                                  ! The factor 0.0455633 converts from micron wavelengths
                                  ! to a.u. frequencies
                        afreqarray(1) =   0.0455633/atomic
                CASE('AF','af')   ! A single frequency is read in directly from micro_1d.inp
                        afreqarray(1) =   atomic

                CASE('M','m')     ! Creates array of length 'iterate' of atomic frequencies
                                  ! The values range from 0 to twice the fundamental frequency
                        fund_freq = r_freq(1,1)
                        afreqarray(1)=fund_freq
                        IF(iterate.GT.1) THEN
                                afreqarray(1)=0.0
                                step = 2*fund_freq/(iterate-1)
                                DO i=2,iterate
                                        afreqarray(i)=afreqarray(i-1)+step
                                END DO
                        END IF
        END SELECT
!       Create an array of field frequencies using either the r_freq function
!       or read-in wavelength values from f_or_g.in
        ffreqarray = 0.0d0
        SELECT CASE(fmethod)
                CASE('AA','aa')              ! calculate field resonant frequencies
                        DO i=1,mmax
                                ffreqarray(i) = r_freq(i,1)
                        END DO
                CASE('MW','mw')              ! read in field wavelengths
                        IF(gmethod.EQ.'a1' .OR. gmethod.EQ.'m') THEN
                                OPEN(unit=10,action='READ',file='f_or_g.inp',status='old')
                                READ(10,15) fgheader
                                IF(fgheader.EQ.'f') THEN
                                        tempwave=1.0d0
                                        DO i=1,mmax
                                                READ(10,30) tempwave
                                                ffreqarray(i) = 0.0455633/tempwave
                                        END DO
                                ELSE
                                        WRITE(7,'("f_or_g.in -- Verify header matches data")')
                                        STOP
                                END IF
                        ELSE
                                WRITE(7,'("micro_1d.in -- gmethod must not be &
                                & mf {i.e. read wavelengths OR g values from file, not both}")')
                                STOP
                        END IF
                CASE('MF','mf')                 ! read in field frequencies
                        IF(gmethod.EQ.'a1' .OR. gmethod.EQ.'m') THEN
                                OPEN(unit=10,action='READ',file='f_or_g.inp',status='old')
                                READ(10,15) fgheader
                                IF(fgheader.EQ.'f') THEN
                                        tempwave=1.0d0
                                        DO i=1,mmax
                                                READ(10,30) ffreqarray(i)
                                        END DO
                                ELSE
                                        WRITE(7,'("f_or_g.in -- Verify header matches data")')
                                        STOP
                                END IF
                        ELSE
                                WRITE(7,'("micro_1d.in -- gmethod must not be &
```

```
                                          &  mf {i.e. read wavelengths OR g values from file, not both}")')
                                          STOP
                          END IF
                END SELECT

!       The array phot_numarray holds the number of photons in the field
        phot_numarray = phot_num
!       This block initializes the array holding the values of g for each
!       mode which are artificially reduced for increasing mode number
!       arithmetically from gstart down to 0.  Note that gvector(1) is always
!       set to 0 since this corresponds to a dipole forbidden +/+ atomic
!       transition
        SELECT CASE(gmethod)
                CASE('M1','m1','A','a','A2','a2')    !  makes all g values = 1.0; if 'a', gvector
                                                     !  will be overwritten in sub fullham_1d
                        gvector = 1.0d0
                        gvector(1) = 0.0d0
                CASE('MF','mf')                      !  read in g values
                        gvector(1) = 0.0
                        IF(fmethod.EQ.'AA' .OR. fmethod.EQ.'aa') THEN
                                OPEN(unit=10,action='READ',file='f_or_g.inp',status='old')
                                READ(10,15) fgheader
                                IF(fgheader.EQ.'g') THEN
                                        DO i=1,mmax
                                                READ(10,30) tempg
                                                gvector(i+1) = tempg
                                        END DO
                                ELSE
                                        WRITE(7,'("f_or_g.in -- Verify header matches data")')
                                        STOP
                                END IF
                        ELSE
                                WRITE(7,'("micro_1d.in -- gmethod must not be &
                                &  mf {i.e. read wavelengths OR g values from file, not both}")')
                                STOP
                        END IF
                CASE('A1','a1')                              !  calculate g values from field frequencies
                        gvector(1) = 0.0
                        DO i=1, mmax
                                gvector(i+1) = SQRT(ffreqarray(i))
                        END DO
        END SELECT

!       Initialize the bare state expansion coefficients
        IF(istate.GT.imax) THEN
                WRITE(7,'("micro_1d.in Error -- Verify istate <{mmax+2}")')
                STOP
        ELSE
                bareinitial(istate) = 1.0
        END IF

1       FORMAT('Date/Time: ',a9,1X,a10)
5       FORMAT(a11)
10      FORMAT(a)
15      FORMAT(a5)
20      FORMAT(i5)
30      FORMAT(f16.10)
35      FORMAT(f20.10)
40      FORMAT(a8)
        RETURN
        END                             !  Subroutine readin_1d
```

```
! ----------------------------------------------------------------------------
!       Subroutine fullham_1d:
!
!       This subroutine populates the full Hamiltonian then diagonalizes it using the
!       LAPACK routine DSYEVD.  The eigenvectors and eigenvalues are saved to
!       'combined.dat' for later use.
! ----------------------------------------------------------------------------

        SUBROUTINE fullham_1d

        USE decs_module                 ! declarations
        USE funct_module                ! common functions
        IMPLICIT NONE

        INTEGER i, j, count                             ! iterators
        INTEGER mtemp                                   ! temporary mode numbers
        DOUBLE PRECISION g_const                        ! constants in g
        DOUBLE PRECISION element                        ! spatial/mode-dependent component of g
        DOUBLE PRECISION rad_freq                       ! field frequency
        DOUBLE PRECISION, ALLOCATABLE :: evarray(:,:)   ! temporarily holds eigenvalues
!       LAPACK declarations

        INTEGER lwork
        INTEGER liwork
        INTEGER info
        INTEGER, ALLOCATABLE :: iwork(:)
        DOUBLE PRECISION, ALLOCATABLE :: work(:)
!       Define several functions for use in populating the arrays:
!
!               element(m):     combines the field frequency computation
!                                               with the spatial dependence of the matrix
!                                               element
!
!               rad_freq(m): calculates field frequency using spec'd dimensions
        element(m) = SQRT(r_freq(m,1))
        rad_freq(m) = r_freq(m,1)

!       Initialize LAPACK parameters

        lwork = (1+5*imax+2*imax*(INT(LOG10(REAL(imax))/LOG10(2.0)) + 1) + 3*imax**2) * lworkfactor
        liwork = 2 + 5*imax

        ALLOCATE(work(lwork))
        ALLOCATE(iwork(liwork))

        work = 0.0
        iwork = 0


!:::::::::::::::::::::::::::::::::::::::::::::::::::::::::::::::::::::::::::::::::::::::::
!
!       INTERACTION HAMILTONIAN
!
!       This section populates the interaction hamiltonian using the
!       coupling term g = - (e rba / 2 hbar) [4 hbar Wn / V e0]^1/2 f(x,y,z)
!       if using gmethod = 'a' (automatic) or forces g's to specified values
!       if gmethod = 'm'.

!       Open a series of files for output data including uncoupled hamiltonian
!       terms, interaction terms, dressed state eigenvalues, and the full
!       hamiltonian
        OPEN(unit=9,file='combined.dat',status='replace')
        OPEN(unit=12,file='fullham.dat',status='replace')
!       Determine whether to calculate or force g values and carry it out

        SELECT CASE (gmethod)
                CASE('M1','m1','MF','mf','A1','a1')         ! Sets Hint(1,i) = g(i)
                        DO i=1, imax
                                intarray(1,i) = gvector(i) * SQRT(DBLE(phot_num))
                        END DO
                CASE('A','a')                               ! Calculates g(i) for Hint(1,i)
                        g_const = - e * rba * SQRT( hbar/(1*eps0) ) / (2*hbar)
                        intarray(1,1) = 0.0
                        gvector(1) = 0.0
                        m = 1
                        DO i=2, imax            ! this step overwrites initial gvector values
                                mtemp = m
                                gvector(i) = g_const * element(mtemp) * g_spatial(mtemp,1,z)
                                intarray(1,i) = gvector(i) * SQRT(DBLE(phot_num))
                                m = mtemp+1
                        END DO
                CASE('A2','a2')                             ! Calculates g(i) for Hint(1,i)
                        g_const = - e * rba * SQRT( hbar/(1*eps0) ) / (2*hbar)
```

```fortran
                              intarray(1,1) = 0.0
                              gvector= 0.0
                              gvector(2) = g_const * element(1) * g_spatial(1,1,z)
                              DO i=2, imax
                                      intarray(1,i) = gvector(i) * SQRT(DBLE(phot_num))
                              END DO
                      END SELECT
!        First column is same as first row
         DO i=2, imax
                 intarray(i,1) = intarray(1,i)
         END DO
!        Interaction hamiltonian created
!:::::::::::::::::::::::::::::::::::::::::::::::::::::::::::::::::::::::::::::::::::::::

!        Repeat the calculation countmax times to process each atomic frequency
!        specified
!        This block determines how many times (countmax) to repeat the calculation
         SELECT CASE(amethod)
                 CASE('AF','af','AW','aw')
                         countmax=1
                 CASE('M','m')
                         countmax=iterate
         END SELECT

         ALLOCATE(evarray(imax,countmax))

         DO count=1,countmax
!*********************************** DO BLOCK ********************************************

!:::::::::::::::::::::::::::::::::::::::::::::::::::::::::::::::::::::::::::::::::::::::
!        ATOM-FIELD UNCOUPLED HAMILTONIAN
!        The following block populates the atom-field uncoupled array
         a_f_array(1,1) = afreqarray(count)/2        ! + (phot_num-1)*rad_freq(mtemp)
         m = 1
         DO i=2, imax
                 mtemp = m
                 a_f_array(i,i) = -afreqarray(count)/2 + phot_num*ffreqarray(i-1)
                 m = mtemp+1
         END DO
!        Uncoupled hamiltonian created
!:::::::::::::::::::::::::::::::::::::::::::::::::::::::::::::::::::::::::::::::::::::::

!:::::::::::::::::::::::::::::::::::::::::::::::::::::::::::::::::::::::::::::::::::::::
!        FULL HAMILTONIAN:
!        Simple statement to add the uncoupled and interaction Hamiltonians;
!        Since the input array to dseyvd is altered to hold the eigenvectors,
!        create a temporary full hamiltonian to pass to the diagonalizing routine
         fullarray = hbar * (a_f_array + intarray)
!        DO i=1,imax
!                If(fullarray(1,i)/fullarray(i,i) .LT. testval) THEN
!                        fullarray(1,i)=0.0
!                        fullarray(i,1)=0.0
!                END IF
!        END DO
         tempfull = fullarray
!        Diagonalize
         CALL dsyevd('V','U',imax,tempfull,imax,eigenvalues,work,lwork,iwork,liwork,info)

!        Write the resulting eigenvalues to a file and append for each iteration over
!        the atomic frequencies
         WRITE(7, '("Diagonalizing routine output:  ")')
         WRITE(7, 1) info
         WRITE(9,5)        count, afreqarray(count)
         DO i=1,imax
                 WRITE(9,20) (tempfull(i,j), j=1,imax)
         END DO
         WRITE(9,20) (eigenvalues(i), i=1,imax)
         DO i=1,imax
                 evarray(i,count)=eigenvalues(i)
         END DO
```

```
!       Write the full and interaction hamiltonians to a file and append
!       for each iteration


!*************************************** END DO BLOCK ***************************************
        END DO
!       Write results to appropriate files

!       DO i=1,imax
!               WRITE(11,40) (evarray(i,j), j=1,countmax)
!       END DO
        DO i=1,imax
                WRITE(12,50) (fullarray(i,j), j=1,imax)
        END DO

1       FORMAT(i4)
5       FORMAT(i4,2X,e12.6)
10      FORMAT(' ', 100000(e9.3, 1X))
20      FORMAT(100000(e18.10,1X))
30      FORMAT(' ', 100000(e12.6, 1X))
40      FORMAT(' ', 100000(e13.7, 1X))
50      FORMAT(' ', 100000(e12.6, 1X))
!print *, 'pre-deallocation okay'
        DEALLOCATE(iwork)
        DEALLOCATE(work)
        DEALLOCATE(a_f_array)
        DEALLOCATE(intarray)
!       DEALLOCATE(fullarray)
        DEALLOCATE(afreqarray)
        DEALLOCATE(ffreqarray)
        DEALLOCATE(phot_numarray)
        DEALLOCATE(gvector)
        DEALLOCATE(eigenvalues)
!print *, 'fullham completed'
        RETURN
        END                     !  Subroutine fullham_1d
```

```
!--------------------------------------------------------------------------------
!       Subroutine timedev_1d:
!
!       Uses the eigenvectors and eigenvalues generated in fullham1d to
!       evolve the system in time and translate the result to the
!       bare state basis
!--------------------------------------------------------------------------------

        SUBROUTINE timedev_1d

        USE decs_module
        IMPLICIT NONE

        INTEGER i, j, count, timeiteration
        INTEGER dummy1
        DOUBLE PRECISION dummy2
        DOUBLE PRECISION t
        DOUBLE PRECISION eigencheck
        COMPLEX(8), ALLOCATABLE :: Uii(:,:)
        COMPLEX(8), ALLOCATABLE :: eigen(:,:)
        COMPLEX(8), ALLOCATABLE :: eigentranspose(:,:)
        COMPLEX(8), ALLOCATABLE :: time_evolve(:)
        DOUBLE PRECISION, ALLOCATABLE :: probarray(:)
        DOUBLE PRECISION, ALLOCATABLE :: evprodarray(:,:)
        DOUBLE PRECISION, ALLOCATABLE :: hamtest(:,:)
        DOUBLE PRECISION, ALLOCATABLE :: newham(:,:)
!       Allocate space for the arrays

        ALLOCATE(Uii(imax,imax))
        ALLOCATE(eigen(imax,imax))
        ALLOCATE(eigentranspose(imax,imax))
        ALLOCATE(time_evolve(imax))
        ALLOCATE(probarray(imax))
        ALLOCATE(evprodarray(imax,imax))
        ALLOCATE(newham(imax,imax))
        ALLOCATE(hamtest(imax,imax))

        OPEN(unit=13,file='timedev.dat',status='replace')
        OPEN(unit=14,file='firstate.dat',status='replace')
        OPEN(unit=15,file='probsq.dat',status='replace')
        OPEN(unit=16,file='conserv.dat',status='replace')
        OPEN(unit=17,file='evproduct.dat',status='replace')
        OPEN(unit=18,file='hamtest.dat',status='replace')
        OPEN(unit=19,file='realtime.dat',status='replace')
        OPEN(unit=20,file='imtime.dat',status='replace')

        REWIND(9)         !  resets the read pointer back to the beginning of the file
!       Initialize some arrays

        Uii = CMPLX(0.0,0.0)
        time_evolve = CMPLX(0.0,0.0)
!       Iterate the time-evolution computation for each of the atomic frequencies

        DO count=1, countmax

!*******************************DO BLOCK*****************************************

!       Read the eigenvalues and vectors from the file 'combined.dat'

                READ(9,5) dummy1,dummy2
!       'tempfull' now becomes a temporary holder for eigenvectors then
!       eigenvalues
!               Read eigenvectors

                tempfull = 0.0d0
                DO i=1, imax
                        READ(9,20) (tempfull(i,j), j=1,imax)
                END DO

                evprodarray = MATMUL(tempfull,TRANSPOSE(tempfull))

                DO i=1, imax
                        WRITE(17,20) (evprodarray(i,j), j=1,imax)
                END DO
!       The following matrices are the eigenvector matrix and its transpose
!       for calculating the transition probabilities

                eigen = CMPLX(tempfull)
                eigentranspose= TRANSPOSE(eigen)

!       Verify that the eigenvectors are orthomormal

                eigencheck = REAL(SUM(MATMUL(tempfull,TRANSPOSE(tempfull))))
                WRITE(7,'("Sum of the elements of eigenvectors x (eigenvectors)T:")')
```

```fortran
                        WRITE(7,30) eigencheck
!                       Read eigenvalues
                        tempfull = 0.0d0
                        READ(9,20) (tempfull(1,i), i=1,imax)
!            Write the eigenvalues back to 'combined.dat' to verify they're read correctly
                        WRITE(9,20) (tempfull(1,i), i=1,imax)
!            Verify the diagonalization is accurate by multiplying Ev. Uii . EvT to recover Hfull
            newham=0.0
            DO i=1,imax
                        newham(i,i) = tempfull(1,i)
            END DO

            hamtest = MATMUL(REAL(eigen), MATMUL(newham,REAL(eigentranspose)))
            DO i=1,imax
                        WRITE(18,20) (hamtest(i,j), j=1,imax)
            END DO
!            Now the fun...for t=0 to tmax in steps of tstep, the vector of time-
!            dependent bare-state expansion coefficients is calculated from
!
!            || Ci(t) || = || Eigenvec || . || Uii || . || EigenvecT || . || Ci(0) ||
                        timeiteration = 1
                        t = tmin

                        DO WHILE(t.LE.tmax)
                            DO i=1, imax
                                        Uii(i,i) = CMPLX(COS(tempfull(1,i) * t),-SIN(tempfull(1,i) * t),8)
                            END DO

                            time_evolve=MATMUL(eigen,MATMUL( Uii,MATMUL(eigentranspose,bareinitial)))
!            Write real and imaginary parts of time_evolve to files for diagnostic purposes
                                WRITE(19,25) t, REAL(time_evolve(1))
                                WRITE(20,25) t, AIMAG(time_evolve(1))
!            Compute probabilities
                                DO i=1,imax
                                        probarray(i) = REAL(CONJG(time_evolve(i)) * time_evolve(i),8)
                                END DO

!            Write the results for the current value of t to files:
                                WRITE(13,25) t, (probarray(i), i=1,imax)
                                WRITE(14,25) t, probarray(1)
!            Verify conservation of probability and energy
                                WRITE(15,25) t, SUM(probarray)
                                WRITE(16,25) t, DOT_PRODUCT(time_evolve,MATMUL(fullarray,time_evolve))

                                timeiteration = timeiteration + 1
                                t = t + tstep
                        END DO                    !  end of time iterations

            END DO                    !  end of atomic frequency iterations

!~~~~~~ Notes: ~~~~~~~~~~~~~~~~~~~~~~~~~~~~~~~~~~~~~~~~~~~~~~~~~~~~~~~~~~~~~~~~~~~~
!
!      Uii contains the terms
!
!                  | Exp[-i E1 t/hbar]        0                  0          ...|
!                  |        0           Exp[-i E2 t/hbar]        0          ...|
!      Uii(i,i) =  |        0                 0           Exp[-i E3 t/hbar] ...|
!                  |        .                 .                  0          ...|
!                  |        .                 .                  .      .   ...|
!                  |        .                 .                  .          .  |
!
!      where E1, E2, ..., are the eigenvalues
!~~~~~~~~~~~~~~~~~~~~~~~~~~~~~~~~~~~~~~~~~~~~~~~~~~~~~~~~~~~~~~~~~~~~~~~~~~~~~~~~~~

!      Format statements
5      FORMAT(i4,2X,e12.6)
10     FORMAT(a)
20     FORMAT(100000(e18.10,1X))
25     FORMAT(e14.6,1x,100000(e18.10,1X))
30     FORMAT(f10.5)

       RETURN
       END                        !  Subroutine timedev_1d
```

Appendix C. Inhibited Spontaneous Emission Plots

For the sake of completeness, several plots demonstrating the suppression of decay out of the excited atomic state alluded to in Chapter 6 are provided on the following pages. No additional discussion of the phenomenon is provided at this time.
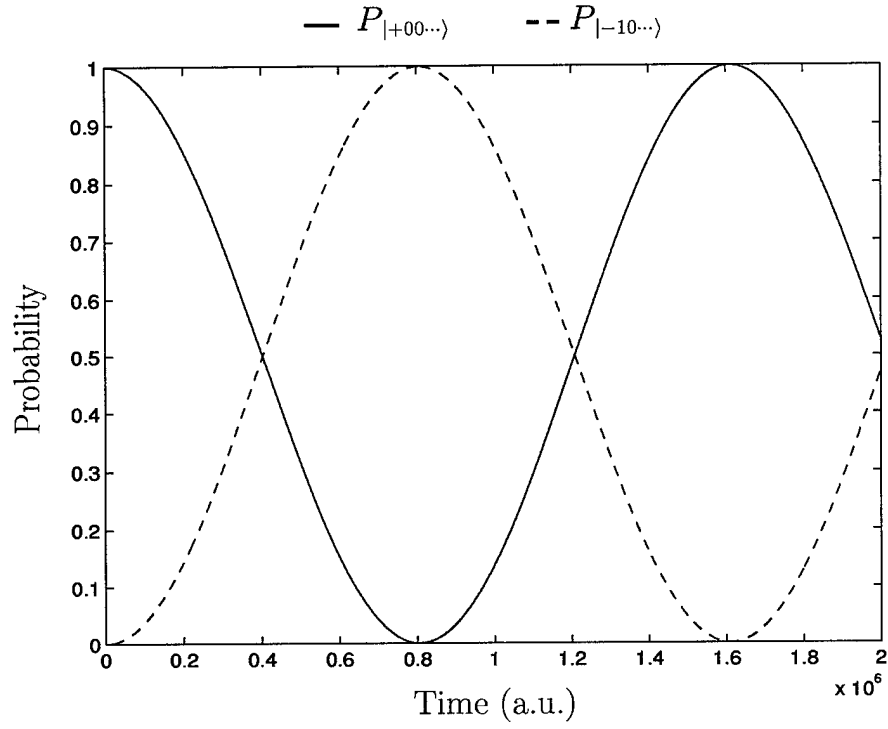
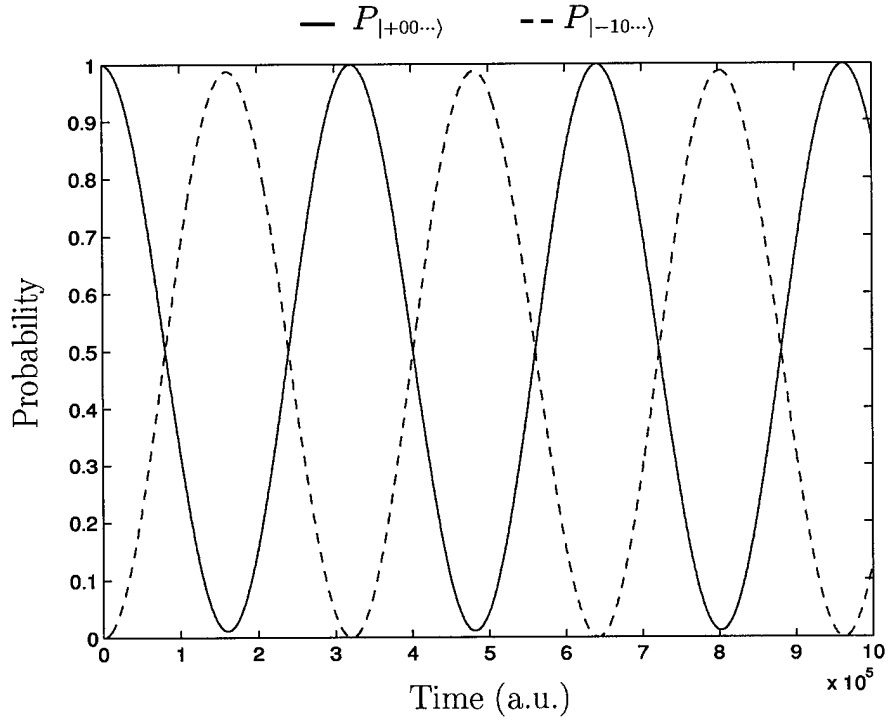Figure C.1   Atom perfectly tuned to the fundamental mode of a 100 mode field. $r_{+-} = 0.01$.
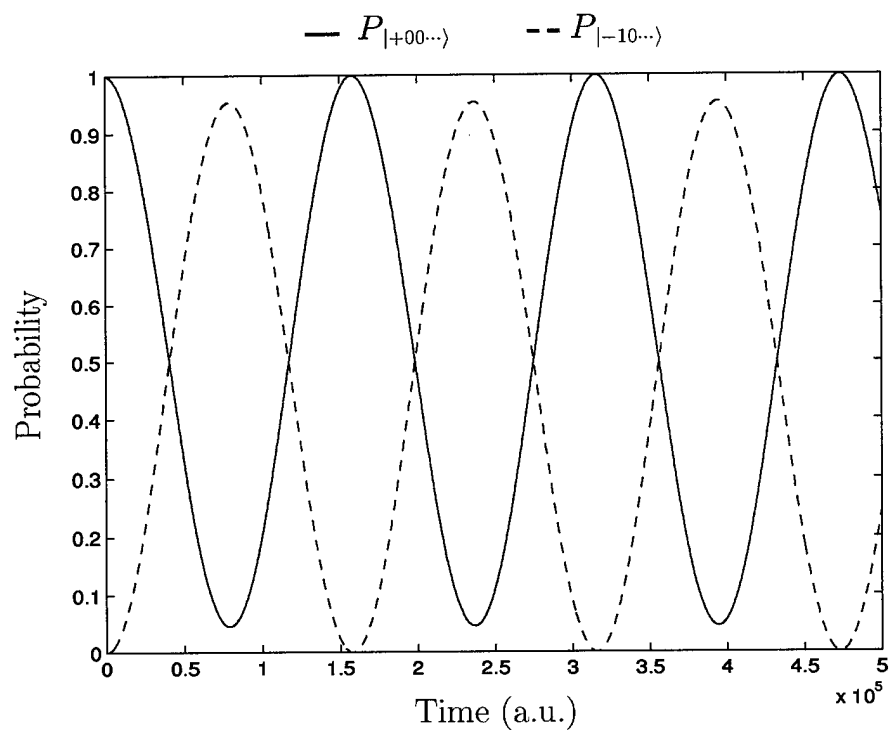

Figure C.2   Same system for $r_{+-} = 0.05$.

Figure C.3 $r_{+-} = 0.1.$
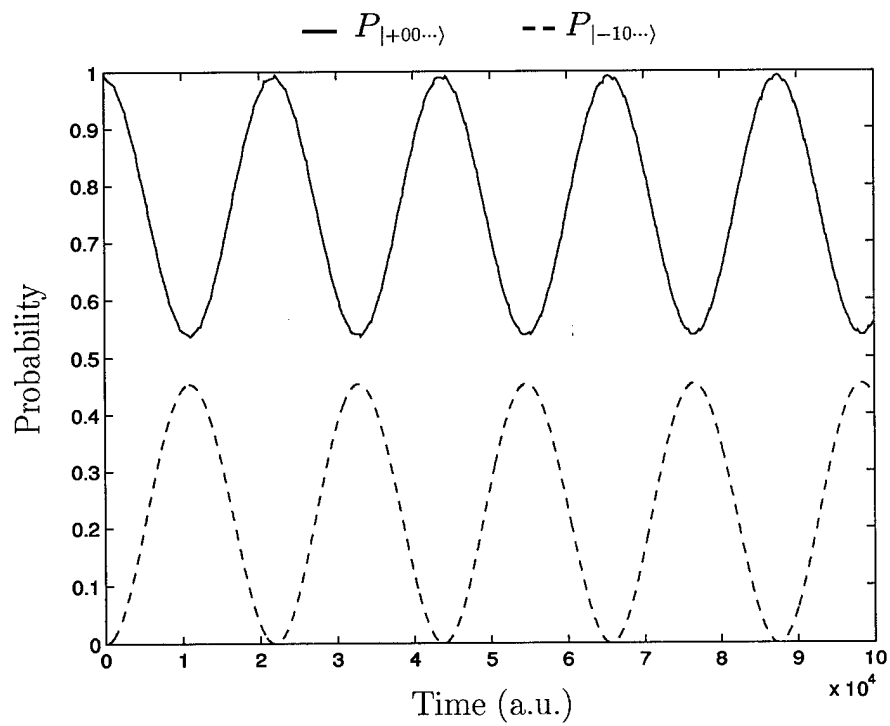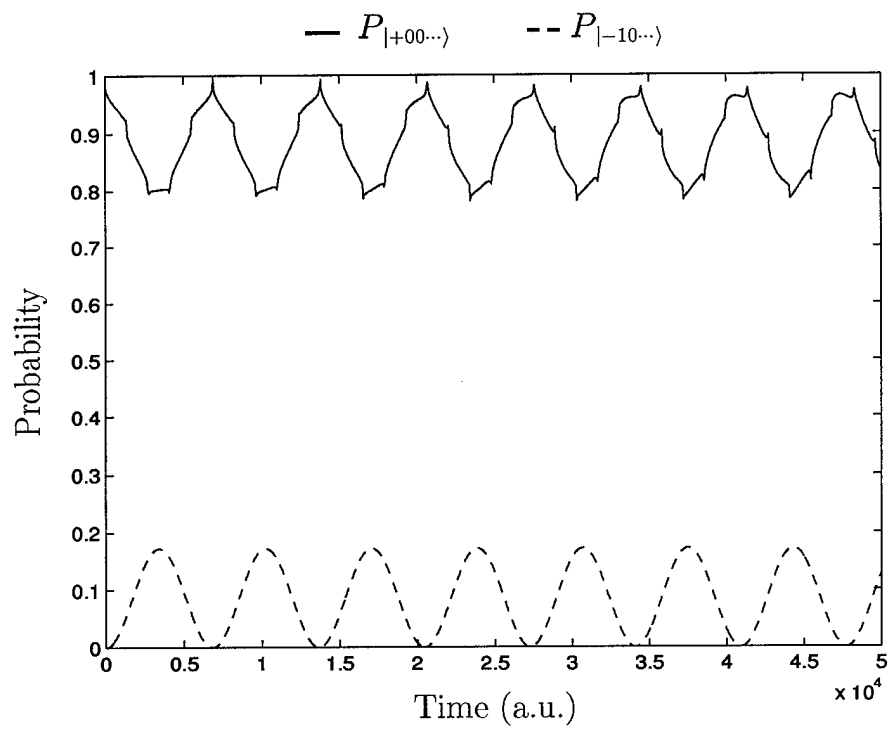

Figure C.4 $r_{+-} = 0.5.$

Figure C.5 $r_{+-} = 1.0$.

Appendix D. Unit Conversions

Listed below are several conversions for converting between atomic units and other unit systems. Values are taken from Bransden and Joachain Appendix 11 [7] as well as the Naval Research Laboratory *Plasma Formulary* [6].

Quantity	Atomic Units	MKS	Gaussian
Angular Momentum	$\hbar$	1.0546×10^{-34} J s	1.0546×10^{-27} erg s
Charge	e	1.6022×10^{-19} C	4.8032×10^{-10} statcoul
Length	a_0	5.2918×10^{-11} m	5.2918×10^{-9} cm
Velocity	v_0	2.1877×10^{6} m s^{-1}	2.1877×10^{8} cm s^{-1}
Time	$\frac{a_0}{v_0}$	2.4189×10^{-17} s	2.4189×10^{-17} s
Frequency	$\frac{v_0}{2\pi a_0}$	6.5797×10^{15} s^{-1}	6.5797×10^{15} s^{-1}
Energy	$\frac{e^2}{4\pi\epsilon_0 a_0}$	4.3598×10^{-18} J	4.3598×10^{-11} erg

Note that the value of ϵ_0 in atomic units is $\frac{1}{4\pi}$.

Following is a graphical representation of a portion of the electromagnetic spectrum to provide a scale for comparison of atomic unit frequencies to more familiar quantities.

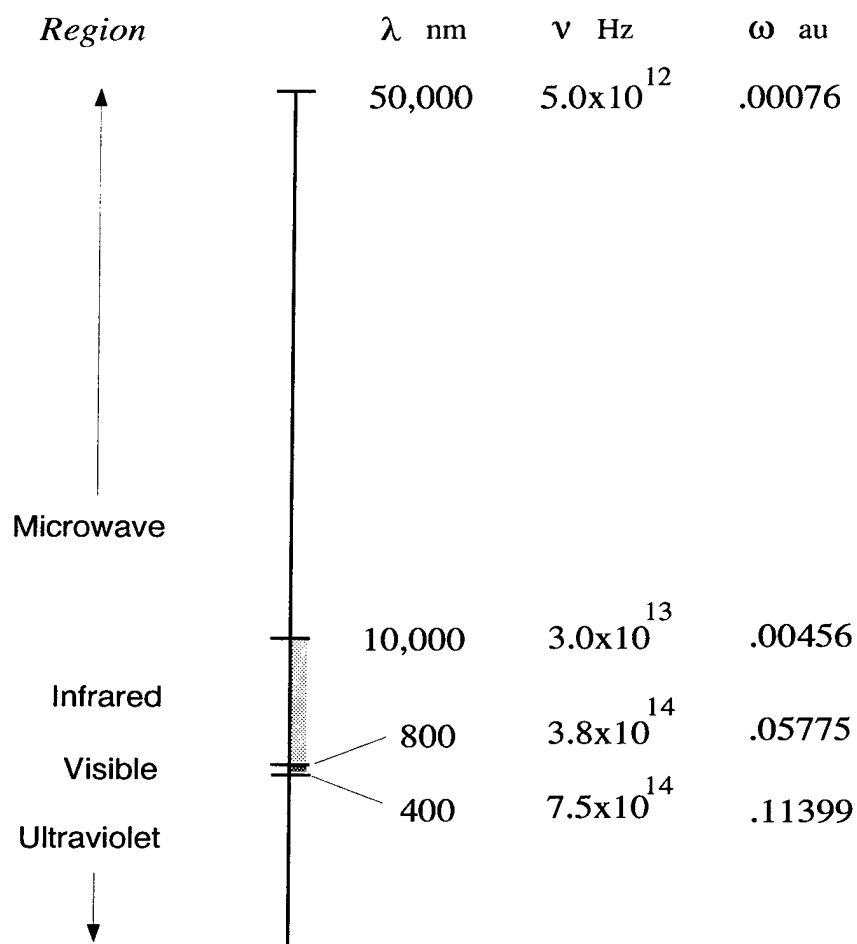| Region	λ nm	ν Hz	ω au
	50,000	5.0×10^{12}	.00076
Microwave			
	10,000	3.0×10^{13}	.00456
Infrared			
	800	3.8×10^{14}	.05775
Visible			
	400	7.5×10^{14}	.11399
Ultraviolet			

Figure D.1   A portion of the electromagnetic spectrum for comparison of atomic units of frequency to transition wavelengths (nm) and transition frequencies (Hz).

Bibliography

1. Abdel-Hafez, A. M., A.-S. F. Obada and M. M. A. Ahmad. "N-Level Atom and N-1 Modes: Statistical Aspects and Interaction with Squeezed Light," *Physical Review A, 35*:1634–1647 (February 1987).

2. Ackerhalt, J. R. and J. HY. Eberly. "Quantum Electrodynamics and Radiation Reaction: Nonrelativistic Atomic Frequency Shifts and Lifetimes," *Physical Review D, 10*(10) (November 1974).

3. Bagnell, Richard J. *Design and Characterization of Optically Pumped Vertical Cavity Surface Emitting Lasers*. MS thesis, Air Force Institute of Technology, 1992.

4. Benivenga, G. and A. Messina. "New Quantum Effects in the Dynamics of a Two-Mode Field Coupled to a Two-Level Atom," *Journal of Modern Optics, 41*(5) (1994).

5. Björk, Gunnar, et al. "Modification of Spontaneous Emission Rate in Planar Dielectric Microcavity Sturctures," *Physical Review A, 44*(1) (July 1991).

6. Book, David L. "NRL Plasma Formulary,". Naval Research Laboratory, Washington, DC, 1990.

7. Bransden, B. H. and C. J. Joachain. *Physics of Atoms and Molecules*. New York: John Wiley and Sons Inc., 1995.

8. Cohen-Tannoudji, Claude, et al. *Quantum Mechanics, Vol. I*. New York: John Wiley and Sons, 1977.

9. Gou, Shih-Chuan. "Quantum Behavior of a Two-Level Atom Interacting with Two Modes of Light in a Cavity," *Physical Review A, 40*(9) (November 1989).

10. Guo, Guang-Can and Shi-Biao Zheng. "Generation of Schrödinger Cat States via the Jaynes-Cummings Model with Large Detuning," *Physics Letters A, 223* (December 1996).

11. Hillery, Mark and Robert John Schwartz. "Time-Averaged Properties of the Jaynes-Cummings Model: Effects of Detuning," *Physical Review A, 43*(3) (February 1991).

12. Janowicz, Maciej W. and J. M. Ashbourn. "Dynamics of the Four-Level Λ System in a Two-Mode Cavity," *Physical Review A, 55*(3) (March 1997).

13. Jaynes, E. T. and F. W. Cummings. "Comparison of Quantum and Semiclassical Radiation Theories with Application to the Beam Maser." *Proceedings of the IEEE 51*. 89–109. January 1963.

14. Kressel, Henry and J.K. Butler. *Semiconductor Lasers and Heterojunction LEDs*. Quantum Electronics Series, Academic Press, Inc., 1977.

15. Loudon, R. *The Quantum Theory of Light* (2nd Edition). Oxford: Clarendon Press, 1983.

16. Marion, Jerry B. and Mark A. Heald. *Classical Electromagnetic Radiation* (2nd Edition). Harcourt Brace Jovanovich, 1980.

17. Meystre, P. and M. Sargent III. *Elements of Quantum Optics* (Second Edition). New York: Springer-Verlag, 1991.

18. Noble, Michael J. "Physics of Surface Emitting Lasers." Dissertation prospectus, Air Force Institute of Technology, Wright-Patterson AFB OH, September 1996.

19. Schlicher, Rainer R. "Jaynes-Cummings Model with Atomic Motion," *Optics Communications*, *70*(2) (February 1989).

20. Shore, Bruce W. and Peter L. Knight. "The Jayne-Cummings Model," *Journal of Modern Optics*, *40*:1195–1238 (1993).

21. Takahashi, Ichiro and Kikuo Ujihara. "Quantum Mechanical Description of Spontaneous Emission in a Microcavity in Terms of Admittance," *Physica B*, *227* (1996).

22. Tavis, Michael and Frederick W. Cummings. "Exact Solution for an N-Molecule-Radiation-Field Hamiltonian," *Physical Review*, *170*:379–384 (June 1968).

23. Towe, Elias. *A Research Report on Vertical-Cavity Surface-Emitting Lasers*. Technical Report RL-TR-95-97, Air Force Materiel Command Griffiss Air Force Base, New York: Rome Laboratory, September 1995 (AAL-9631).

24. United States Air Force Scientific Advisory Board. *New World Vistas: Air and Space Power for the 21st Century: Directed Energy Volume*. Washington, D. C.: USAF Scientific Advisory Board, 1995 (AAM-4728).

25. Vurgaftman, Igor and Jasprit Singh. "Semiconductor Microcavity Light-Emitting Structures." *Proceedings of the SPIE 2397*. 515–525. 1995.

26. Wu, Ying and Xiaoxue Yang. "Jaynes-Cummings Model for a Trapped Ion in Any Position of a Standing Wave," *Physical Review Letters*, *78*(16) (April 1997).

27. Xie, Y. B. "Two-Level Atom and Multichromatic Waves in a Lossless Cavity," *Journal of Modern Optics*, *44*(2) (1997).

28. Yamamoto, Y., S. Machida and G. Bjork. "Microcavity Semiconductor Laser with Enhanced Spontaneos Emission," *Physical Review A*, *44*(1) (July 1991).

29. Yang, Xiaoxue and Yuanjie Li. "Unified and Standardized Procedure to Solve Various Nonlinear Jaynes-Cummings Models," *Physical Review A*, *55*(6) (June 1997).

Vita

Capt Dustin Ziegler was born in Burlington, Vermont in 1971. He attended Mount Mansfield Union High School in Jericho, Vermont, and graduated in the spring of 1989. Later that year, he enrolled at the University of Vermont in Burlington on an Air Force Reserve Officer Training Corps scholarship through a cross-town program with St. Michael's College in Colchester, Vermont. In 1993, he graduated Cum Laude with a Bachelor of Science Degree in Physics and received his commission as a Second Lieutenant.

His first assignment was at Los Angeles Air Force Base where he worked in the Space Test and Evaluation Directorate as the Satellite Payload Engineer for the Advanced Research and Global Observation Satellite. In June of 1996, he entered study at the Air Force Institute of Technology.

Permanent address: HCR Box 227
Richmond, Vermont 05477

REPORT DOCUMENTATION PAGE

1. AGENCY USE ONLY (Leave blank)	2. REPORT DATE	3. REPORT TYPE AND DATES COVERED
	December 97	Master's Thesis

4. TITLE AND SUBTITLE
SPONTANEOUS EMISSION IN MICROCAVITY LASERS

5. FUNDING NUMBERS

6. AUTHOR(S)
Dustin P. Ziegler, Capt, USAF

7. PERFORMING ORGANIZATION NAME(S) AND ADDRESS(ES)
Air Force Institute of Technology
2750 P Street
WPAFB OH 45433-7765

8. PERFORMING ORGANIZATION REPORT NUMBER

AFIT/GAP/ENP/97D-11

9. SPONSORING/MONITORING AGENCY NAME(S) AND ADDRESS(ES)
Dr John P. Loehr
Heterojunction Physics Branch
Avionics Directorate (WL/AADP)
Wright Patterson AFB OH 45433-7765

10. SPONSORING/MONITORING AGENCY REPORT NUMBER

11. SUPPLEMENTARY NOTES

12a. DISTRIBUTION AVAILABILITY STATEMENT
APPROVED FOR PUBLIC RELEASE; DISTRIBUTION UNLIMITED.

12b. DISTRIBUTION CODE

13. ABSTRACT (Maximum 200 words)

An understanding of spontaneous emission processes within microcavities is crucial in addressing the need to make tomorrow's microlasers more efficient. One approach to improving the device efficiency is to reduce the threshold input energy at which lasing begins to occur. It has been suggested that the threshold in a microcavity laser can be decreased by increasing the fraction of spontaneous emission into the lasing mode. this can be accomplished by preferentially coupling the gain medium of the laser to the electromagnetic cavity mode of interest. It therefore becomes necessary to understand the mechanism by which this coupling takes place. This research develops a fully quantum mechanical description of the interaction between a gain medium modeled as a two level atom and a multimode electromagnetic field in a microcavity. Atomic transition probabilities are computed for systems in which the atom couples through a single photon process to electromagnetic cavity modes which range in number from two to 2000. Calculations performed for cavities with widely spaced modes demonstrate that atoms exhibit Jaynes-Cummings behavior when closely tuned to one mode. Detuning of the atom from the mode inhibits the exchange of energy, while increasing the strength of the coupling to the mode amplifies this exchange. Two level systems strongly coupled to many closely spaced modes exhibit spontaneous emission rates characteristic of an atom in free space.

14. SUBJECT TERMS
Quantum Electrodynamics, Field Theory, Diode Lasers, Laser Cavities, Spontaneous Emission

15. NUMBER OF PAGES
119

16. PRICE CODE

17. SECURITY CLASSIFICATION OF REPORT	18. SECURITY CLASSIFICATION OF THIS PAGE	19. SECURITY CLASSIFICATION OF ABSTRACT	20. LIMITATION OF ABSTRACT
Unclassified	Unclassified	Unclassified	UL